UNIVERSITY OF CALIFORNIA
RIVERSIDE

Sensory-Motor Transformation in a Selective Detection Task in Mice

A Dissertation submitted in partial satisfaction
of the requirements for the degree of

Doctor of Philosophy

in

Psychology

by

Behzad Zareian

December 2022

Dissertation Committee:
Dr. Edward Zagha, Chairperson
Dr. Khaleel A. Razak
Dr. Aaron Seitz

The Dissertation of Behzad Zareian is approved:

_____

_____

_____

Committee Chairperson

University of California, Riverside

Acknowledgements

The chapters of this dissertation, in part or in whole, are reprints of materials as they appear in Aruljothi et al., 2020, Zareian et al., 2021 and Zareian et al., 2022 (under review). Chapter 2 is in part from Aruljothi et al. 2020. Chapters 3 and 4 are full reprints of Zareian et al., 2021 and Zareian et al.,2022, respectively.

I want to thank all my family and friends who have supported me in my journey. To my lovely mom and dad who are the reason that I am a successful person. Thank you for your love and solace. To my brothers, Faraz and Mehrdad, thank you for always being encouraging. To Jordan and Kathleen, my hiking, painting, and gaming buddies, and neuroscience peers.

I also want to thank Zagha lab members, for being such great and lovely colleagues. We grew up together. I learned a lot from you. I taught you a lot of things, too. Thank you for your great work and professionalism, Krithiga, Zhaoran, Krista, and Angelina. I also want to thank other members of the lab, outstanding postdocs and researchers, rotating students, undergraduate research assistants, and everyone who helped with establishing this lab.

I am grateful for the help of my committee members, Dr. Aaron Seitz and Dr. Khaleel A. Razak, for their support and for being great mentors. I also want to thank other faculty members that have helped me with my research and never-ending questions, Dr. Aerika Loyd, Dr. Anu Goel, Dr. Hongdian Yang, Dr. Megan Peters, Dr. Peter Hickmott, Dr. David Rosenbaum, Dr. Weiwei Zhang, Dr. Kate Sweeney and many other ones. Also, I must especially thank the Barrels community, who have always been

curious about Zagha lab research. I am also grateful to the staff of the Department of Psychology and Life Sciences; thank you Renee Young, Marissa Ruth Skari, Jay Malekonsho, Sarah Turnbull, Kirsten Alonso, Alisha Janet, and others. You have helped a lot with all the procedures and growth of our lab.

I want to thank all my mice, Tiny, Carlos, and many other ones, who helped with the experiments and were always cooperative. You are amazing.

Lastly and most importantly, thank you Dr. Edward Zagha for your guidance at different stages of my journey. It would not have been possible for me to learn neuroscience and electrophysiology, without your patience and care. I am also appreciative of the fact that you were always supportive, especially in the harsh circumstances of my PhD. I want to thank you for all the smart solutions and for your care about being professional, orderly, and respectful of people's time and efforts.

ABSTRACT OF THE DISSERTATION

Sensory-Motor Transformation in a Selective Detection Task in Mice

by

Behzad Zareian

Doctor of Philosophy, Graduate Program in Psychology
University of California, Riverside, December 2022
Dr. Edward Zagha, Chairperson

In our everyday lives, we receive information from our environment and respond to this received information by performing motor actions. A transformation between sensory information and motor action that is not a mere reflex occurs inside our brain. Most of our goal-directed behavior involves this transformation, which may become impaired in different neurological and psychiatric disorders such as Parkinson's disease. Therefore, it becomes important to know where and how this transformation happens in the brain. I trained mice in a whisker-based selective detection task to discover mechanisms of sensory-motor transformation. In this type of behavior, mice learned to selectively respond to a brief whisker stimulation by licking a waterspout. Using wide-field calcium imaging during task performance, my colleagues revealed regions in the cortex that became active during sensory and motor behavior. I performed whisker imaging as well as recording local field potentials to give insights into the mouse behavior as well as the relationship between fast dynamics of sensory and motor signals and whisker movements (Chapter 2). Among active regions in the frontal cortex, I localized the site of

transformation to the whisker motor cortex using single-unit recording and advanced data analysis (Chapter 3). Importantly, I discovered a subcortical site of sensory-motor transformation in the dorsolateral striatum, residing downstream of the whisker motor cortex (Chapter 4). Thus, my research describes a network composed of cortical and subcortical regions involved in sensory-motor transformation. Our findings may contribute toward developing therapeutics that target the motor cortex and dorsolateral striatum in health conditions that impair these regions and sensory and motor behavior in general.

Contents

List of Figures

List of Tables

Abbreviations

Primary Whisker Somatosensory Cortex (S1, wS1)
Primary Whisker Motor Cortex (M1, MC or wMC)
Anterior Lateral Motor Cortex (ALM)
Dorsolateral Striatum (DLS)
Local Field Potentials (LFPs)
Current Source Densities (CSDs)

Chapter 1 : General Introduction

I used to get a taxi every day when I was going to high school. I waited patiently until my eyes detected a target—one of those yellow taxis—and then I would wave my hand or hold out my arm straight, so the taxi drivers knew that I wanted a taxi and would stop for me. Or when we go to a doctor's appointment, they may test our sensory-motor reflex or knee-jerk reaction by tapping below our knees. We can also think of when we see food, our mouth starts to secrete saliva. The only difference between the latter example and the former two is in the apparent motor action. Would a signal appear in my brain when I detect a yellow taxi? If that is the case, then how would a signal related to seeing a yellow target transform into a hand waving signal that controls my arm movement?

In this dissertation, I am going to talk about what is 'sensory', what is 'motor', and what happens in the brain when we perform behaviors such as in the taxi example (henceforth called sensory-motor behavior). A sensory-motor behavior is when a sensory input related to the five senses leads to motor action. I studied these concepts in mice as a model organism with generalizations to primate and human behavior systems. Studies in human subjects bring forth limitations in studying the human brain. For instance, it is hard to access the brain internally using methods such as electrophysiological recording to monitor its activity. This is especially the case for deep regions inside the brain. Also, it is hard to link the scientific findings about the brain to impairment conditions, solely by doing research on humans. I studied the brain and behavior of mice, amazing creatures with a lot of differences, yet similar in many fundamental features to humans. I first trained mice in sensory-motor behavior. I then analyzed their behavior. Finally, I

recorded different regions during their behavior, using advanced electrophysiology techniques. We see that there exist regions in the brains of mice that can sense environmental information, trigger action, and connect sense and action after learning a sensory-motor behavior.

The knowledge in this dissertation can be applied to diseases that may impede sensory-motor behavior such as in Parkinson's disease, but those diseases are not discussed here. There exists a vast amount of knowledge obtained by experimentally changing the gene expression patterns and observing their effects on brain health in mice as future directions. In the end, I am hoping for the reader can appreciate the ideas regarding sensory-motor transformation to further use them to investigate brain diseases that impair this transformation in their research. Now, let us take a closer look at the definition of a sensory-motor transformation.

What is Sensory-Motor Transformation?

Definition of Sensory-Motor Transformation. The most straight-forward description of sensory-motor transformation is at the level of the spinal cord. Sensory-motor 'pathways' are composed of a chain of sensory and motor neurons, that could receive sensory stimulation as a signal (for example when something hits our knee) and reflexively generate action in response to stimuli (knee-jerk reaction). If the level of sensory input is sufficient to generate a motor response, a sensory-motor transformation happens. A sensory-motor transformation can be more than just a reflex, such as the taxi example

mentioned in the beginning. In this case, the brain may become involved in the transformation.

For the sake of clarity, I assume that the sensory information that is received by one of the sensory organs travels further to the brain to be processed. In turn, the brain may generate motor plans and execute motor commands to make a response. Compared to the spinal cord, the complexity in connectivity of the neurons increases drastically in the brain. The neurons in the brain may receive input from sources other than the external environment such as from inside the body. So, the definitions of 'sensory' and 'motor' become blurred when compared to pathways in the spinal cord. Extensive histology and tracing experiments have been performed to determine the pathways of connecting neurons, from primary sensory organs (such as skin, eyes, ears, or whiskers of mice) to regions deep inside the brain (BARRIS, 1935; Lund et al., 1979; Woolsey & Van der Loos, 1970). Similarly, tracing experiments can be used to find returning pathways of connecting neurons, from 'motor regions' inside the brain to the moving organs (Grinevich et al., 2005).

Experimental Ways of Finding the Sensory and Motor Regions in the Brain. Sensory regions in the brain could be identified by stimulating sensory organs and recording activities in the brain in those regions. For instance, Hubel and Wiesel measured the neuronal responses in the visual cortex of cats in response to different patterns of light (Hubel & Wiesel, 1962). On the other hand, motor areas could be identified by stimulating regions and finding their corresponding movement of the body organs

(Penfield & Rasmussen, 1950). For example, stimulating the frontal eye field in the cortex evokes saccadic movements of the eyes (Tehovnik et al., 2000).

Methodological Definition of Sensory and Motor Signals. Methodologically, a sensory signal in the brain could be defined using the following set of rules: 1) A sensory signal is 'time-locked' to the time of experimentally defined stimulus onset (Chapter 3). For instance, in the primary visual cortex of anesthetized macaques, the sensory signal appears within about 34 milliseconds (ms) after stimulus onset (Schmolesky et al., 1998). In awake mice, the somatosensory or touch sensory signal appears, about 20 ms after stimulus onset in the primary somatosensory cortex (S1) (Crochet & Petersen, 2006). 2) Sensory signals are graded based on the amplitude of sensory stimulation. For instance, different levels of coherence of moving dot patterns lead to different amplitudes of sensory signals in area middle temporal visual area (V5), one of the sensory regions in the extrastriate visual cortex of primates (Britten et al., 1992). 3) Sensory signals are present irrespective of the behavioral outcome of the trial. For instance, regardless of whether a subject misses a sensory stimulus during a visual experiment or not, there is a sensory peak in sensory regions of the brain (although this is contingent upon whether the sensory stimulus is strong enough to evoke a sensory signal) (Britten et al., 1996; de Lafuente & Romo, 2006). 4) Sensory signals are transient, meaning that they have a sharp rise and fall (within a few milliseconds) (Chapter 3). 5) Sensory signals are heavily related to features of the environment, such as space or frequency. For instance, the

auditory cortex of echolocating Pallid Bats has shared neural substrates for sound localization in the space and frequency modulation (Razak & Fuzessery, 2002)

Motor signals are different from sensory signals. 1) They are time-locked to the reaction time and they happen prior to action (Chapter 3). 2) In contrast to sensory signals, motor signals are highly dependent on the behavioral outcome of the trial. For instance, they appear only in hit (correct response) trials but not miss (no response) trials (Britten et al., 1996; de Lafuente & Romo, 2006). In cases where a subject initiates movement in specific directions for an experiment, motor signals may only encode those directions (Georgopoulos et al., 1982; Li et al., 2015). 3) These signals may be less transient than sensory signals and show "ramp-like" features until the time of motor response (Roitman & Shadlen, 2002).

Traditional View About Sensory and Motor Areas in the Brain and the Challenges. Based on decades of experiments, multiple brain regions have been found to be involved with sensory and motor signal processing. For instance, the thalamus is a region that receives sensory information from all the sensory modalities (other than olfactory sensors) and it is also known as the 'relay' of sensory information to the cortex (Ahissar & Oram, 2015). On the other hand, the brainstem generates rhythmic movements (e.g., respiratory, cardiac rhythms, and whisking in mice) (McElvain et al., 2018). There are also regions with more interesting functionality; for instance, the striatum within the basal ganglia, which leads to a motor action only when there is a cue directing to the motor action (Graybiel et al., 1994).

The superficial part of the brain which is usually what we see in pictures of a brain is called the cerebral cortex (or cortex, for simplicity). Sensory and motor areas have clear spatial anatomical boundaries and definitions in the cortex of human and non-human primates (e.g., monkeys, chimpanzees, etc.). There are fundamental differences between sensory and motor areas in the cortex such as the absence of layer 4 in the motor cortex (Geyer et al., 2000). The most important sensory and motor areas in the cortex are called "primary areas", for instance, the primary motor cortex (M1). Aside from primary regions in the cortex, there are other cortical regions that may be involved in the processing of sensory information and planning motor actions. These are called high order, secondary or association areas.

It becomes hard to distinguish what is 'sensory' and what is 'motor' at the level of the cortex in rodents. Clear boundaries of sensory and motor areas in the cortex in primates, may be due to cortical expansion on the outer surface of the brain across evolution. Part of my efforts during my Ph.D. was to untangle definitions of sensory and motor in the cortex and the basal ganglia in the brains of mice. For instance, we used temporal alignment in Chapter 2 to separate these possibilities in three cortical regions.

Although the cortex is evolutionarily preserved across rodents and primates, there are fundamental differences among the species (other than the size and expansion). Damage to the motor cortex in humans leads to spastic paralysis (Brown, 1994), while extensive lesions of the motor cortex in mice may not even lead to the smallest deficits in task performance, especially in skilled actions (Kawai et al., 2015).

Mechanism: Brain Regions Related to Sensory-Motor Transformation

Here I focus on introducing the features of and controversies around individual brain regions. Although there is a growing appreciation that pathways between brain regions and their interaction are more important than individual ones. There is a lot of overlap amongst the functionality of regions in sensory-motor behavior, as we will see in more detail in chapters 3 and 4. But there are fundamental differences among brain regions such as architecture, cell type, electrophysiology, and other features; that become important in specificity with limitations in functionality and interpretation, regarding behavior and the role of these brain regions in larger networks.

Primary Sensory Cortices. Primary sensory regions in the cortex have been shown to exhibit changes in neuronal activation when sensory information arrives at sensory organs, in the form of an increase in firing rate (Hubel & Wiesel, 1962) or changes in rhythmic voltage fluctuations (Fries et al., 2001; Jones et al., 2010; Zareian et al., 2020).

Rodents use their whiskers to detect information in the environment. Whiskers are connected to muscle fibers that move and that movement sends information as a proprioception signal to the cortex. The part of the cortex that receives information from whiskers is called the primary whisker somatosensory cortex (wS1 or S1). S1 is also called the barrel cortex, because of individual whisker representations that look like barrels in the input layers of S1 (Woolsey & Van der Loos, 1970). This region has been a source of major controversy in recent years due to its ability to evoke whisker movement, which is not expected for a traditionally defined sensory cortex (Matyas et al., 2010).

Primary Motor Cortices. The motor cortex is important in movement planning (Georgopoulos et al., 1982; Rothwell et al., 1987; Svoboda & Li, 2018). Deficits in the motor cortex development lead to impairment in movement which can be seen in cases such as cerebral palsy patients (Richards & Malouin, 2013).

The primary whisker motor cortex (wMC, MC, or M1) is responsible for the control of whisker movement in rodents (Hill et al., 2011). wMC receives sensory input from S1 and thalamus and is heavily interconnected with them (Hooks et al., 2013). This region shows signals in anticipation of licking behavior (Zagha et al., 2015). Aside from wMC, in recent years, the anterior lateral motor cortex (ALM), a region within the frontal cortex has been investigated and has shown to be related to directional licking in rodents (Svoboda & Li, 2018).

The Striatum. My research mostly involved the investigation of two brain regions: wMC and the striatum. There are stark structural differences between this region and the cortex, such as the absence of layered structure. Also, the striatum does not have long-range excitatory projections like the cortex does, so it is a mutually inhibitory network.

Realizing from the first experiments performed with my colleague Angelina Lam (a co-author of Chapter 4), lesions of this brain region sometimes result in a circling type of movement in mice (especially when the extent of the lesion is large, unpublished data), showing that fundamental movement aspects of the body are dependent on this region. This may be due to the removal of tonic input to downstream regions such as superior

colliculus which has been shown to be important in spatial orienting (Masullo et al., 2019).

The striatum receives dopaminergic input from the substantia nigra which is important in reinforcement learning. It has been proposed that the striatum detects the co-activation of multiple cortical and thalamic inputs. This integration function is reinforced by dopamine (Shepherd, 2003). Damage to the striatum impairs learning severely (Dang et al., 2006). This proposes the great importance of the striatum in instrumental learning. In this study, Dang et al. showed that when they knocked out the NMDAR1 subunit of the NMDAR receptors in the striatum of mice, the mice failed to learn to stay on an accelerating rotarod. Along the same line, the sensory-motor part of the striatum has been suggested to be involved in automated movements after learning a motor task. This may be related to a shift in the involvement of the active networks in the brain from the cortex to the striatum, across learning. This shift has been suggested to become impaired in diseases such as Parkinson's disease (Wu et al., 2015). In my research, I particularly focus on a part of the striatum that receives projections from S1, which is the dorsolateral portion of the striatum (DLS) (Hintiryan et al., 2016). Researchers show that lesion in this region impairs whisker detection behavior (Hong et al., 2018).

Why is it Important to Study Sensory and Motor Activities?

Sensory and motor activities are the primary ways that our brain and body interact with the environment in everyday functions. For instance, we find objects of interest by actively moving our hands and sensing the shape and location of the objects. Similarly,

we may suppress our movements when we are about to detect an important object. These activities may be compromised in brain diseases such as cortical blindness, cerebral palsy, and Parkinson's disease.

There are cognitive functions in the brain that are critically dependent on or related to sensory and motor activities and the transformation between them, for instance, attention and decision-making. Decision-making is defined as a function of sensory information in a deliberative or accumulative form to commit to a category to further trigger one of the multiple motor programs (Gold & Shadlen, 2007). Based on studying the brain mechanisms of decision-making, we realized that a region involved in decision-making may have different features such as the following (Crapse et al., 2018; Guo et al., 2014; Luo & Maunsell, 2015; Roitman & Shadlen, 2002; Znamenskiy & Zador, 2013): 1) A region that is involved in decision making has both sensory and motor properties; 2) It shows heightened choice probability, a measure of the difference between hit (correct response) and miss (no response) trials; 3) It tracks changes in subjective threshold or criterion (as calculated by signal detection theory); across sessions or even trials. 4) It shows evidence of accumulation or categorization of sensory evidence; 5) Lesions of this region impair the ability to make appropriate decisions; 6) Microstimulation of this region biases decision-making performance. Obtaining any of these evidence in the mouse brain could be valuable to connect non-human primate and primate literature to mouse literature. In chapters 3 and 4, we investigated a few of these measures, most importantly the sensory and motor evidence in the cortex and the striatum.

References

Ahissar, E., & Oram, T. (2015). Thalamic relay or cortico-thalamic processing? Old question, new answers. *Cerebral Cortex*, *25*(4), 845-848.

BARRIS, R. W. (1935). Disposition of fibers of retinal origin in the lateral geniculate body: Course and termination of fibers of the optic system in the brain of the cat. *Archives of Ophthalmology*, *14*(1), 61-70.

Britten, K. H., Newsome, W. T., Shadlen, M. N., Celebrini, S., & Movshon, J. A. (1996). A relationship between behavioral choice and the visual responses of neurons in macaque MT. *Visual neuroscience*, *13*(1), 87-100.

Britten, K. H., Shadlen, M. N., Newsome, W. T., & Movshon, J. A. (1992). The analysis of visual motion: a comparison of neuronal and psychophysical performance. *Journal of Neuroscience*, *12*(12), 4745-4765.

Brown, P. (1994). Pathophysiology of spasticity. *Journal of neurology, neurosurgery, and psychiatry*, *57*(7), 773.

Crapse, T. B., Lau, H., & Basso, M. A. (2018). A role for the superior colliculus in decision criteria. *Neuron*, *97*(1), 181-194. e186.

Crochet, S., & Petersen, C. C. (2006). Correlating whisker behavior with membrane potential in barrel cortex of awake mice. *Nature neuroscience*, *9*(5), 608-610.

Dang, M. T., Yokoi, F., Yin, H. H., Lovinger, D. M., Wang, Y., & Li, Y. (2006). Disrupted motor learning and long-term synaptic plasticity in mice lacking NMDAR1 in the striatum. *Proceedings of the National Academy of Sciences*, *103*(41), 15254-15259.

de Lafuente, V., & Romo, R. (2006). Neural correlate of subjective sensory experience gradually builds up across cortical areas. *Proceedings of the National Academy of Sciences*, *103*(39), 14266-14271.

Fries, P., Reynolds, J. H., Rorie, A. E., & Desimone, R. (2001). Modulation of oscillatory neuronal synchronization by selective visual attention. *Science*, *291*(5508), 1560-1563.

Georgopoulos, A., Kalaska, J., Caminiti, R., & Massey, J. (1982). On the relations between the direction of two-dimensional arm movements and cell discharge in primate motor cortex. *The Journal of Neuroscience*, *2*(11), 1527-1537.

Geyer, S., Matelli, M., Luppino, G., & Zilles, K. (2000). Functional neuroanatomy of the primate isocortical motor system. *Anatomy and embryology*, *202*(6), 443-474.

Gold, J. I., & Shadlen, M. N. (2007). The neural basis of decision making. *Annu Rev Neurosci*, *30*, 535-574.

Graybiel, A. M., Aosaki, T., Flaherty, A. W., & Kimura, M. (1994). The basal ganglia and adaptive motor control. *Science*, *265*(5180), 1826-1831.

Grinevich, V., Brecht, M., & Osten, P. (2005). Monosynaptic pathway from rat vibrissa motor cortex to facial motor neurons revealed by lentivirus-based axonal tracing. *Journal of Neuroscience*, *25*(36), 8250-8258.

Guo, Z. V., Li, N., Huber, D., Ophir, E., Gutnisky, D., Ting, J. T., Feng, G., & Svoboda, K. (2014). Flow of cortical activity underlying a tactile decision in mice. *Neuron*, *81*(1), 179-194.

Hill, D. N., Curtis, J. C., Moore, J. D., & Kleinfeld, D. (2011). Primary motor cortex reports efferent control of vibrissa motion on multiple timescales. *Neuron*, *72*(2), 344-356.

Hintiryan, H., Foster, N. N., Bowman, I., Bay, M., Song, M. Y., Gou, L., Yamashita, S., Bienkowski, M. S., Zingg, B., & Zhu, M. (2016). The mouse cortico-striatal projectome. *Nature neuroscience*, *19*(8), 1100-1114.

Hong, Y. K., Lacefield, C. O., Rodgers, C. C., & Bruno, R. M. (2018). Sensation, movement and learning in the absence of barrel cortex. *Nature*, *561*(7724), 542-546.

Hooks, B. M., Mao, T., Gutnisky, D. A., Yamawaki, N., Svoboda, K., & Shepherd, G. M. (2013). Organization of cortical and thalamic input to pyramidal neurons in mouse motor cortex. *Journal of Neuroscience*, *33*(2), 748-760.

Hubel, D. H., & Wiesel, T. N. (1962). Receptive fields, binocular interaction and functional architecture in the cat's visual cortex. *The Journal of physiology*, *160*(1), 106.

Jones, S. R., Kerr, C. E., Wan, Q., Pritchett, D. L., Hämäläinen, M., & Moore, C. I. (2010). Cued spatial attention drives functionally relevant modulation of the mu rhythm in primary somatosensory cortex. *Journal of Neuroscience*, *30*(41), 13760-13765.

Kawai, R., Markman, T., Poddar, R., Ko, R., Fantana, A. L., Dhawale, A. K., Kampff, A. R., & Ölveczky, B. P. (2015). Motor cortex is required for learning but not for executing a motor skill. *Neuron, 86*(3), 800-812.

Li, N., Chen, T.-W., Guo, Z. V., Gerfen, C. R., & Svoboda, K. (2015). A motor cortex circuit for motor planning and movement. *Nature, 519*(7541), 51-56.

Lund, J., Henry, G., MacQueen, C., & Harvey, A. (1979). Anatomical organization of the primary visual cortex (area 17) of the cat. A comparison with area 17 of the macaque monkey. *Journal of Comparative Neurology, 184*(4), 599-618.

Luo, T. Z., & Maunsell, J. H. (2015). Neuronal modulations in visual cortex are associated with only one of multiple components of attention. *Neuron, 86*(5), 1182-1188.

Masullo, L., Mariotti, L., Alexandre, N., Freire-Pritchett, P., Boulanger, J., & Tripodi, M. (2019). Genetically defined functional modules for spatial orienting in the mouse superior colliculus. *Current Biology, 29*(17), 2892-2904. e2898.

Matyas, F., Sreenivasan, V., Marbach, F., Wacongne, C., Barsy, B., Mateo, C., Aronoff, R., & Petersen, C. C. (2010). Motor control by sensory cortex. *Science, 330*(6008), 1240-1243.

McElvain, L. E., Friedman, B., Karten, H. J., Svoboda, K., Wang, F., Deschênes, M., & Kleinfeld, D. (2018). Circuits in the rodent brainstem that control whisking in concert with other orofacial motor actions. *Neuroscience, 368*, 152-170.

Penfield, W., & Rasmussen, T. (1950). The cerebral cortex of man; a clinical study of localization of function.

Razak, K. A., & Fuzessery, Z. M. (2002). Functional organization of the pallid bat auditory cortex: emphasis on binaural organization. *Journal of neurophysiology, 87*(1), 72-86.

Richards, C. L., & Malouin, F. (2013). Cerebral palsy: definition, assessment and rehabilitation. *Handbook of clinical neurology, 111*, 183-195.

Roitman, J. D., & Shadlen, M. N. (2002). Response of neurons in the lateral intraparietal area during a combined visual discrimination reaction time task. *Journal of Neuroscience, 22*(21), 9475-9489.

Rothwell, J. C., Thompson, P. D., Day, B. L., Dick, J., Kachi, T., Cowan, J., & Marsden, C. D. (1987). Motor cortex stimulation in intact man: 1. General characteristics of EMG responses in different muscles. *Brain, 110*(5), 1173-1190.

Schmolesky, M. T., Wang, Y., Hanes, D. P., Thompson, K. G., Leutgeb, S., Schall, J. D., & Leventhal, A. G. (1998). Signal timing across the macaque visual system. *Journal of neurophysiology*, *79*(6), 3272-3278.

Shepherd, G. M. (2003). *The Synaptic Organization of the Brain* (G. M. Shepherd, Ed. 5th ed.). Oxford University Press.

Svoboda, K., & Li, N. (2018). Neural mechanisms of movement planning: motor cortex and beyond. *Current opinion in neurobiology*, *49*, 33-41.

Tehovnik, E. J., Sommer, M. A., Chou, I.-H., Slocum, W. M., & Schiller, P. H. (2000). Eye fields in the frontal lobes of primates. *Brain Research Reviews*, *32*(2-3), 413-448.

Woolsey, T. A., & Van der Loos, H. (1970). The structural organization of layer IV in the somatosensory region (SI) of mouse cerebral cortex: the description of a cortical field composed of discrete cytoarchitectonic units. *Brain research*, *17*(2), 205-242.

Wu, T., Hallett, M., & Chan, P. (2015). Motor automaticity in Parkinson's disease. *Neurobiology of disease*, *82*, 226-234.

Zagha, E., Ge, X., & McCormick, D. A. (2015). Competing neural ensembles in motor cortex gate goal-directed motor output. *Neuron*, *88*(3), 565-577.

Zareian, B., Maboudi, K., Daliri, M. R., Abrishami Moghaddam, H., Treue, S., & Esghaei, M. (2020). Attention strengthens across-trial pre-stimulus phase coherence in visual cortex, enhancing stimulus processing. *Scientific reports*, *10*(1), 1-12.

Znamenskiy, P., & Zador, A. M. (2013). Corticostriatal neurons in auditory cortex drive decisions during auditory discrimination. *Nature*, *497*(7450), 482-485.

Chapter 2 : Relationship Between Sensory-Motor Signals and Movements

Introduction

In the previous chapter, I defined the term sensory-motor transformation and features of sensory and motor signals. However, it is important to investigate the relationship between a presumed sensory and motor signal and the actual movement of the subject since the relationship may not be direct and there may be alternative explanations.

Different Factors may Influence the Interpretation of Presumed Motor Signals. A presumed motor signal that appears in the brain, especially in sensory cortices, may not always be related to the initiation or suppression of the apparent task-instructed movements (Zagha et al., 2022). A signal that is a direct consequence of stimulation of sensory organs and a result of activating 'afferent' nerve projections, generates an afferent signal. For instance, seeing a moving object with our eyes, moving an object inside the whisker fields of mice, or when mice sweep an object with their whiskers, are examples of afferent signals. However, a signal could be a result of self-generated movements. 1) An 'efferent' signal (motor command) is a signal that directly drives the movement. 2) A copy of a motor command might be fed back from regions that initiated motor signals to other regions, which is known as 'corollary discharge' (Also efference copy). 3) A 'reafferent' signal is the case that self-generated movements generate sensory signals that are consequences of those movements. For instance, movements of the head and body would also change the reference frames of our vision (as if we are seeing a moving object, though an object is fixed). With repetition, multiple close instances of

triansient afferent or reafferent sensory signals in time might as well look like motor signals, with ramping or sustained profiles. Thus, it is important to account for and possibly record all types of task-instructed and task-uninstructed movements and determine how they correlate with the presumed motor signals in active regions of the brain. Especially, mice are used to conduct behavioral experiments and they move a lot when they are head-fixed and waiting for stimuli. In the project described in this chapter, I used measures of movement and neuronal activities to obtain insights into the nature and delay of signals that appear in the cortex in relationship to task-instructed (licking) movement (Musall et al., 2019).

Selective Whisker Detection Task. At the time we started with our experiments, there was a surge in the investigation of brain activities while mice perform a whisker-dependent task. Unlike most of the other behavioral tasks, we used a paradigm exploiting bilateral whisker fields, choosing one of the stimuli to be a distractor stimulus, to which the mouse had to withhold responding. One of our goals was to determine mechanisms of impulse control and attenuation of sensory information by comparing the behavioral and neuronal responses of the distractor stimulus to a target stimulus in the contralateral whisker field, in which the mice had to respond by licking a waterspout.

Since the whisker system is highly lateralized, testing Triesman's attenuation framework works best for this system to find out any insights about brain mechanisms of selective attention (Treisman, 1964). Based on this framework, the stream of unattended signals gets filtered at different stages of information flow. Mechanistically and

considering brain resources involved, an implementation of the framework could be related to the attenuation of the sensory signals in different regions of the brain along the sensory pathways. In this way, the whisker system is unique since the sensory pathways of the two fields are mostly isolated in the two hemispheres of the brain. We did not know how far the sensory signals could reach inside the brain in our task, especially in the case of distracting information propagation through the cortex. Also, most of the similar studies were performed in non-human primates, but our goal was to study attenuation in mice to bridge the gap between non-human primate literature and the research in rodents related to disease models such as mouse models of attention deficit hyperactivity disorder (ADHD) (Yamashita et al., 2013).

Results

Brief Overview of Aruljothi et al. 2020. Aruljothi et al. characterized a selective detection behavior across many mice trained in the lab and found that the mice learn to withhold their licking in response to a distractor stimulus (more than 86% of distractor trials) and they responded with high accuracy to target trials (80% of the target trials), resulting in discrimination value of 2, which indicates the mice separate the target from distractor information very well (Aruljothi et al., 2020). Using a widefield calcium imaging method of the dorsal cortex, they found that although both target and distractor signals appear in sensory cortices of both hemispheres to the same extent, the distractor signals undergo drastic attenuation in wMC and ALM in the distractor-aligned frontal cortex. This attenuation was detected in a time window immediately after the stimulus

onset, in which the mice were instructed to withhold licking for an additional 200 ms until the start of a response window. The paper further controls for two important effects: 1) The target-distractor assignment of the whisker fields (whether the target is assigned to the left or right whisker field), and 2) Whether a hit trial is preceded by a correct rejection trial or not. In either case of both experiments, they showed that the main results of the paper were still valid. Thus, Aruljothi et al. found possible regions for attenuation of sensory stream in the cortex.

Whisker Imaging of the Selective Detection Task. We recognized two possible strategies mice could use to solve the selective detection task. First, the mice could fix their whiskers (fixate) until the arrival of the stimuli for optimal detection. Fixation of whiskers on piezo-controlled paddles was comparable to fixating saccades on to-be-attended items in visual attention tasks in primates. However, it was also possible that mice use the movement of their whiskers to find an alternative strategy for better detection of the target stimulus in contrast to the distractor (See also (Zagha et al., 2022) for a related discussion). Figuring out a difference in the movement of whiskers in the target and distractor whisker fields, became also important in terms of correct interpretation of differential attenuation in the two hemispheres, observed in the cortex. In the Aruljothi et al. project, I designed a method for collecting images of whiskers. I further analyzed and visualized whisker data to figure out whether whiskers are fixed before the stimuli and whether their movements had any relationship with task performance. I found bilateral whisking in general increases in target trials compared to

distractor trials after the onset of the stimuli (Figure 2.1, A and B compared to C and D or E and F compared to G and H). The increase in whisking happened about 100 ms after the stimulus onset. Considering that the mice were instructed to not lick until 200 ms after the stimulus onset, we speculated that the whisker movement may be part of a larger overt sequence of whisking-licking that happens after the stimulus onset. In distractor trials and times before stimulus onset in all types of trials, we observed lower whisking than after the target trials. This suggests that the mice used a fixed or quiet whisking strategy to maximize detection of the stimuli. Also, we concluded that at least based on the amplitude of whisking, the mice did not choose a different type of whisking in the two whisker fields. Thus, together with symmetric positioning of the stimuli, detection and amplification of target signals and attenuation of distractor signals may not be driven by a difference in whisking in the two whisker fields. In addition to the data described here, I used the same methodology for whisking data analysis on different outcome types of trials, published in another widefield calcium imaging study of the same task (Marrero et al., 2022). In Marrero et al., I showed that more whisking coincided with missing target stimuli. Altogether, mice learned to maintain their whiskers largely fixed prior to the stimulus onset and additional whisker movements resulted in reduced ability to detect the target stimuli.

Using Local Field Potentials (LFPs) to Reveal Fast Temporal Dynamics. Following the observation of activation of cortical regions in widefield calcium imaging, I obtained recordings from layer 5 of wMC and ALM and I used it to reveal fast changes in the

population activities of each region. Interestingly, LFPs confirmed the same trend of increase in active regions (downward deflection after stimulus onset), similar to what was observed in widefield calcium imaging (Figure 2.2). In terms of details of Figure 2.2, we depicted LFPs of target trials, recorded from the target-aligned hemisphere (Figure 2.2, A-C), and distractor trials recorded from the distractor-aligned hemisphere (Figure 2.2, D-F). We overlapped the average of traces across sessions to reveal the differences between the two streams (Figure 2.2, G-I). Although the first peak (as defined in Figure 2.2, H) was highly similar in both streams, the traces started to diverge from peak 2 in wMC and ALM, validating the findings revealed by widefield calcium imaging regarding the attenuation of the distractor sensory stream. The first feed-forward sweep of the activities likely reflected a sensory signal that appeared in both contexts.

The contextual divergence of the second peak in LFPs of wMC and ALM happened earlier than the increase in whisking observed around 100 ms after the stimulus onset. Thus, the early divergence of LFP signals suggests that cortical attenuation precedes the initiation of whisking and licking. This excludes the possibility that the apparent attenuation is caused by the movement itself.

The way that I implemented the whisker imaging method in Aruljothi et al. was to continuously image the whiskers using a camera, while the mice were performing the task. The continuous method was suffering from drifts in frame rate. In a more recent project (striatum project), I realized that the more recent versions of cameras from Thorlabs had an external trigger (trigger mode), which could be used to image the whiskers only during the trial events. In the trigger mode method, the trials could be

averaged to give a single whisking trace which was also less time-consuming to analyze than the continuous method. Aside from that, I realized there existed an output port that could be used to track the changes in the frame rate directly from the camera. I imaged a new set of mice using the trigger mode method. Importantly, in these experiments, I used faster stimuli than what I used in Aruljothi et al. (faster deflection of piezo-controlled paddles). I observed a faster rise time for whisking signals (around 60 ms after the stimulus onset) (unpublished). In light of these new findings, I speculate the following: 1) In the continuous method, I generally observed a gradual increase of frame rate throughout a session (due to drift), meaning that the whisking traces captured by imaging were increasingly expanded throughout the session (in an accordion-like manner). It is possible that an early average increase in whisking after the stimulus onset (such as the one observed in later experiments), was smeared by averaging over slow-rising whisking traces. Thus, the actual increase in whisking may be faster than what I reported before. This suggests that an early increase in whisking may influence the attenuation observed in wMC and ALM (for instance the continuous decrease in peak 3 in LFPs of figure 2.2, H may be related to whisking). Nevertheless, 2) the changes between the two experiments may be due to a difference in the amplitude and duration of whisker stimuli. In this case, LFPs of bilateral wMC should show a fast divergence, preceding the increase in whisking in the trigger mode method (faster than 60 ms), to be consistent with Aruljothi et al. (the continuous method). Altogether, these emphasize the importance of precise movement imaging for the correct interpretation of neuronal activities.

Discussion

We found an increase in neuronal activities and whisking behavior after the stimulus onset, during a 200 ms lockout window, and before the earliest onset of reaction times. Since the mice were instructed to not lick in the lockout window, we made sure that the increase in neuronal activities and whisking are not directly related to licking. However, there remain multiple interpretations of the observed data: 1) Our behavioral measurements do not rule out small movements of the tongue and jaw, which cannot be captured by our lick detector. These movements may exist and be a sign of preparatory activity or working memory (Mayrhofer et al., 2019), 2) Along the same line, the movement of the whiskers may also be a sign of motor preparation or working memory, or in general a way of retaining sensory signals, since the whisking continues until the onset of licking after the 200 ms lockout window. Also, there is a possibility that the overt movement of the tongue is contingent upon the overt movement of the whiskers, thus driving one type of movement may drive the other. 3) We cannot rule out whether neuronal signals observed in regions such as the whisker motor cortex causally drive the whisking and licking or whether they reflect motor signals that are generated elsewhere.

A way of addressing some of these possibilities is by performing simultaneous recordings of brain activity and imaging whisker movements (and possibly other parts of the body). In this case, the onset of whisking can be correlated with the activity of wMC on a trial-by-trial basis. Alternatively, a regression or temporal correlation of whisking (and licking or other types of movements) and neuronal activities could be done to reveal the true nature of signals observed in active regions. Lastly, optogenetics activation or

inhibition of active cortical regions could provide insights into whether the observed signals are causally important in driving or suppressing movements.

Aside from global attenuation of distractor sensory signal reaching the frontal cortex, Aruljothi et al. revealed possible sites of target signal propagation, showing up in target-aligned wMC and ALM during response hit trials. The paper further revealed a choice signal that appears in the frontal cortex. These signals appeared when the frames were aligned to either sensory (stimulus onset) or motor events. Thus, along with S1, these sites are potentially reflective of sensory-motor transformation in the dorsal cortex. To be clear in the remainder of this dissertation, the usage of 'motor' in the term sensory-motor transformation refers to a licking motor signal. But in general, and based on the content of this chapter, the reader should keep in mind that a limitation of my study and many other similar studies is a need for imaging body movements (especially imaging whiskers in whisker-based tasks) at the same time with experiments of interest such as recording brain activity, to clearly define the sensory and motor signals and the transformation. In the next chapter, using single-unit recording, we investigate which of the active regions is most likely related to sensory-motor transformation in the cortex.

Figures and Legends

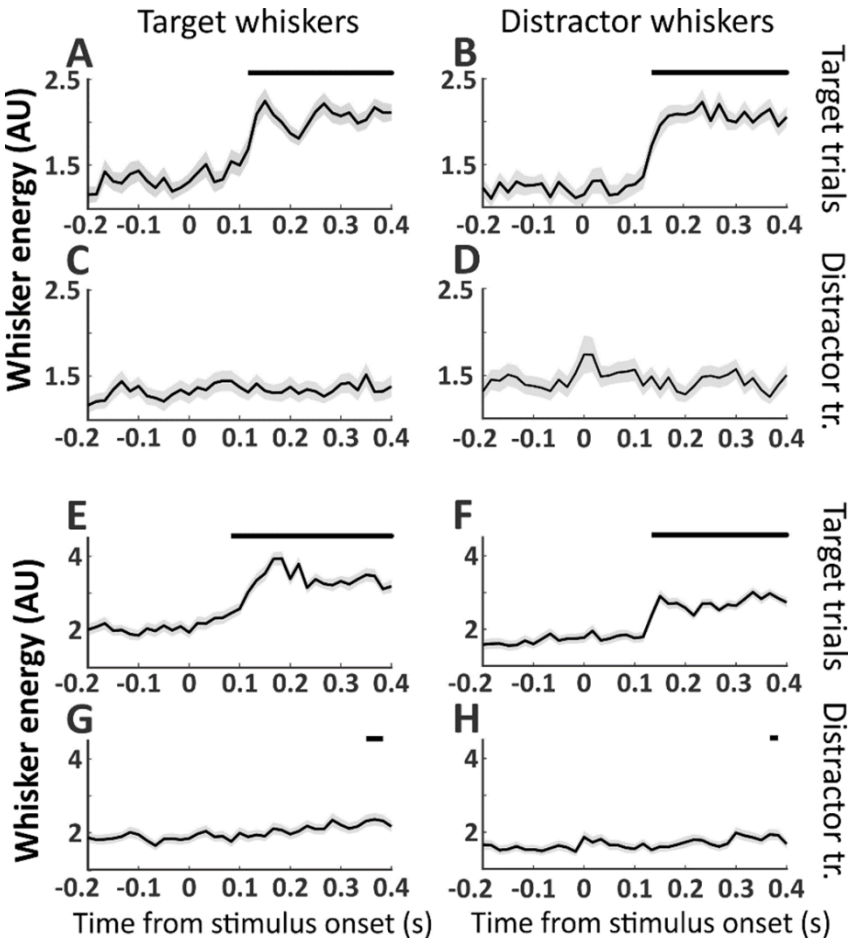

Figure 2.1. Bilateral whisker movements on target trials.

Whisker movement energy was calculated from target or distractor whisker fields and plotted separately for target and distractor trials. Significant changes in post-stimulus compared to pre-stimulus whisker movements are indicated as black bars above each plot. Two example sessions are shown, session 1 **(A-D)** and session 2 (E-H). **(A, E)** Target whisker energy on target trials; **(B, F)** distractor whisker energy on target trials; **(C, G)** target whisker energy on distractor trials; **(D, H)** distractor whisker energy on distractor trials. Significant increases in whisker movements occurred for both target and distractor whiskers approximately 0.1 seconds after target stimulus onset **(A, B, E, F)**. Target and distractor whisker movements to distractor stimuli were either non-significant throughout the trial **(C, D)** or delayed **(G, H)**.

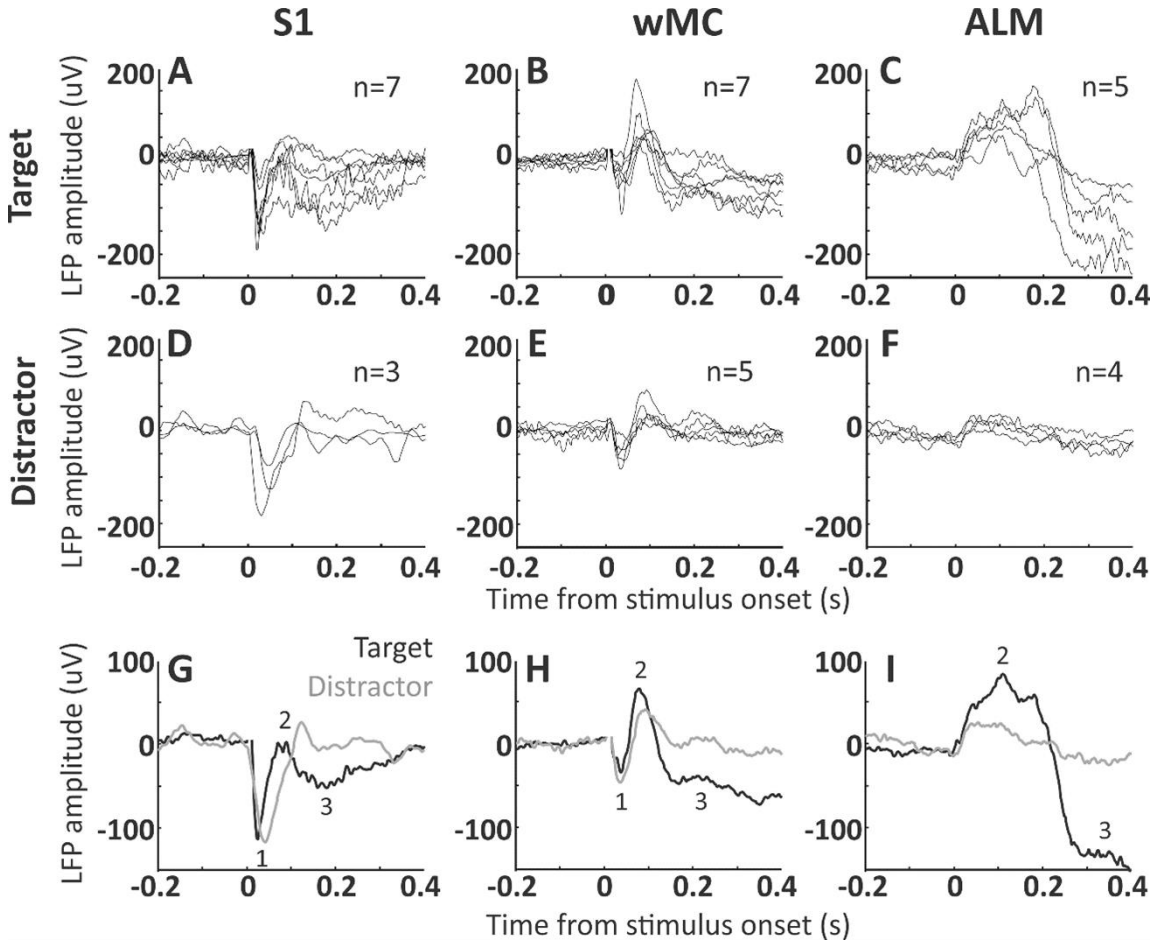

Figure 2.2. LFP signal transformation across S1, wMC and ALM.

LFP signals were recorded from layer 5 of S1, wMC and ALM. **(A-F)** Each trace reflects average LFP signals from one session, across all target trials in target-aligned cortices **(A-C)** and across all distractor trials in distractor-aligned cortices **(D-F)**. The count in each panel refers to the number of recorded sessions included. **(G-I)** Target-aligned (black) and distractor-aligned (grey) LFP signals, averaged across sessions. We observed three distinct event-related potentials, two negative-going (1 and 3) and one positive-going (2). Event 1, which is large in S1, small in wMC and absent in ALM, likely reflects the initial feedforward sensory sweep. This event is similar in target and distractor recordings. Event 3, which is large in ALM and moderate in wMC and S1, is highly dissimilar between target and distractor recordings.

References

Aruljothi, K., Marrero, K., Zhang, Z., Zareian, B., & Zagha, E. (2020). Functional localization of an attenuating filter within cortex for a selective detection task in mice. Journal of Neuroscience, 40(28), 5443-5454.

Marrero, K., Aruljothi, K., Zareian, B., Gao, C., Zhang, Z., & Zagha, E. (2022). Global, Low-Amplitude Cortical State Predicts Response Outcomes in a Selective Detection Task in Mice. Cerebral Cortex, 32(9), 2037-2053.

Mayrhofer, J. M., El-Boustani, S., Foustoukos, G., Auffret, M., Tamura, K., & Petersen, C. C. (2019). Distinct contributions of whisker sensory cortex and tongue-jaw motor cortex in a goal-directed sensorimotor transformation. Neuron, 103(6), 1034-1043. e1035.

Musall, S., Kaufman, M. T., Juavinett, A. L., Gluf, S., & Churchland, A. K. (2019). Single-trial neural dynamics are dominated by richly varied movements. Nature neuroscience, 22(10), 1677-1686.

Treisman, A. M. (1964). Selective attention in man. British medical bulletin, 20(1), 12-16.

Yamashita, M., Sakakibara, Y., Hall, F. S., Numachi, Y., Yoshida, S., Kobayashi, H., Uchiumi, O., Uhl, G. R., Kasahara, Y., & Sora, I. (2013). Impaired cliff avoidance reaction in dopamine transporter knockout mice. Psychopharmacology, 227(4), 741-749.

Zagha, E., Erlich, J. C., Lee, S., Lur, G., O'Connor, D. H., Steinmetz, N. A., Stringer, C., & Yang, H. (2022). The importance of accounting for movement when relating neuronal activity to sensory and cognitive processes. Journal of Neuroscience, 42(8), 1375-1382.

Chapter 3 : Cortical Localization of the Sensory-Motor Transformation in a Whisker Detection Task in Mice

At the time we started the project described in this chapter, methods to relate neuronal activities and behavior was relatively unknown in the mouse literature. An established method that had been used more in the neuroscience of non-human primates, was signal detection theory. Signal detection theory had been shown to be important in separating sensitivity and criterion as critical components of behavior. We used this method to investigate sensory and motor activities in multiple regions in the cortex and relate them to behavior.

A major debate in the field was whether the sensory-motor transformation is distributed in the brain or localized to any specific region, especially in our case of an investigation, within the cortex. The correlates of sensory-motor transformation have been found in S1, wMC, and ALM in separate labs. Another major debate was whether the motor regions in the brain were responsible for triggering a motor action or whether their activity was related to the suppression of an action.

This is a collaborative paper, a follow-up of the study presented in Chapter 2. Based on widefield calcium imaging of the dorsal cortex presented in Chapter 2, active regions during task performance were determined as follows: S1, wMC, and ALM. Here I contributed by performing in vivo electrophysiology from wMC and analyzing the data. The single unit and population activities were investigated and contrasted with each other. Thus, the analyses presented in this chapter could be used to relate multiple measures of regional activities to behavior. In addition, the methodological definition of

sensory and motor activities, based on measures such as temporal alignment, could be used as a starting point to answer more complicated questions about any regions in the brain (also explained in Chapter 1 in detail). Lastly, this study revealed wMC as the most plausible site of sensory-motor transformation in the dorsal cortex.

Cortical Localization of the Sensory-Motor Transformation in a Whisker Detection Task in Mice

Abbreviated Title: Cortical Localization of Sensory-Motor Transformation

Authors: Behzad Zareian[1*], Zhaoran Zhang[2*], Edward Zagha[1,2]

[1] Department of Psychology, [2] Neuroscience Graduate Program, University of California Riverside, 900 University Avenue, Riverside CA 92521 USA

* equal contributors

Correspondence to: edward.zagha@ucr.edu

Number of Figures: 8

Number of words abstract (209), introduction (716), discussion (930)

Acknowledgements

We thank Dr. Hongdian Yang, Krista Marrero and Krithiga Aruljothi for many helpful discussions throughout the project.

Conflicts of Interest

The authors declare no competing financial interests.

Funding Sources

This project was supported by the Whitehall Foundation (Research Grant 2017-05-71 to E.Z.) and the National Institutes of Health (R01NS107599 to E.Z.).

Abstract

Responding to a stimulus requires transforming an internal sensory representation into an internal motor representation. Where and how this sensory-motor transformation occurs is a matter of vigorous debate. Here, we trained male and female mice in a whisker detection go/no-go task in which they learned to respond (lick) following a transient whisker deflection. Using single unit recordings, we quantified sensory-, motor- and choice-related activities in whisker primary somatosensory cortex (S1), whisker primary motor cortex (wMC) and anterior lateral motor cortex (ALM), three regions that have been proposed to be critical for the sensory-motor transformation in whisker detection. We observed strong sensory encoding in S1 and wMC, with enhanced encoding in wMC, and a lack of sensory encoding in ALM. We observed strong motor encoding in all three regions, yet largest in wMC and ALM. We observed the earliest choice probability in wMC, despite earliest sensory responses in S1. Based on the criteria of having both strong sensory and motor representations and early choice probability, we identify whisker motor cortex as the cortical region most directly related to the sensory-motor transformation. Our data support a model of sensory encoding originating in S1, sensory amplification and sensory-motor transformation occurring within wMC, and motor signals emerging in ALM after the sensory-motor transformation.

Significance Statement

This study addresses the fundamental question of where within the neocortex a sensory stimulus representation transforms into a motor response representation during stimulus detection. We recorded and analyzed single unit activity of three cortical regions during a passive whisker detection Go/NoGo task in mice. Using quantitative assessments of sensory- motor- and choice- encoding across these regions, we showed that a cortical region traditionally defined as whisker motor cortex is most directly related to the transformation process. In addition, our study shows how sensory and motor signals are amplified and propagated throughout cortex. These findings open up new directions to studying the cellular and circuit mechanisms of sensory-motor transformations.

Introduction

To accomplish goal-directed behavior, the brain selects task-relevant stimuli and outputs the appropriate motor responses. A crucial component of this process is the transformation of an internal representation of a sensory stimulus into an internal representation of a motor response. Identifying where this occurs is an essential first step in developing mechanistic understandings of this process. Correlates of sensory-motor transformations in neocortex have been identified in non-human primates (Kim and Shadlen, 1999; Shadlen and Newsome, 2001; de Lafuente and Romo, 2006; Siegel et al., 2015). More recent efforts are now underway to study sensory-motor transformations in mouse neocortex (Matyas et al., 2010; Guo et al., 2014; Yang et al., 2015; Zagha et al., 2015; Goard et al., 2016; Le Merre et al., 2018; Pho et al., 2018; Mayrhofer et al., 2019; Aruljothi et al., 2020; Salkoff et al., 2020), which benefits from less neocortical arealization and the application of novel genetic and physiological tools. Yet, despite these efforts, there is still no agreement on the location of the sensory-motor transformation.

In this study, we use two major criteria for localizing the site of transformation in mouse neocortex. Our first criterion is the coexistence of robust sensory and motor representations. This has been elegantly demonstrated in the primate lateral intraparietal (LIP) cortex during a visual discrimination task; early in the decision process LIP neurons encode sensory stimulus strength whereas late in the decision process this activity converges to the anticipated response (Roitman and Shadlen, 2002). Regions

with only sensory or only motor representation could be upstream or downstream, respectively, of the transformation process, but cannot mediate the transformation.

Our second criterion is early and robust choice probability (Britten et al., 1996; de Lafuente and Romo, 2006; Crapse and Basso, 2015). Choice probability is a measure of the relationship between neural activity and a behavioral response, independent of stimulus content (Britten et al., 1996). For identical stimulus and behavioral conditions, choice probability is significant only after the initiation of the transformation process. Notable primate studies using multi-site recordings during sensory-motor task performance compared the onset and magnitude of choice probability across multiple cortical regions (de Lafuente and Romo 2006; Siegel, Buschman, and Miller 2015). Regions showing early and robust choice probability are more likely to be initiating the transformation; conversely, regions showing late choice probability are likely reflecting transformations that occurred elsewhere.

We studied a sensory-motor transformation in the context of sensory detection, in which mice learned to respond (lick) following the presence of a transient whisker deflection stimulus. In a recent study using widefield calcium imaging of dorsal neocortex, we identified the following regions as potentially contributing to the transformation process by expressing robust activity between stimulus onset and response: whisker representation of primary somatosensory cortex (S1), whisker region of primary motor cortex (wMC), and anterior lateral motor cortex (ALM) (Aruljothi et al., 2020). Previous studies of similar sensory-motor pairings (whisker stimulus→lick) provide partial support for the transformation occurring within each region. S1 shows

robust sensory encoding (Stüttgen and Schwarz, 2008; O'Connor et al., 2010; Wang et al., 2012; Sachidhanandam et al., 2013), can evoke motor responses (Matyas et al., 2010), and displays significant choice probability (Sachidhanandam et al., 2013; Yang et al., 2015; Chen et al., 2016; Kwon et al., 2016). wMC shows robust sensory and motor encoding (Ferezou et al., 2007; Huber et al., 2012; Zagha et al., 2015) and displays neural dynamics consistent with linking a sensory stimulus to a motor response (Zagha et al., 2015). ALM shows robust motor encoding (Li et al., 2015; Chen et al., 2017) and displays neural dynamics consistent with motor planning (Inagaki et al., 2018). Moreover, acute perturbation of all three regions impairs whisker detection (Huber et al., 2012; Guo et al., 2014; Yang et al., 2015; Zagha et al., 2015). However, previous studies have not compared sensory-, motor-, and choice-related content across all three regions in the same task. Moreover, it is critical that such studies are conducted with sufficient temporal resolution to determine the precise timing of these signals in each region.

In this study we measured single unit spiking activity in S1, wMC and ALM during a whisker detection task. Based on analyses of sensory and motor encoding and choice probability, we find that activity in wMC is most correlated with a sensory-motor transformation process.

Materials and Methods

Subjects. Animals and experiments were approved by the IACUC of University of California, Riverside. Both male and female, adult mice were used in the experiments, of C57BL/6J or BALB/c backgrounds (age: mean +/- std: 145+/-45 days old at the time of recording experiments). The mice were kept in 12 hours light and dark cycle and the experiments were conducted predominantly during the light cycle.

Surgery. Mice were anesthetized using an induction of ketamine (100 mg/kg) and xylazine (10 mg/kg) and maintained under isoflurane (1-2%) anesthesia. A 10x10 mm portion of the scalp was removed and a lightweight metal headpost was attached to the skull using cyanoacrylate glue. The headpost includes an 8×8 mm central window, leaving the skull over dorsal cortex exposed. The exposed skull was sealed with a thin layer of cyanoacrylate glue and covered with silicone gel. Mice were treated with meloxicam (0.3 mg/kg) and enrofloxacin (5 mg/kg) on the day of the surgery and for 2 additional days after the surgery. After recovery from surgery for a minimum of three days, water restriction was initiated, and the mice were introduced to the behavioral task.

Behavior. MATLAB software and Arduino boards were used to control the behavioral task flow. The mice were head-fixed in the setup during a behavioral session. Piezoelectric benders with attached paddles were placed within the whisker fields bilaterally. One side was assigned as target and the other as distractor at the onset of training and remained consistent throughout training and recording. The location of the

paddles was in the mid-ventral whisker fields (targeting D2/E2-D3/E3 whiskers), with movement in the caudal direction of 1 mm for our largest stimuli. A voltage generator (Thorlabs) was used to drive the piezo benders. Whisker deflections were triangular waves of 2 to 200 ms. Amplitude and velocity of deflections were varied to operate within the dynamic range of each mouse's psychometric curve. In any single recording session, two stimulus amplitudes were applied: one near the saturation of the psychometric curve and one 2x or 4x lower within the dynamic psychometric range. For each session, equal strength stimuli were presented for target and distractor trials. Licking responses were detected by an infrared beam break circuit positioned immediately in front of a central lickport. Reward was approximately 5 μL of water. Mice were trained in three stages, progressing from 1) classical condition to 2) operant conditioning to 3) the full task with punishment for incorrect responses (see (Aruljothi et al., 2020) for training details and learning trajectories). Intertrial intervals (ITI) varied from 6 to 10.5 seconds, drawn from a decreasing exponential distribution, to correct for an expectation hazard function and thereby minimize a timing strategy (Elithorn and Lawrence, 1955). Trial types consisted of target trials (deflection of the target paddle), distractor trials (deflection of the distractor paddle) or catch trials (no stimulus). The initial percentages of each trial-type were set as follows: target trials 15%, distractor trials 60%, catch trials 25%. Immediately following stimulus onset was a lockout period of 200 (46 sessions) or 300 ms (8 sessions). Licking during the lockout period resulted in aborting the current trial. Following the lockout period was a 1 second response window. Responses within the response window following target stimuli (hits) were rewarded with a fluid reward.

Withholding (not responding) on a distractor trial was rewarded with a shortened ITI (1.4 to 3.1 second distribution) and subsequent target trial. In expert mice, the percentage of target and distractor trials were similar across each session. All licking outside the post-target response window (including during the ITI) was punished by resetting the ITI. Behavioral sessions typically lasted between one to two hours, which included 200 to 400 trials. Mouse weights were maintained above 85% of their initial weights by either receiving all the water from task or receiving additional water and wet food after the task.

Engagement Period. For behavioral and recording analyses, the trials were truncated to engaged periods using a gap of 60 seconds as a disengagement criterion. For sessions with more than one engaged period, the longest continuous bout was used for further analyses. Sessions without continuous engagement for 10 minutes were excluded from further analysis. We also excluded the trials in which the mice responded prematurely (licking during the lockout period).

Behavioral Analysis. For behavioral metrics, hit rate was obtained by dividing the number of hits by the total number of target deflection trials. Spontaneous rate was obtained by dividing the number of catch trials containing spontaneous licking during the equivalent response window by the total number of catch trials. For the sessions that did not contain catch trials (n=10 out of 54 sessions), the 1 second pre-stimulus response rate was used as a replacement of the spontaneous rate. For the purpose of d-prime

calculations, response rates of 0 and 1 were estimated at 0.01 and 0.99, respectively. Behavioral d-prime and criterion were calculated as (Swets, 1961):

$$Dprime_{behavior} = \phi^{-1}_{Hit\ rate} - \phi^{-1}_{Spont\ rate}$$

$$Criterion_{behavior} = -(\phi^{-1}_{Hit\ rate} + \phi^{-1}_{Spont\ rate})/2$$

ϕ^{-1} is the inverse phi function which outputs the z score of the input rates. Electrophysiological recordings were conducted immediately after the mice reached expert status. For behavioral performance measures during the electrophysiological recording sessions, see Figure 3.1D.

Electrophysiology. All of the recordings were obtained from 19 mice. On average, 3 sessions were recorded from each mouse (range 1-9). Craniotomies and durotomies of less than 0.5 mm in diameter were established on the day of recording, under isoflurane anesthesia. After 30 to 60 minutes post-surgery, mice were tested in the behavioral task without electrode implantation to ensure recovery to normal behavior. Upon evidence of normal expert behavior, a silicon probe (Neuronexus A1x16-Poly2-5mm-50s-177) was advanced into the brain using a Narishige micro-manipulator under stereoscope guidance. Recording sites were targeted to the barrel field of primary somatosensory cortex (S1), the whisker region of primary motor cortex (wMC) and anterior lateral motor cortex (ALM), based on the functional mapping studies of (Aruljothi et al., 2020) . Precise coordinates (mm, from bregma): S1 3.2-3.7 lateral, 1-1.5 posterior; wMC 0.5-1.5 lateral, 1-2 anterior; ALM 1-2 lateral, 2-2.5 anterior. We positioned the recording sites to target

layer 5, from 500 to 1000 μm below the pial surface (midpoint of the silicon probe recording sites, mean +/- standard deviation, S1: 650+/-68 μm; wMC: 647+/-145 μm; ALM: 692+/-84 μm).

Whisker alignment for S1 recordings was verified by two methods. First, after electrode implantation we verified correct alignment by hand mapping of several individual whiskers and observing LFP responses. Second, we only included sessions with clear peaks in the combined multi-unit post-stimulus time histogram (peak response >1.4x above baseline within 40 ms post-stimulus). In contrast, inclusion of wMC and ALM sessions were based solely on anatomical location. For wMC, we targeted our recordings to the sub-region that displays the earliest onset sensory responses (Matyas et al., 2010), which correlates with anatomical projection sites from whisker primary somatosensory (barrel) cortex at the transition zone between agranular medial and agranular lateral cortices (Smith and Alloway, 2013).

Electrophysiology Pre-Processing and Spike Sorting. Neuralynx software was used for data acquisition and spike sorting. Electrophysiological signals were sampled at 32 kHz; wideband signals were band-pass filtered from 0.1Hz to 8000 Hz and signals for spike sorting were additionally high pass filtered at 600 Hz to 6000 Hz. Putative spikes were identified as threshold crossings over 20 to 40 μV, set at the beginning of each recording session to be well isolated from baseline noise. Spike sorting and clustering was done offline using KlustaKwik algorithm in SpikeSort3D software. The clusters were further manually inspected and merged based on the similarity of waveform and cluster location

in peaks and valleys feature space; clusters indicative of movement artifacts (non-spike waveform, equal amplitude in all channels) were removed. We used isolation distance (ID) and L ratio to verify cluster quality (Schmitzer-Torbert et al., 2005) (mean +/- standard error of mean (SEM): ID 15.6180+/- 0.7378, L ratio 0.2312+/- 0.0172). Clusters were rejected if the spike rate was lower than 0.1 Hz. The number of units included in each recording session (mean +/- standard deviation): S1: 18+/-5, wMC: 26+/-4, ALM: 24+/-4. Further data analyses were conducted using MATLAB software (Mathworks). Spike times were binned within 5 ms non-overlapping bins. Reaction time (RT) binning in Figure 3.2 used the following bins: (ms) sensory: fast RT 201-249, medium RT 250-330, slow RT 335-547; sensory-motor: fast RT 322-374, medium RT 374-447, slow RT 459-982; motor: fast RT 301-326, medium RT 329-399, slow RT 407-1240.

Sensory Encoding. Sensory encoding was quantified using a neurometric approach based on signal detection theory that enables the direct comparison of neural performance to behavioral performance (Britten et al., 1992; Stüttgen and Schwarz, 2008). For this analysis, the target and distractor trials were used regardless of their outcome (hits, misses, false alarms and correct rejections). Data presented for sensory encoding used the larger of the two stimuli for neurometric and psychometric comparisons. 'Stimulus present' data were spike counts within 100 ms immediately post-stimulus; 'stimulus absent' data were spike counts within three consecutive 100 ms epochs pre-stimulus onset. Distributions based on single trials were compared using receiver operating characteristic (ROC) curve, by plotting the cumulative distribution function of each

distribution against each other. The area under the ROC (AU-ROC) was converted to neurometric d-prime as (Simpson and Fitter, 1973):

$$Dprime_{neuron} = \sqrt{2} \times \phi^{-1}_{AU-ROC}$$

AU-ROC was bounded by 0.003 and 1-0.003 for population encoding, to ensure the output of real numbers.

Combining Units. In Figure 3.4, sensory encoding was calculated not only for single units, but also for different combinations of units. In Figure 3.4B set 3, the spikes were summed together for each 5 ms bin across all the units recorded in a session. This results in a single multi-unit per session, for which sensory encoding was calculated similar to single units. In Figure 3.4B set 4, the spikes of all units in each region were combined across all sessions. To equalize the number of trials across sessions, the sessions with less trials had their trials duplicated and appended to the original trials to match the trial number of the session with the most trials; for the sessions with the trial numbers not a common divisor of the trial number in the longest session, the trials were randomly sampled (with replacement) from these sessions accordingly and added to that session to fill in. The sensory encoding for these combined units and trials were calculated similar to the previous cases.

Random Sampling. In addition to combining all units from each session or region, we ran additional analyses to assess encoding for random sets of units (Figure 3.4C and D). We randomly selected units to be added sequentially and computed d-prime values for each

group, with group size spanning 1 to total number of units per region. We permutated this ordering and d-prime calculation 300 times and plotted the mean +/- standard deviation curve in Figure 3.4C. For the purpose of neurometric-psychometric comparison, we transposed the data by creating a histogram in d-prime bins (bin width of 0.02 spanning 0 to 4.5), with the entries (dependent variable) as the neuronal pool size. Mean +/- standard deviation for the neuronal pool size needed to achieve a specific d-prime is plotted in Figure 3.4D.

Sensory-Motor Alignment. A common method used to assess sensory and motor content is to determine the temporal alignment of neural activity to stimulus and response onsets (Hanes and Schall 1996; Mountcastle et al. 1974; Romo et al. 2002). To quantify sensory and motor content, we used a similar neurometric approach as described above. Because the motor alignment requires responding to a stimulus, we only considered hit trials in this analysis. For sensory alignment, we used the same 100 ms post-stimulus window as for sensory encoding. For motor alignment, we used a 100 ms pre-response window. Both conditions were compared to the same pre-stimulus baseline as described above.

Latency Estimation. Latencies of activation after the stimulus onset was estimated by using a 20 ms sliding window (75% overlap) post-stimulus, comparing to a pre-stimulus baseline, for all target trials. Baseline activity was the average activity in 20 ms sliding windows (75% overlap), during the 1 second pre-stimulus epoch. We excluded the first 10 ms after the stimulus onset due to possible contamination with stimulus artifacts.

Choice Probability. Choice probability was calculated as the separation of neural activity on hit versus miss trials. All spikes from each session were combined to increase spike density for comparisons. To ensure an adequate number of trial types and ensure valid comparisons: 1) we calculated the hit rate for small and large amplitude stimuli separately 2) if the difference between those was below 15%, trials from both types of stimuli were pooled together 3) if the difference was above 15%, the stimulus type with larger number of hits and misses were considered 4) all sessions with fewer than 5 misses were removed. The total number of trials used for each session are (max/mean/min) 89/24.9/5 (hits) and 102/22.7/5 (misses). We used the AU-ROC method along sliding time windows to calculate choice probability as the separation between spiking distributions on hit vs miss trials. The duration of the sliding window was set to 50 ms with 90% overlap.

General Statistics. We used permutation statistics for comparing sensory-motor variance and slope differences (10,000 repetitions). We shuffled the units between the conditions (for instance, S1 and wMC sensory encoding d-primes), and we pooled two new putative sets and calculated the difference in variable of interest (for instance, variance). Then we assessed the position of the actual variance difference among these 10,000 repetitions and we reported the p-value as the proportion of the repetitions above the actual variance (two-sided calculation). For each repetition, the shuffling was done by randomly sampling from each condition, with replacement, then mixing the samples. The new

putative sets were set to have equal numbers of samples from each condition (half of each condition's initial size). For comparing random sampling results, Cohen's d was used by dividing mean difference of the two groups by their pooled standard deviation. For calculating significant choice probability within each region across sessions, for each time window, we calculated a one sample t-test between the reported choice probability and chance level (0.5) (p-value=0.01). For comparing choice probability amplitudes across regions, we used unpaired t-tests with an alpha level of 0.01. For latency estimation, paired t-test was used (between each 20 ms window and baseline) with alpha level of 0.05. Data are presented as mean +/- SEM unless otherwise indicated.

Results

Behavioral Task and Electrophysiological Recordings. Head-fixed mice were trained to perform a whisker detection go/no-go task in which they learned to lick a lickport following a transient whisker deflection in one whisker field (target) to obtain a fluid reward (Figure 3.1A). Stimuli were piezo-controlled caudal deflections of a paddle contacting multiple whiskers. We imposed a minimum lockout period of 200 ms between stimulus onset and response window to separate sensory from motor encoding. Trials were aborted if any responses occurred during the lockout period. Target trials were interleaved with two other trial types: distractor trials, in which there was a transient deflection of the same amplitude in the opposite whisker field, and catch trials, in which there was no stimulus deflection (Figure 3.1B and 3.1C). Mice were considered expert in this task once they achieved a detection d-prime (separation between hit rate and

spontaneous rate) greater than 1 for three consecutive days. Electrophysiological recordings were conducted in expert mice while performing the detection task. For the recording sessions included in this study, the behavioral performance measures: hit rate 88.0% +/- 2.3%; spontaneous rate 15.7% +/- 1.4%; d-prime 2.6 +/- 0.1 (n=54 sessions from n=19 mice, Figure 3.1D).

Based on a concurrent widefield calcium imaging study (Aruljothi et al., 2020), we targeted our electrophysiological recordings to three cortical regions contralateral to the target whisker field: whisker representation of primary somatosensory cortex (S1), whisker region of primary motor cortex (wMC) and anterior lateral motor cortex (ALM). Each of these regions were significantly active post-stimulus and pre-response (Aruljothi et al., 2020), and therefore may contribute to the sensory-motor transformation process. We used silicon probes with contact sites spanning layer 5 to record multiple single units in each region (S1: 445 units, 25 sessions, 8 mice; wMC: 424 units, 16 sessions, 9 mice; ALM: 315 units, 13 sessions, 8 mice). To establish the functional hierarchy of these regions, we calculated post-stimulus response latency for each session. Latency measurements are consistent with the functional ordering of S1→wMC→ALM (mean +/- standard deviation: S1 30 +/- 15 ms, wMC 48 +/- 28 ms, ALM 95 +/- 43 ms; ANOVA $F(2,51)=23.56$, $p<0.01$; Tukey post-hoc comparison: S1-ALM $p<0.01$, wMC-ALM $p<0.01$, S1-wMC $p=0.11$).

Justification of 'Sensory' and 'Motor' Temporal Windows. The next set of analyses quantify the sensory and motor content within each cortical region. We used spiking

activity within specific time windows to assess putative sensory content (100 ms post-stimulus onset) and putative motor content (100 ms pre-response onset). To justify our time windows, we present three example neurons in Figure 3.2 with robust sensory, sensory-motor, and motor context, respectively. The 'sensory' unit shows robust alignment to the stimulus onset as a sharp peak in the average spiking activity across trials (Figure 3.2A, left column). In contrast, this unit lacks a sharp peak in average activity when aligned to the response (Figure 3.2A, right column). This is further apparent when grouping the trials based on reaction times (Figure 3.2A, bottom row): peak activity levels overlap regardless of reaction time when aligned to stimulus onset, whereas peak activity levels vary according to reaction time when aligned to the response. Note that this time-locked sensory activity occurs within the first 100 ms post-stimulus. On the other hand, the 'motor' unit shows prominent alignment to the response (Figure 3.2C, right column) with activity that is delayed when aligned to the stimulus onset (Figure 3.2C, left column). In further contrast with the 'sensory' unit, peak activity levels in the 'motor' unit overlap when aligned to the response but not to the stimulus onset (Figure 3.2C, bottom row). Note that this time-locked motor activity peaks within the last 100 ms pre-response. The 'sensory-motor' unit shows a mixture of both features, with sharp, transient activity aligned to the stimulus followed by activity that is sustained until the response (Figure 3.2B).

Single Unit and Population Sensory Encoding Across Cortical Regions. We show in Figure 3.3A the average spiking activity for an example unit from target-aligned S1,

contralateral to the target whisker field. On target trials (Figure 3.3A blue), this unit displayed a prominent increase in spiking immediately after stimulus presentation, followed by a lower level of persistent activity. Spiking activity on distractor trials (Figure 3.3A, black), in contrast, appeared only slightly elevated from pre-stimulus levels. In order to quantify stimulus encoding, we used the neurometric d-prime approach (Figure 3.3B-E), which accounts for single trial variability and allows for comparisons between neuronal performance and behavioral performance (Britten et al., 1992). We compared trial by trial distributions of pre-stimulus and post-stimulus spiking activities (Figure 3.3B and 3.3C). For the post-stimulus condition, we included spikes in the first 100 ms post-stimulus onset. We calculated the d-prime value of each unit from area under the curve (AUC) of the receiver operating characteristic (ROC) function (AU-ROC) between the pre-stimulus and post-stimulus distributions (Figure 3.3D). For this analysis, a d-prime greater than zero indicates higher spiking activity post-stimulus compared to pre-stimulus. Plotting the d-prime values for all units in this S1 recording session (Figure 3.3E) shows target versus distractor stimulus encoding across the population. As shown in this example session, target stimulus encoding is highly variable yet positively skewed across these units, whereas distractor stimulus encoding is considerably more restricted.

Shown in Figure 3.4A is target and distractor stimulus encoding for S1, wMC and ALM across all recorded neurons, indexed to the average behavioral performance of the mice during the corresponding recording sessions. Both S1 and wMC neurons showed prominent target stimulus encoding across their populations. ALM neurons, in contrast,

showed minimal target stimulus encoding. We analyzed these data with both single unit and population approaches (Figure 3.4B-D). First, we compared the group means of single unit target encoding across these three regions (Figure 3.4B set 2). We found mean target stimulus encoding to be significantly higher for S1 and wMC compared to ALM, and, interestingly, for wMC to be significantly higher than S1 (S1: 0.23 +/- 0.02; wMC: 0.37 +/- 0.03; ALM: 0.03 +/- 0.01; ANOVA $F(2,1181)=47.036$, $p<0.01$; Tukey post-hoc comparison: S1-ALM $p<0.01$, wMC-ALM $p<0.01$, wMC-S1 $p<0.01$; effect size: wMC 61% larger than S1). Additionally, we compared the summed spiking from multiple neurons in each trial (summed within each recordings session, Figure 3.4B set 3, and summed across all units within each region, Figure 3.4B, set 4). When combined across each population, the neurometric d-prime for S1 and wMC, but not ALM, outperformed the behavioral d-prime.

To quantify population coding within each region, we randomly sampled different numbers of units in each region and plotted the resulting neurometric target d-prime values (see Methods) (Figure 3.4C). As the number of sampled units increased, the target d-prime increased well beyond behavioral performance for S1 and wMC, but not for ALM. Furthermore, this trend rose faster for wMC than for S1 (Figure 3.4C). To perform neurometric-psychometric comparisons, we first transformed the data across axes (Figure 3.4D). This allowed us to assess, for each region, the mean and variance in neural pool size that outputs each d-prime value. Next, we determined the neural pool size needed to match the average behavioral d-prime values from the same sessions. Both S1 and wMC populations were able to match behavioral performance (Figure 3.4D, red arrows),

whereas the ALM population was not. Moreover, fewer units were required to match behavioral performance for wMC compared to S1 (mean +/- standard deviation: S1 95 +/- 44 units; wMC 52 +/- 25 units; Cohen's d=1.2).

We also used an additional method to quantify sensory encoding. Instead of using a fixed 100 ms window, we replicated the above analyses for a 20 ms window of peak sensory encoding for each recording session. The peak window analyses also demonstrated larger single unit d-prime values in wMC compared to S1 (average d-prime: S1: 0.16, wMC: 0.22, $p<0.01$, Tukey post-hoc comparison) and fewer wMC neurons needed to match behavioral performance (mean +/- standard deviation: S1 199 +/- 84 units; wMC 121 +/- 56 units; Cohen's d=1.0). Altogether, these results demonstrate robust sensory encoding in S1 and wMC but not in ALM, with increased sensory encoding in wMC compared to S1.

Sensory and Motor Alignments Across Cortical Regions. Next, we sought to assess the sensory versus motor alignment across these three cortical regions. For quantification, we used a similar neurometric d-prime method as above, yet for only hit trials and for both sensory and motor alignments (Figure 3.5). For sensory alignment, we again analyzed spiking within 100 ms following stimulus onset; for motor alignment, we analyzed spiking within 100 ms preceding the reaction time (Figure 3.5A). Due to our imposed lockout between stimulus onset and response window, these analysis epochs did not overlap. In Figure 3.5B, we plot the sensory vs. motor alignment for each unit across all three regions. Interestingly, much of the variance of the S1 and wMC populations lies

along the diagonal, indicating equal sensory and motor alignment in these regions. In contrast, the variance of the ALM population is largely along the x-axis, indicating predominant motor alignment. We quantified this by calculating a sensory-motor variance ratio: variance along sensory axis divided by variance along motor axis. Indeed, this variance ratio was similar for S1 and wMC, and both were significantly larger than ALM (variance ratio: S1=0.90, wMC=0.86, ALM=0.09; permutation statistics, S1-wMC, $p=0.79$, S1-ALM, $p<0.01$, wMC-ALM, $p<0.01$). We also used the mean and variance of each alignment as measures of representation and compared these values within and between regions (Figure 3.5C and D, respectively). Similar to the findings depicted in figure 3.4, we found that sensory representation increased from S1 to wMC, then fell dramatically in ALM. Additionally, we found that motor representation increased from S1 to wMC and ALM, with similar means and variance in wMC and ALM.

The above analyses support the observation that S1 and wMC show both sensory-aligned and motor-aligned content, and therefore meet our first criterion for identifying the location of the sensory-motor transformation. ALM, in contrast, shows only motor-aligned content, which we interpret as being downstream of the transformation process.

Choice Probability Across Cortical Regions. To determine the temporal onset of activity related to the sensory-motor transformation, we calculated choice probability across time for each of the three regions. Choice probability quantifies the separation between hit and miss trials, thereby isolating response-related activity (Britten et al., 1996; de Lafuente and Romo, 2006; Crapse and Basso, 2015). According to our second criterion, the region

with early and robust choice probability is most likely to initiate the sensory-motor transformation. For these analyses we combined spikes from all units within each recording session to enhance spike density per comparison. Figure 3.6 shows the average spiking activity on hit and miss trials from three example sessions (Figure 3.6A-C) and across all recording sessions (Figure 3.6D-F). All panels show higher activity on hit trials during some portion of their post-stimulus response, indicating positive choice probability. However, there are notable differences between regions. The S1 and wMC data show increased activity on hit trials immediately post-stimulus and during the response window. However, the separation of hit and miss activity appears to be larger and more sustained for wMC. In contrast, the ALM data show post-stimulus responses only on hit trials, which emerges gradually after stimulus onset.

We calculated choice probability in 50 ms sliding windows across sessions for each region (Figure 3.7A). All three regions showed significant increases in choice probability post-stimulus (Figure 3.7B, gray bars; one-sample t test, comparing to chance level at 50% and alpha level of 0.01), indicating higher spiking rate on hit trials. Interestingly, S1 additionally showed significant negative choice probability pre-stimulus (Figure 3.7B, purple bars), indicating that lower spike rates immediately before the stimulus onset predicts a hit response. For all three regions, significant post-stimulus choice probability preceded the reaction time, which was always >200 ms due to our lockout period. Yet, significant post-stimulus choice probability emerged earliest in wMC compared to S1 and ALM (S1 165 ms, n=21 sessions; wMC 70 ms, n=13 sessions; ALM: 175 ms, n=9 sessions). Notably, choice probability latencies are not merely reflections of

neural activity latencies of these regions (Figure 3.7B, red bars); while stimulus response latency was earliest in S1, choice probability emerged earliest in wMC.

To compare amplitude and time course, in Figure 3.8 we overlay choice probability signals from all three regions. After stimulus onset, choice probability rose faster in wMC compared to S1 and ALM (Figure 3.8A). We further assessed differences in choice probability magnitude in each time window by conducting pairwise comparisons between regions (Figure 3.8B). Choice probability was significantly larger during the post-stimulus lockout window in wMC compared to S1 and ALM (two-sample t test, alpha level of 0.01). Based on these analyses, wMC meets our second criterion for identifying the location of a sensory-motor transformation, in displaying early onset and robust choice probability.

Discussion

The focus of this study is to localize within neocortex the region most directly related to the sensory- motor transformation process. This was studied in a whisker detection task, in which mice were trained to respond to passive whisker deflections by licking a central lickport. Our recordings within the neocortex focused on three regions which have been identified in a recent calcium imaging study (Aruljothi et al., 2020) as potentially contributing to the transformation. Our analyses indicate wMC as the cortical region most directly related to the transformation processes based on having the strongest sensory encoding (Fig 3.4), robust sensory and motor alignment (Fig 3.5) and early and robust choice probability (Fig 3.7 and 3.8). Our findings are consistent with sensory integration

occurring between S1 and wMC, sensory-motor transformation occurring within wMC, followed by the propagation of motor signals in ALM.

Choice encoding initiating downstream of primary sensory cortices has been demonstrated in studies of non-human primates (Romo et al., 2002; de Lafuente and Romo, 2006; Siegel et al., 2015) and studies of visual detection/discrimination in mouse (Goard et al., 2016; Pho et al., 2018; Salkoff et al., 2020). Our study is also consistent with this finding. However, our study and other studies of the mouse whisker system show significant choice encoding in S1 as well (Sachidhanandam et al., 2013; Yang et al., 2015; Kwon et al., 2016; Aruljothi et al., 2020). Choice encoding in S1 consistently occurs 'late', after the initial feedforward sensory peak activity (Sachidhanandam et al., 2013) (Figure 3.8). Our findings do not support S1 as initiating the sensory-motor transformation (Figures 3.7 and 3.8). We consider two possible causes for S1 choice encoding. First, S1 choice encoding may reflect feedback from choice signals originating in higher order cortices, such as wMC or S2 (Yang et al., 2015; Kwon et al., 2016), as has been described in non-human primates (Siegel et al., 2015). Alternatively, S1 choice probability measurements may not relate to choice encoding at all, but instead reflect re-afferent signals related to the behavioral response sequence. In a related study of the same task, we found whisking to increase approximately 100 ms after stimulus onset, which preceded the onset of licking by approximately 100 ms (Aruljothi et al., 2020). We report here significant choice probability in S1 at 160 ms, 60 ms *after* the onset of whisking. Since whisking is largely absent on miss trials (Aruljothi et al., 2020), re-afferent signals likely contribute to measures of S1 choice probability. In contrast, we

find significant choice probability in wMC at 70 ms, 30 ms *before* the onset of whisking. Additionally, we find significant choice probability in ALM at 175 ms, 25 ms before the onset of licking. These neural and behavioral temporal latencies are consistent with the choice-related signals in wMC and ALM initiating the whisking and licking response sequence, respectively.

wMC is a frontal region traditionally studied in the context of whisking initiation and modulation (Carvell et al., 1996; Kleinfeld et al., 1999; Hill et al., 2011). However, it is now certain that wMC has additional functions related to whisker sensory processing. wMC receives whisker sensory inputs (Farkas et al., 1999; Kleinfeld et al., 2002; Ferezou et al., 2007; Chakrabarti et al., 2008). In one study, sensory representations in wMC better matched perceptual reports than sensory representations in S1 (Fassihi et al., 2017). wMC may also mediate sensory selection, by attenuating the propagation of distractor stimuli (Aruljothi et al., 2020). The current study proposes an additional function of sensory-motor transformation, potentially mediated by winner-take-all dynamics in converting a transient, sensory stimulus into a sustained, motor response (Zagha et al., 2015).

We recognize that it is highly unlikely that the sensory-motor transformation occurs exclusively within neocortex. In particular, we suspect that, in our task, interactions between neocortex and the striatum are essential for action selection and initiation (Frank, 2011). The question then is, what are the specific contributions of wMC to the transformation process? First, we propose that wMC contributes to sensory integration. An unexpected finding in this study is that sensory encoding is enhanced in

wMC compared to S1. This finding is based on a larger average neurometric d-prime of wMC neurons and fewer wMC neurons required for the neurometric d-prime to match the psychometric d-prime of the same behavioral sessions (Figure 3.4). This enhancement may occur by summing the spiking activity of random sets of S1 neurons, as simulated in our pooling analysis. Thus, a general function of wMC may be to integrate whisker sensory responses. The integrated sensory representations within wMC, rather than S1, may reflect the 'decision variables' that ultimately drive behavior (Gold and Shadlen, 2007).

Less clear, however, are the contributions of wMC to response initiation. Previous studies that have suppressed this region and neighboring regions during sensory-motor tasks have reported variable effects on hit rates, but significant increases in false alarm rates (Narayanan and Laubach, 2006; Huber et al., 2012; Zagha et al., 2015; Goard et al., 2016; Kamigaki and Dan, 2017) or non-significant trends towards increased false alarm rates (Le Merre et al., 2018; Mayrhofer et al., 2019). In contrast to wMC suppression, S1 suppression consistently results in reduced hit rates (O'Connor et al., 2010; Miyashita and Feldman, 2013; Zagha et al., 2015; Le Merre et al., 2018; Mayrhofer et al., 2019). Thus, for wMC, we note an apparent contradiction between our neural recording data and these causal studies. We report strong positive choice probability, suggesting that wMC *promotes* response initiation. Yet these causal studies suggest that wMC *suppresses* response initiation. Resolving these contradictory findings is an important focus of future research.

Figures and Legends

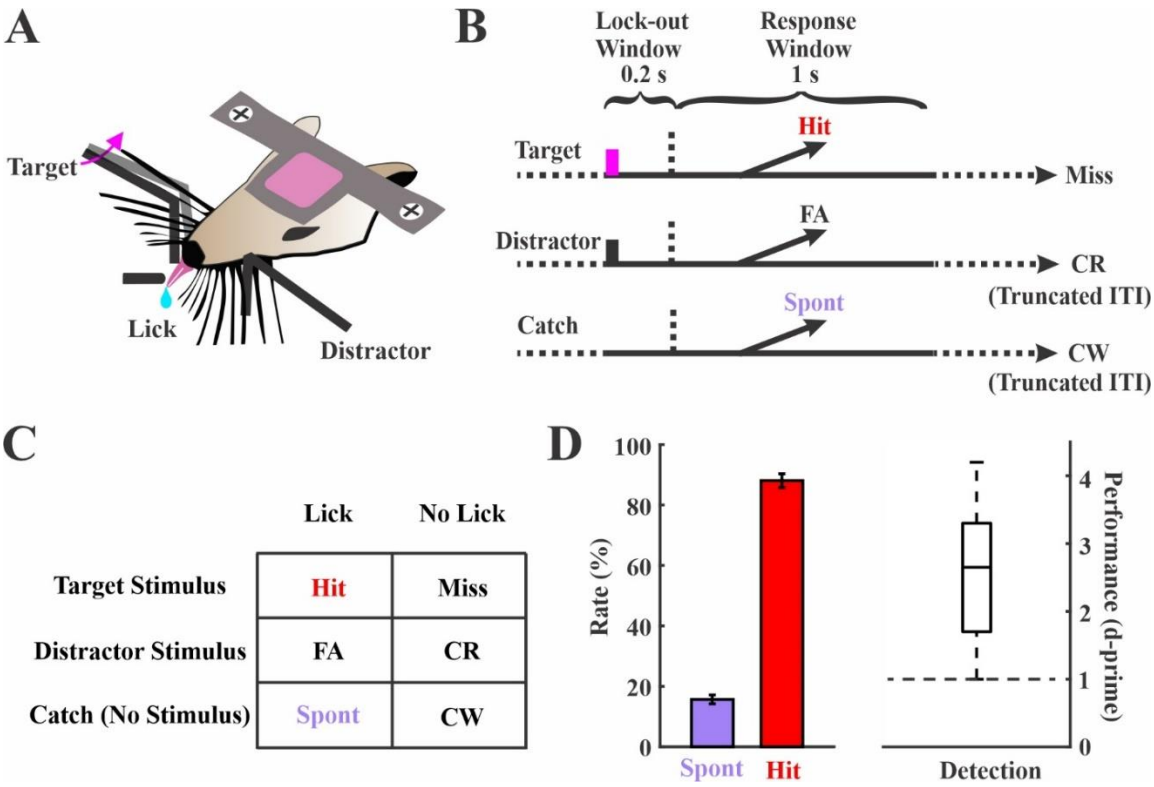

Figure 3.1. Sensory detection task structure and performance.

(**A**) A side-view of the task showing bilateral paddle placement and the central lickport. Head-fixed mice learned to respond to whisker deflections on one side (target) by licking the central lickport to obtain a fluid reward, and to ignore the deflections on the contralateral side (distractor) by withholding a licking response. (**B**) Trial structures. Each trial starts either with a target deflection (magenta bar, target), a distractor deflection (black bar, distractor) or no stimulus (catch). Responding during the lockout window (indicated by the horizontal dashed lines) aborts the current trial. (**C**) Possible outcomes based on trial type and response: Hit, Miss, False Alarm (FA), Correct Rejection (CR), Spontaneous Response (Spont) and Correct Withholding (CW) (**D**) Behavioral performance of all the 54 sessions that were included in this study collected from 19 expert mice. Boxplot for d-prime values shows min, max, median and 25th and 75th percentiles.

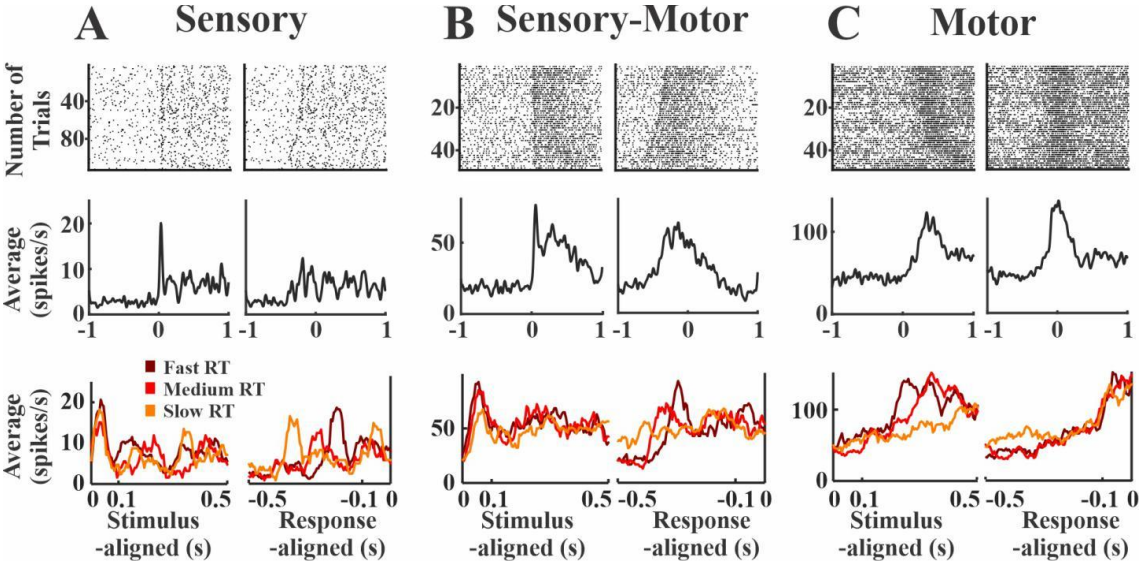

Figure 3.2. Examples of sensory, sensory-motor and motor single unit spiking activity.

(**A**) A sample sensory unit from S1. (Top) Raster plots show spiking activity for all trials within a session, aligned to the stimulus onset (left) and the mouse's reaction time (right). The trials in all raster plots are sorted according to the mouse's reaction time. (Middle) Average spiking rates across all trials. A transient peak immediately post-stimulus is observable with stimulus alignment (left) but not with response alignment (right). (Bottom) Trials were further grouped into slow, medium and fast reaction times. The sensory peak overlaps in all groups when aligned to the stimulus onset (left) but varies when aligned to the reaction time (right). (**B**) Same structure as panel [A], but for a sample sensory-motor unit in wMC. (Middle) A transient sensory peak is observable with stimulus alignment (left), along with a sustained activity prominent in the response alignment (right). (**C**) Same structure as panel [A] but for a sample motor unit in ALM. (Middle) Response alignment shows prominent ramping activity immediately prior to the reaction time. (Bottom) Unlike the sensory unit, the stimulus-aligned peak activity varies with reaction time (left) whereas the response-aligned peak activity overlaps for all reaction times (right).

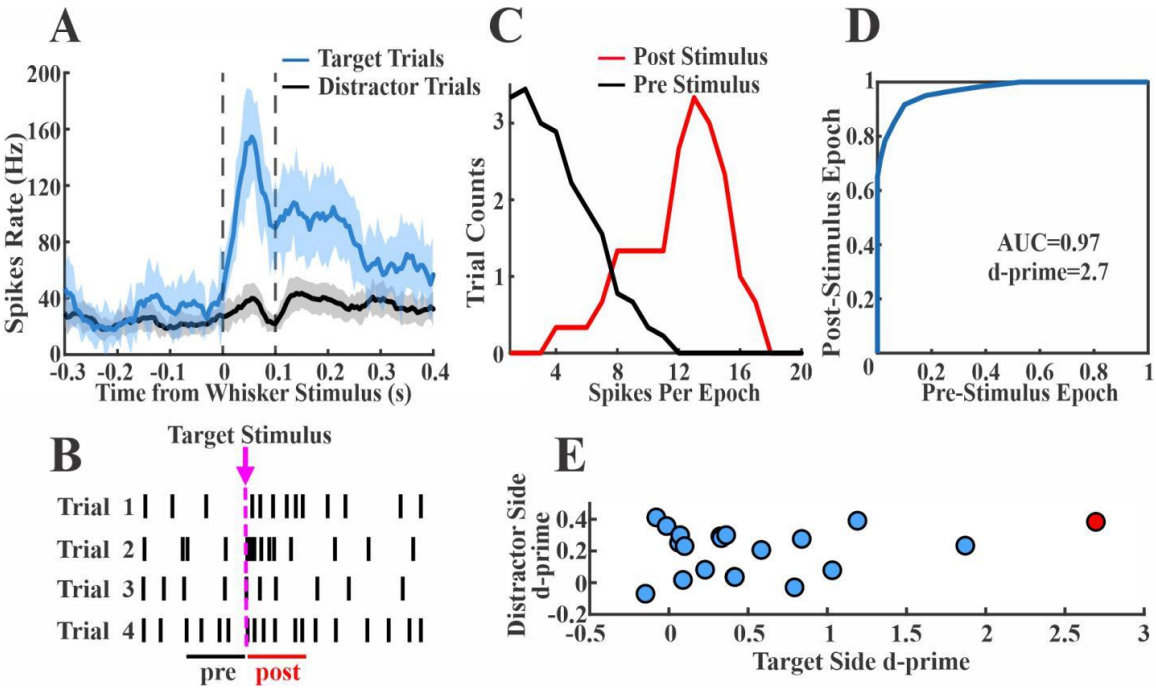

Figure 3.3. Quantification of target and distractor stimulus encoding.

(**A**) A sample S1 unit firing rate averaged across target (blue) and distractor (black) trials. This unit shows a prominent increase in spiking after target stimulus onset. Dashed lines reflect the post-stimulus window used for quantification of sensory encoding. (**B**) Illustration of the single trial pre-stimulus and post-stimulus windows. (**C**) Plot of pre-stimulus and post-stimulus spike count distributions from target trials of the example unit shown in [A]. (**D**) Plotting of the pre-stimulus and post-stimulus cumulative distribution functions to create a receiver operating characteristic curve for the example unit shown in [A]. The area under the curve is transformed into a neurometric d-prime value. The large response in [A] is reflected in the large separation of pre-stimulus and post-stimulus distributions in [C] and the highly convex ROC curve in [D]. (**E**) Scatter plot of all single units in this recording session, plotting target stimulus d-prime vs distractor stimulus d-prime values (example unit indicated in red). Note that target d-prime values are more positively skewed than distractor d-prime values.

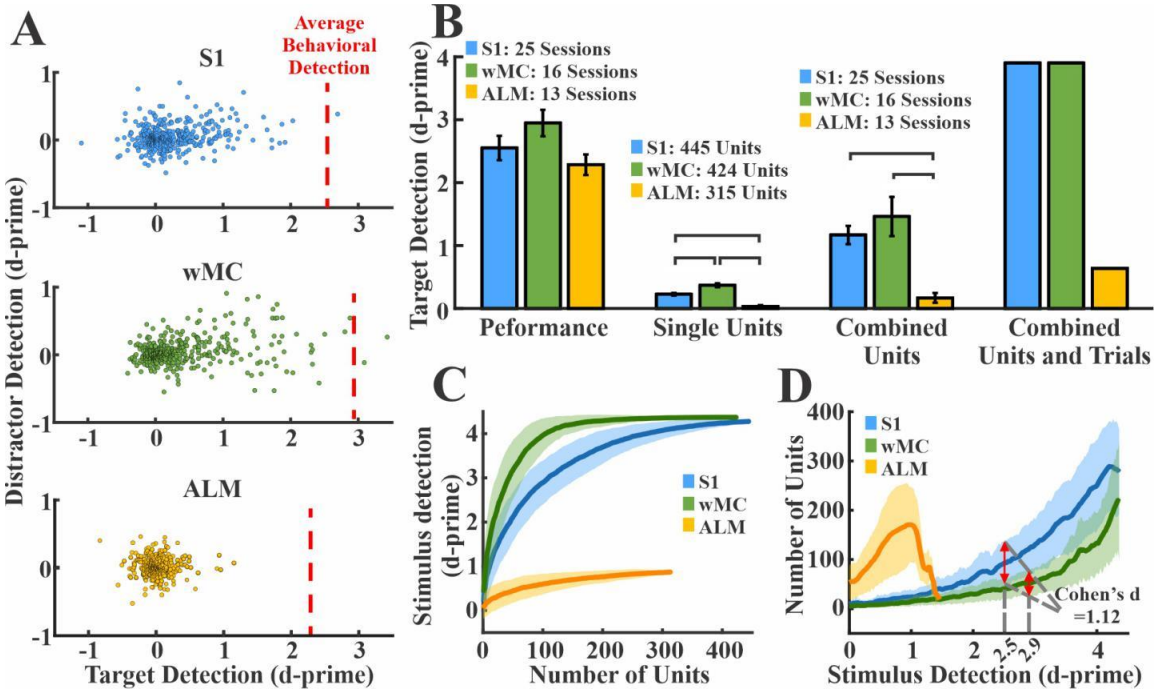

Figure 3.4 Sensory encoding and neurometric-psychometric comparisons across cortical regions.

(**A**) Distribution of single unit target and distractor d-prime values for all S1 (top, blue, n=445 units), wMC (middle, green, n=424 units), and ALM (bottom, yellow, n=315 units) units. The average behavioral detection performance (behavioral d-prime) during these recording sessions is depicted by the red dashed lines (S1=2.5, wMC=2.9 and ALM=2.2). Note that S1 and wMC target d-prime values are highly positively skewed along the x-axis (target detection) but ALM units are not. (**B**) Behavioral and neural d-prime measures across regions. Lines connecting columns within each set denote differences of statistical significance. Set 1, psychometric d-prime across all regions. Set 2, neurometric d-prime averaged across all single units within each region. Set 3, neurometric d-prime of summed spiking within each session averaged across all sessions. Set 4, neurometric d-prime of summed spiking of all units within each region. Combining units results in neurometric performance surpassing psychometric performance for S1 and wMC, but not ALM. (**C**) Randomly selected units were added sequentially to determine the resulting d-prime values of pooled neuronal activity. Shown are the distributions from 300 iterations of each region. Increasing the number of combined units increased d-prime values, with the fastest rate of rise in wMC. (**D**) Transformation of data in panel [C], depicting the size of the neural pools achieving the corresponding d-prime values. Red arrows overlaying S1 and wMC data indicate the number of units needed to match behavioral performance. Fewer wMC units were required to match behavioral performance compared to S1 and ALM. The traces and shades in panels [C] and [D] are the mean +/- SD.

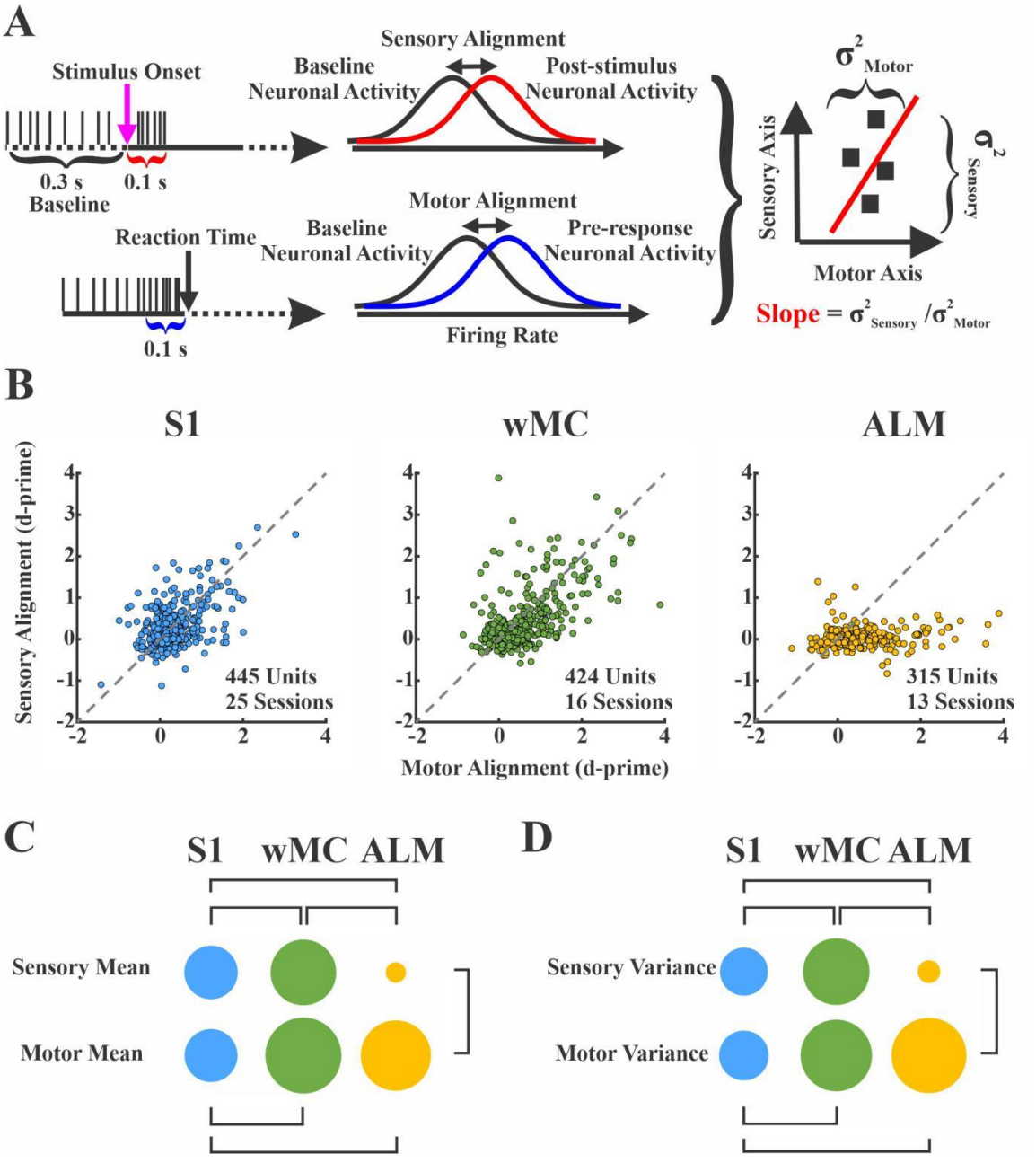
A
Stimulus Onset
0.3 s
Baseline
0.1 s
Sensory Alignment
Baseline
Neuronal Activity
Post-stimulus
Neuronal Activity
Reaction Time
0.1 s
Motor Alignment
Baseline
Neuronal Activity
Pre-response
Neuronal Activity
Firing Rate
σ² Motor
Sensory Axis
σ² Sensory
Motor Axis
Slope = σ² Sensory /σ² Motor
B
S1
wMC
ALM
Sensory Alignment (d-prime)
445 Units
25 Sessions
424 Units
16 Sessions
315 Units
13 Sessions
Motor Alignment (d-prime)
C
S1 wMC ALM
Sensory Mean
Motor Mean
D
S1 wMC ALM
Sensory Variance
Motor Variance

Figure 3.5 Sensory and motor representations on hit trials across cortical regions.

(**A**) A schematic showing how the sensory and motor alignments were calculated. 100 ms windows, after stimulus onset (magenta arrow) and preceding time reaction time (black arrow), were referenced as sensory (red) and motor (blue) epochs, respectively. Spike counts in these windows were compared to a pre-stimulus baseline (black). (Right) Sensory-aligned vs motor-aligned values were plotted for each unit. Population measurements of each region included the sensory and motor alignment mean, variance (sigma squared), and slope (sensory variance / motor variance). (**B**) Sensory and motor alignment for all of the recorded units of S1 (left, n=445), wMC (middle, n=424) and ALM (right, n=315). In each plot, the x-axis and the y-axis show motor and sensory alignment d-prime values, respectively. The dashed line indicates equal sensory and motor alignment. Note that S1 and wMC populations both show high variance along the unity line, whereas the ALM population shows high variance nearly exclusively along the motor-aligned axis. (**C**) Each circle's area is proportional to the mean value along the indicated axis. Statistically significant differences are indicated by bars (permutation statistics). Note the increase in both sensory and motor mean values from S1 to wMC and reduction in sensory mean value in ALM. (**D**) Similar to [C], with each circle's area proportional to the variance of d-prime along the indicated axis.

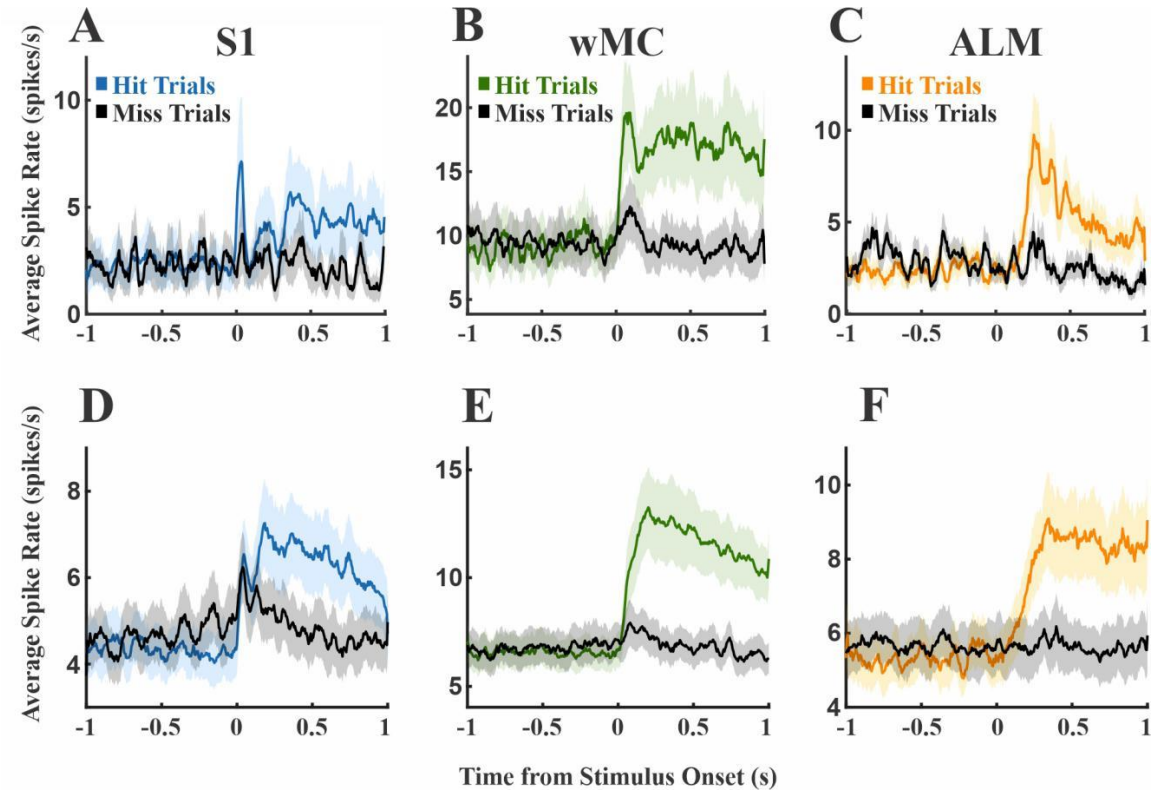

Figure 3.6. Comparison of spike rates on hit versus miss trials.

Colored plots denote hit trials, black plots denote miss trials. (**A**) An example S1 session, showing moderately higher hit-related spiking immediately post-stimulus and during the response window. (**B**) An example wMC session, showing robust increased and sustained hit-related spiking that emerges immediately post-stimulus. (**C**) An example ALM session, showing robust increased hit-related spiking that emerges late post-stimulus. (**D**,**E**,**F**) Average spike rates across all sessions for S1, wMC and ALM recordings, respectively.

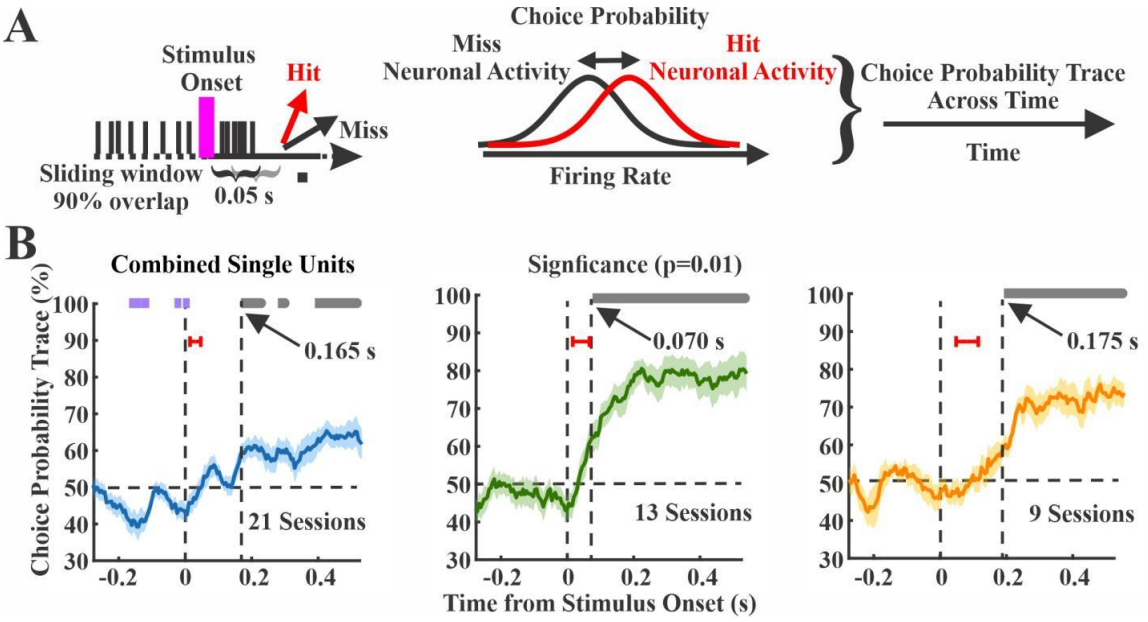

Figure 3.7. Choice probability within each cortical region.

(**A**) A schematic that shows the calculation of the choice probability. Choice probability was calculated by 50 ms sliding window, comparing spike counts on hit (red) versus miss (black) trials. (**B**) Choice probability as a function of time for each region, with overlapping hit and miss distributions at 50% (horizontal dashed line). Data are averages of recording sessions (left, S1, n=21 sessions; middle, wMC, n=13 sessions; right, ALM, n=9 sessions). Significant choice probability is indicated by bars above each plot, gray bars indicate significant positive choice probability (>50%) whereas purple bars indicate significant negative choice probability (<50%). Vertical dashed lines indicate latency to significant post-stimulus choice probability. Red bars indicate +/- 1 standard deviation of the sensory response latency for the same recording sessions. Left, S1 shows pre-stimulus negative choice probability and post-stimulus positive choice probability at a latency of 165 ms. Middle, wMC shows post-stimulus positive choice probability at a latency of 70 ms. Right, ALM shows post-stimulus positive choice probability at 175 ms.

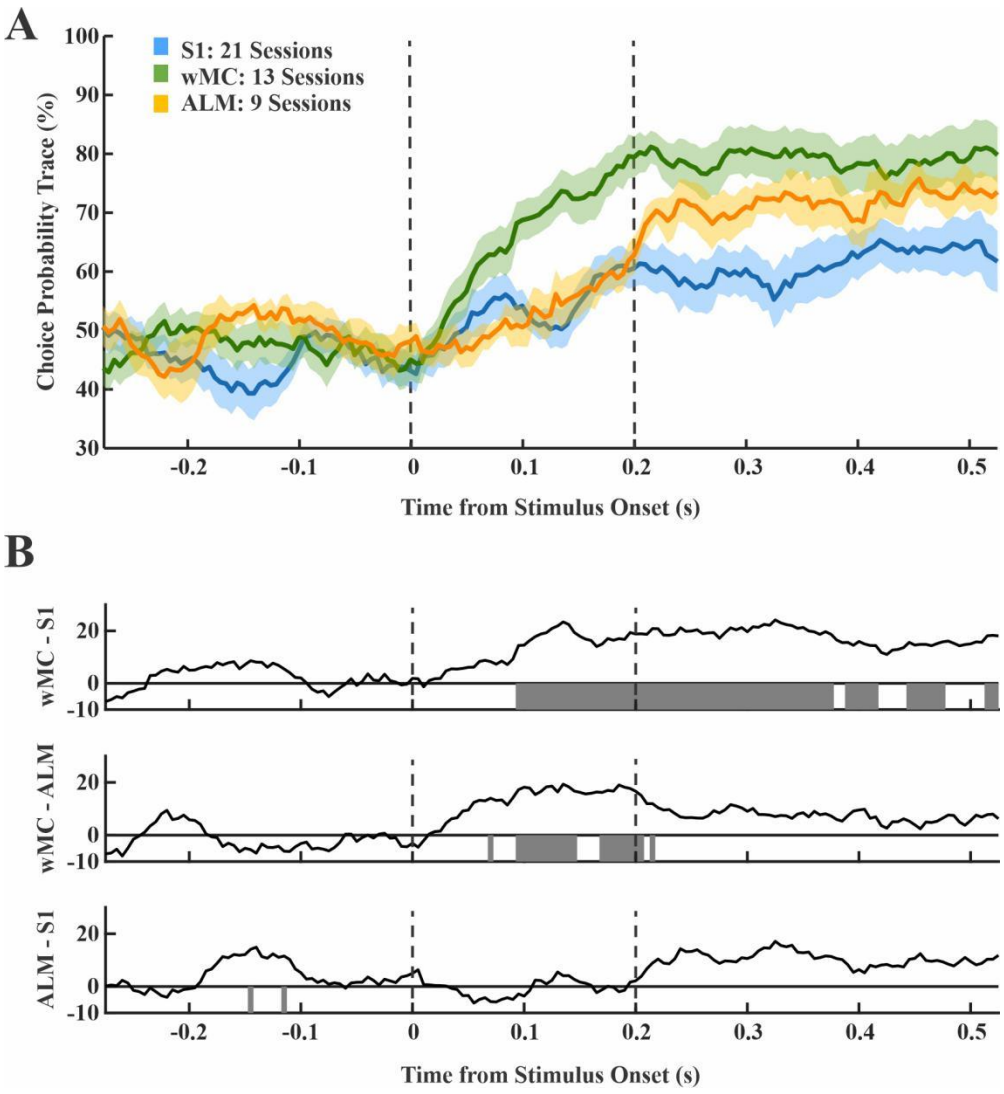

Figure 3.8. Comparison of choice probability between cortical regions.

(**A**) Overlap of traces from Figure 3.7B. Vertical bars indicate the lockout period, between stimulus onset and start of the response window. Note that wMC rises faster than S1 and ALM and remains elevated throughout the lockout period. (**B**) Inter-regional difference of choice probability and null hypothesis testing for comparisons at each time point. The gray bars denote statistical significance. Choice probability in wMC is greater than S1 and ALM during the lockout period.

References

Aruljothi K, Marrero K, Zhang Z, Zareian B, Zagha E (2020) Functional Localization of an Attenuating Filter within Cortex for a Selective Detection Task in Mice. J Neurosci 40:5443–5454.

Britten KH, Newsome WT, Shadlen MN, Celebrini S, Movshon JA (1996) A relationship between behavioral choice and the visual responses of neurons in macaque MT. Vis Neurosci 13:87–100.

Britten KH, Shadlen MN, Newsome WT, Movshon JA (1992) The analysis of visual motion: A comparison of neuronal and psychophysical performance. J Neurosci 12:4745–4765.

Carvell GE, Miller SA, Simons DJ (1996) The relationship of vibrissal motor cortex unit activity to whisking in the awake rat. Somatosens Mot Res 13:115–127.

Chakrabarti S, Zhang M, Alloway KD (2008) MI neuronal responses to peripheral whisker stimulation: relationship to neuronal activity in SI barrels and septa. J Neurophysiol 100:50–63.

Chen JL, Voigt FF, Javadzadeh M, Krueppel R, Helmchen F (2016) Long-range population dynamics of anatomically defined neocortical networks. Elife 5:e14679.

Chen TW, Li N, Daie K, Svoboda K (2017) A Map of Anticipatory Activity in Mouse Motor Cortex. Neuron 94:866–879.

Crapse TB, Basso MA (2015) Insights into decision making using choice probability. J Neurophysiol 114:3039–3049.

de Lafuente V, Romo R (2006) Neural correlate of subjective sensory experience gradually builds up across cortical areas. Proc Natl Acad Sci U S A 103:14266–14271.

Elithorn A, Lawrence C (1955) Central Inhibition—Some Refractory Observations. Q J Exp Psychol 7:116–127.

Farkas T, Kis ZS, Toldi J, Wolff J-R (1999) Activation of the primary motor cortex by somatosensory stimulation in adult rats is mediated mainly by associational connections from the somatosensory cortex. Neuroscience 90:353–361.

Fassihi A, Akrami A, Pulecchi F, Diamond ME (2017) Transformation of Perception from Sensory to Motor Cortex. Curr Biol 27:1585–1596.

Ferezou I, Haiss F, Gentet LJ, Aronoff R, Weber B, Petersen CCH (2007) Spatiotemporal Dynamics of Cortical Sensorimotor Integration in Behaving Mice. 56:907–923.

Frank MJ (2011) Computational models of motivated action selection in corticostriatal circuits. Curr Opin Neurobiol 21:381–386.

Goard MJ, Pho GN, Woodson J, Sur M (2016) Distinct roles of visual, parietal, and frontal motor cortices in memory-guided sensorimotor decisions. Elife 5:1–30.

Gold JI, Shadlen MN (2007) The Neural Basis of Decision Making. Annu Rev Neurosci 30:535–574.

Guo Z V., Li N, Huber D, Ophir E, Gutnisky D, Ting JT, Feng G, Svoboda K (2014) Flow of cortical activity underlying a tactile decision in mice. Neuron 81:179–194.

Hanes DP, Schall JD (1996) Neural control of voluntary movement initiation. Science (80-) 274:427–430.

Hill DN, Curtis JC, Moore JD, Kleinfeld D (2011) Primary motor cortex reports efferent control of vibrissa motion on multiple timescales. Neuron 72:344–356.

Huber D, Gutnisky DA, Peron S, O'Connor DH, Wiegert JS, Tian L, Oertner TG, Looger LL, Svoboda K (2012) Multiple dynamic representations in the motor cortex during sensorimotor learning. Nature 484:473–478.

Inagaki HK, Inagaki M, Romani S, Svoboda K (2018) Low-Dimensional and Monotonic Preparatory Activity in Mouse Anterior Lateral Motor Cortex. J Neurosci 38:4163–4185.

Kamigaki T, Dan Y (2017) Delay activity of specific prefrontal interneuron subtypes modulates memory-guided behavior. Nat Neurosci 20:854–863.

Kim JN, Shadlen MN (1999) Neural correlates of a decision in the dorsolateral prefrontal cortex of the macaque. Nat Neurosci 2:176–185.

Kleinfeld D, Berg RW, O'Connor SM (1999) Anatomical loops and their electrical dynamics in relation to whisking by rat. Somatosens Mot Res 16:69–88.

Kleinfeld D, Sachdev RNS, Merchant LM, Jarvis MR, Ebner FF (2002) Adaptive filtering of vibrissa input in motor cortex of rat. Neuron 34:1021–1034.

Kwon SE, Yang H, Minamisawa G, O'Connor DH (2016) Sensory and decision-related activity propagate in a cortical feedback loop during touch perception. Nat Neurosci 19:1243–1249.

Le Merre P, Esmaeili V, Charrière E, Galan K, Salin PA, Petersen CCH, Crochet S (2018) Reward-Based Learning Drives Rapid Sensory Signals in Medial Prefrontal Cortex and Dorsal Hippocampus Necessary for Goal-Directed Behavior. Neuron 97:83–91.

Li N, Chen TW, Guo Z V., Gerfen CR, Svoboda K (2015) A motor cortex circuit for motor planning and movement. Nature 519:51–56.

Matyas F, Sreenivasan V, Marbach F, Wacongne C, Barsy B, Mateo C, Aronoff R, Petersen CCH (2010) Motor control by sensory cortex. Science (80-) 330:1240–1243.

Mayrhofer JM, El-Boustani S, Foustoukos G, Auffret M, Tamura K, Petersen CCH (2019) Distinct Contributions of Whisker Sensory Cortex and Tongue-Jaw Motor Cortex in a Goal-Directed Sensorimotor Transformation. Neuron 103:1034–1043.

Miyashita T, Feldman DE (2013) Behavioral detection of passive whisker stimuli requires somatosensory cortex. Cereb Cortex 23:1655–1662.

Mountcastle VB, Lynch JC, Georgopoulos A, Sakata H, Acuna C (1974) Posterior parietal association cortex of the monkey: command functions for operations within extrapersonal space. J Neurophysiol 38:871–908.

Narayanan NS, Laubach M (2006) Top-Down Control of Motor Cortex Ensembles by Dorsomedial Prefrontal Cortex. Neuron 52:921–931.

O'Connor DH, Peron SP, Huber D, Svoboda K (2010) Neural activity in barrel cortex underlying vibrissa-based object localization in mice. Neuron 67:1048–1061.

Pho GN, Goard MJ, Woodson J, Crawford B, Sur M (2018) Task-dependent representations of stimulus and choice in mouse parietal cortex. Nat Commun 9:1–16.

Roitman JD, Shadlen MN (2002) Response of neurons in the lateral intraparietal area during a combined visual discrimination reaction time task. J Neurosci 22:9475–9489.

Romo R, Hernández A, Zainos A, Lemus L, Brody CD (2002) Neuronal correlates of decision- making in secondary somatosensory cortex. 5:1217–1225.

Sachidhanandam S, Sreenivasan V, Kyriakatos A, Kremer Y, Petersen CCH (2013) Membrane potential correlates of sensory perception in mouse barrel cortex. Nat Neurosci 16:1671–1677.

Salkoff DB, Zagha E, McCarthy E, McCormick DA (2020) Movement and Performance Explain Widespread Cortical Activity in a Visual Detection Task. Cereb cortex 30:421–437.

Schmitzer-Torbert N 1, Jackson J, Henze D, Harris K, Redish AD (2005) Quantitative measures of cluster quality for use in extracellular recordings. Neuroscience 131:1–11.

Shadlen MN, Newsome WT (2001) Neural basis of a perceptual decision in the parietal cortex (area LIP) of the rhesus monkey. J Neurophysiol 86:1916–1936.

Siegel M, Buschman TJ, Miller EK (2015) Cortical information flow during flexible sensorimotor decisions. Science (80-) 348:1352–1355.

Simpson AJ, Fitter MJ (1973) What is the best index of detectability? Psychol Bull 80:481.

Smith JB, Alloway KD (2013) Rat whisker motor cortex is subdivided into sensory-input and motor-output areas. Front Neural Circuits 7:1–15.

Stüttgen MC, Schwarz C (2008) Psychophysical and neurometric detection performance under stimulus uncertainty. Nat Neurosci 11:1091–1099.

Sul JH, Jo S, Lee D, Jung MW (2011) Role of rodent secondary motor cortex in value-based action selection. Nat Neurosci 14:1202–1210.

Swets JA (1961) Detection theory and psychophysics: a review. Psychometrika 26:49–63.

Wang Q, Millard DC, Zheng HJV, Stanley GB (2012) Voltage-sensitive dye imaging reveals improved topographic activation of cortex in response to manipulation of thalamic microstimulation parameters. J Neural Eng 9:26008.

Yang H, Kwon SE, Severson KS, O'Connor DH (2015) Origins of choice-related activity in mouse somatosensory cortex. Nat Neurosci 19:127–134.

Zagha E, Ge X, McCormick DA (2015) Competing Neural Ensembles in Motor Cortex Gate Goal-Directed Motor Output. Neuron 88:565–577.

Chapter 4 : Involvement of the Striatum in a Selective Detection Task: A Bottleneck

We investigated wMC in the previous chapter and realized that, among other regions recorded in the cortex, this region could be a site of sensory-motor transformation. wMC and DLS are major target regions for outputs of S1 (Mao et al., 2011). DLS is a region within the basal ganglia network. Classical models of the basal ganglia propose that this area is involved in action selection (Redgrave et al., 1999). However, we did not know if or how involved DLS is in the task, especially in a causal way. Similarly, we did not know the causal involvement of wMC solely based on the recording that we did in the previous study. Researchers suggest that the motor cortex may be dispensable in expert mice (Kawai et al., 2015). So, we were wondering how and whether these regions are important in the ongoing performance for our task in the first place.

I contributed to this paper by performing in vivo electrophysiology from wMC and DLS. The combination of recording and lesion experiments we introduced here, could be used to find the order of activation and necessity of multiple brain regions in a network, in a behavioral task. In this paper, we showed that the striatum is an important bottleneck of sensory-motor transformation and that the order of activation of regions is as follows: wMC → DLS.

Dorsolateral Striatum, not Motor Cortex, is a Bottleneck for Responding to Task-Relevant Stimuli in a Learned Whisker Detection Task in Mice

Abbreviated Title: Striatum is a Bottleneck for Stimulus Detection

Authors: Behzad Zareian[1], Angelina Lam[2], Edward Zagha[1,2,3]

[1]Department of Psychology, [2] Division of Biomedical Sciences, School of Medicine, [3]Neuroscience Graduate Program, University of California Riverside, 900 University Avenue, Riverside CA 92521 USA

Correspondence to: edward.zagha@ucr.edu

Number of pages: 44

Number of figures: 9

Number of tables: 2

Number of words in abstract (160), introduction (634), discussion (835)

Acknowledgements

This work was support by the National Institutes of Health Grant R01NS107599 (to E.Z.). We thank Trevor Zimmerman-Thompson and Emaan Kaur for helping with training of mice. We are also thankful to Zhaoran Zhang, Krista Marrero and Krithiga Aruljothi for their feedback in all stages of the project.

Conflict of Interest

The authors declare no competing financial interests.

Abstract

A learned sensory-motor behavior engages multiple brain regions, including the neocortex and the basal ganglia. How a target stimulus is selected by these regions remains poorly understood. Here, we performed electrophysiological recordings and pharmacological inactivations of motor cortex and dorsolateral striatum to determine the representations within and functions of each region during performance in a selective whisker detection task in male and female mice. From the recording experiments, peak pre-response activity and significant choice probability emerged in the motor cortex before the dorsolateral striatum, suggesting a sensory-to-motor transformation in which the striatum is downstream of motor cortex. We performed pharmacological inactivation studies to determine the necessity of these brain regions for this task. We found that suppressing the dorsolateral striatum, but not motor cortex, severely disrupts responding to task-relevant stimuli, without disrupting the ability to respond. Together these data support the dorsolateral striatum, and not motor cortex, as an essential node in the sensory-to-motor transformation of this whisker detection task.

Significance Statement

We learn to do various sensory-motor behavior in our daily life, such as clicking on a journal article that looks interesting, among other articles. There are parts of our brain that are active when we do these learned behaviors, such as motor cortex and basal ganglia. But what is the order of activation of these regions? Which of them is necessary for responding to task-relevant sensory information? To answer these questions, we trained mice in a whisker-based target selection task and used recording of neural activity and inactivation of subregions within motor cortex and basal ganglia in expert mice. Our findings show dorsolateral striatum, a region within basal ganglia, is a bottleneck for performing task-related sensory-to-motor transformation.

Introduction

Goal-directed behavior requires the ability to selectively respond to target sensory stimuli (selection), while inhibiting responses to extraneous or distractor stimuli. In simple Go/NoGo tasks, sensory selection involves transforming sensory responses into motor commands. Neuronal recording studies have demonstrated full sensory-to-motor transformations unfolding across the neocortex, with motor planning and motor command signals present most robustly in motor cortices (de Lafuente & Romo, 2006; Esmaeili et al., 2021; Finkelstein et al., 2021; Hanes & Schall, 1996; Inagaki et al., 2019; Li et al., 2015; Li et al., 2016; Moran & Desimone, 1985; Salinas & Romo, 1998; Siegel et al., 2015). These studies provided strong motivation for considering the neocortex as the primary structure implementing goal-directed, sensory-to-motor transformations (Figure 4.1C). Simultaneously, anatomical, physiological, and lesioning studies of the basal ganglia identified these subcortical structures as essential for implementing action selection and initiation (Figure 4.1D) (Alexander & Crutcher, 1990; Bergstrom et al., 2020; Bergstrom et al., 2018; Graybiel et al., 1994; Grillner et al., 2005; Jin & Costa, 2010; Stephenson-Jones et al., 2011; Yin et al., 2004). Motor cortex and dorsolateral striatum are heavily interconnected, as determined by both anatomical and functional studies (Foster et al., 2021; Frank et al., 2001; Gordon et al., 2022; Hintiryan et al., 2016; Hunnicutt et al., 2016; Kupferschmidt et al., 2017; Lee et al., 2019; McGeorge & Faull, 1987; Peters et al., 2021; Saunders et al., 2015), and therefore sensory selection may be mediated by the coordinated activities of both regions. Traditional models of cortico-striatal coordination propose that motor plans are generated in motor cortex and then

selected in the basal ganglia. The output of this striatal selection is propagated via the thalamus back to motor cortex, which ultimately sends out the motor command (Figure 4.1E) (Hoover & Strick, 1999; Middleton & Strick, 2000; Redgrave et al., 1999). And yet, the basal ganglia project to multiple regions besides the neocortex which may also trigger motor commands (Figure 4.1F) (Guo et al., 2017; Mink, 1996; Utter & Basso, 2008; Yin & Knowlton, 2006). Revealing the functional organizations of the motor cortex and the basal ganglia requires conducting representational and causal studies from both structures in subjects performing the same behavioral task (Antzoulatos & Miller, 2011; Brockett et al., 2022; Clarke et al., 2008; Kupferschmidt et al., 2017; Muhammad et al., 2006; Pasupathy & Miller, 2005; Peters et al., 2021; Pimentel-Farfan et al., 2022)

The mouse whisker system is an ideal model system to test this functional organization, due to its simplified and well-characterized neural anatomy. Whisker stimulus responses propagate to the contralateral whisker representation of primary somatosensory cortex (S1). In turn, S1 projects directly and robustly to sub-regions of both the motor cortex (MC) and the dorsolateral striatum (DLS) (Mao et al., 2011). This study focuses on these sub-regions of MC and DLS, as possible signaling pathways for sensory selection. Prior representational and causal studies implicate the involvement of both MC and DLS in whisker detection/discrimination tasks (Aruljothi et al., 2020; Guo et al., 2014; Hong et al., 2018; Lee et al., 2019; Li et al., 2015; Li et al., 2016; Sippy et al., 2015; Zagha et al., 2015; Zareian et al., 2021). And yet, the functional organizations between these regions in the context of whisker sensory selection remains poorly understood. In this study, we directly compared the representational and functional

properties of MC and DLS in a Go/NoGo selective whisker detection task (Figure 4.1). We previously demonstrated robust sensory, motor, and choice signals in whisker-related MC, identifying this region as the most likely site of sensory-motor transformations within dorsal neocortex for this task (Aruljothi et al., 2020; Zareian et al., 2021). In the current study, our data support a functional organization in which DLS is downstream of MC and is an essential bottleneck for transforming whisker stimuli into motor commands.

Materials and Methods

Animals. Experiments performed in this study were approved by the Institutional Animal Care and Use Committee of University of California, Riverside. Male and female mice of two strains were used for the experiments: wild type (C57BL/6J) and Thy1-ChR2 mice (all purchased from The Jackson Laboratory or bred in our own colony). Data from mice of each sex and strain were combined, and the transgenic feature was not exploited in these studies. All mice were housed on a 12h light/12h dark cycle. Food was always accessible to mice outside of the behavioral training sessions.

Surgery. All experiments were performed on head-fixed mice. To attach the headpost to the skull, the mice were first anesthetized with a mixture of ketamine (100 mg/kg), xylazine (10 mg/kg), and isoflurane (1-2%) throughout the surgery. They were additionally administered meloxicam (5 mg/kg) and enrofloxacin (5 mg/kg) at the day of the surgery and for two days post-surgery. A 10 mm × 10 mm part of scalp was resected.

A stainless steel headpost with length of 3 cm and a weight of 1.5 grams with a central window of 8 mm × 8mm, was attached to the skull using cyanoacrylate glue. The 8 mm × 8 mm exposed window was sealed with Kwik-sil. After the surgery, the mice recovered on a heating pad. Behavioral experiments were started a minimum of 3 days after recovery from surgery. At the day of recording or inactivation, small craniotomies (~0.5 mm) were made under isoflurane anesthesia to access the relevant cortical and subcortical regions (see below).

Training. We trained mice in a selective detection task, which we have characterized in previous studies (Aruljothi et al., 2020; Marrero et al., 2021; Zareian et al., 2021). The mice were head-fixed in a custom-made setup. Piezo-controlled paddles were placed symmetrically within bilateral whisker fields contacting multiple whiskers. Target and distractor whisker fields were assigned at the beginning of training (target as the right whisker field) and remained constant throughout. Sensory stimuli consisted of small, rapid deflections of either whisker field. The deflections ranged from 0.01-0.2 seconds (s) in duration with a velocity of 10 mm/s, always equal for target and distractor stimuli. For most of the training sessions, two different stimulus amplitudes were used, one (large) near the saturation of the mouse's psychometric range and the other (small) near the midpoint. Mice reported stimulus detection by licking a central lick port. A lockout of 0.2 s was imposed between stimulus onset and response window, and mice were punished with a timeout for responding during this delay. Following 5-9 s inter-trial intervals, mice received either target, distractor, or catch (no stimulus) trials. All licking outside the post-

target response window were punished by time-out (resetting the inter-trial interval). Water rewards for responding during the post-target response window were delivered from the same lick port used to report stimulus detection. Mice were water restricted throughout the training period, with the goal of receiving all water during behavioral trainings. Supplemental water was given in the home cage if weights fell below 85% of initial weights. Behavioral training was implemented using custom MATLAB scripts and Arduino Uno boards to trigger task stimuli and report licking responses. For further details of the behavioral training and training stages, see (Aruljothi et al., 2020).

Mice were considered expert in the task once they achieved a target-distractor discrimination d-prime > 1, for three consecutive days (d-prime=*norminv* (Hit rate)-*norminv* (False alarm rate), in which *norminv* is the inverse of the standard normal cumulative distribution value). All recording and inactivation experiments were performed in animals that had reached expert performance. For the electrophysiological recording sessions, performance values (discrimination d-prime) were as follows: target-aligned MC: 2.7 +/- 0.6, n=11, distractor-aligned MC: 2.5 +/- 0.6, n=19, target-aligned Str: 2.3 +/- 0.6, n=10, distractor-aligned Str: 2.3 +/- 0.7, n=11 (mean +/- STD). Performance of the mice during muscimol inactivation are reported in the Results, since behavioral performance was the dependent variable under examination.

Electrophysiological Recordings. 20 mice were used for electrophysiological recording experiments (see Table 1 for the number of sessions used in each analysis). Recordings were conducted following at least 20 minutes after recovery from isoflurane anesthesia.

Recovery was assessed based on normal mouse behavior within their home cage and high engagement during the first few minutes of the task. For MC and DLS recordings, Neuronexus laminar probes with 16 sites and 100 µm spacing were used (A1x16-5mm-100-177-OA16LP or A1x16-5mm-100-177-A16). For each recording, the probe was advanced slowly in the brain using hydraulic Narishige micromanipulators. Electrophysiology data were acquired using Neuralynx recording system and Cheetah viewer software. The data were acquired at 32 kHz, then subsequently filtered at 600 to 6000 Hz for spike analyses.

Craniotomies for MC recordings were centered on 1 +/- 0.5 mm lateral, 1 +/- 0.5 mm anterior to bregma. These MC coordinates were chosen to target the S1 projection zone, as in our previous studies (Zareian et al., 2021). The probe was advanced until the last site was barely visible at the surface (16 sites spanning 1.5 mm within cortex and below). At these coordinates, the thickness of layer 1, 2/3 and 5A of MC collectively span the superficial (dorsal) 500-600 µm (Hooks et al., 2013) (also see Figure 4.2C). Therefore, we considered recording sites within this range as 'superficial MC' and the more ventral recording sites as 'deep MC.' DLS coordinates were as follows [from bregma]: 2.5 +/-0.5 mm lateral, 0.7 +/- 0.4 mm posterior (also see Figure 4.2F). The probe was advanced deep inside the DLS (distal tip 2300-2500 µm below the pial surface). The coordinates were initially chosen based on Allen Brain Institute Mouse Connectivity atlas, selecting the region within DLS receiving the highest density inputs from S1.

Muscimol Inactivation. Injections of 2 mM muscimol in normal saline were performed using the Nanoject III Programmable Nanoliter Injector from Drummond Scientific Company fitted with a borosilicate glass micropipette. The same surface coordinates were used for muscimol injections as described above for electrophysiological recordings. For MC injections, 250 nL of muscimol was injected at a rate of 1-3 nL/s at 1 mm deep (from the pial surface) and another 250 nL was administered at 0.5 mm deep, for a total of 500 nL, to target both superficial and deep layers of MC. Based on previous experience using nearly identical protocols, this application causes inactivation of cortex approximately 1 mm in diameter as observed from the dorsal surface [see Figure 4D in (Salkoff et al., 2020)]. For DLS injections, a single bolus of 250 nL of 2 mM muscimol was injected at a rate of 1-3 nL/s at 1.7 mm deep. Based on the descriptions above, we expect this protocol to inactivate a volume of the striatum less than 1 mm in diameter.

For muscimol inactivation studies, expertly performing mice were assigned to alternating control performance days, without muscimol exposure, and experimental performance days, with muscimol inactivation. Sites for muscimol inactivation were randomized for each mouse, such that the order of inactivation varied (both within and across mice). For daily behavioral testing (also see Figure 4.7A), mice were first placed in a classical conditioning version of our task (see (Aruljothi et al., 2020)) for 2 minutes to ensure licking responses were intact when presented with water reward cued by the opening of a solenoid. Then mice were tested in the full selective detection task for 1 hour. After 1 hour of testing if mice collected fewer than 10 rewards, they were considered non-performers. 10 rewards is 2-3 standard deviations below the number of

rewards achieved by non-injected control mice within the same duration (62 +/- 21 rewards [mean +/- SD]). Non-performing mice were placed back in the classical conditioning task for 15 minutes to again assess for licking to solenoid-cued water rewards. If mice were still performing the full selective detection task after 1 hour, they were permitted to perform that task until unmotivated (as determined by time since previous reward greater than 10 minutes). The threshold for consideration as 'performing' in the classical conditioning task was responding to >50% of rewards, in either testing phase.

Histology. Verifications of silicone probe and muscimol injection sites were performed on wildtype C57BL/6J mice not previously utilized for muscimol inactivation experiments. A borosilicate glass micropipette was inserted into MC or DLS using similar protocols as for muscimol inactivation studies. One hour after injection, mice brains were processed to visualize the pipette tract. Mice were sacrificed using Euthasol euthanasia solution and transcardially perfused with 20-40 mL of 1X Phosphate-Buffered Saline solution (PBS) followed by 20-40 mL of 4% Paraformaldehyde (PFA) in 1X PBS before the brain was dissected and stored in 4% PFA overnight. The following day, brains were rinsed with 1X PBS three times, then embedded in a 3% agarose in 1X PBS solution. 120 µM slices were collected using a Leica VT1000 S vibrating blade microtome and mounted onto glass slides using glycerol and a coverslip. 2X images were collected using a Keyence BZ-X710 microscope under brightfield illumination (Figure 4.2A and D).

Comparison tracing studies (Figure 4.2B and E) are from the Allen Brain Mouse Connectivity Atlas, experiment 126907302. For the schematics depicting approximate recording sites (Figure 4.2C and F), we traced the outlines of slices from The Mouse Brain in Stereotaxic Coordinates (-1.06 and 0.98 mm from Bregma for DLS and MC, respectively) (Paxinos & Franklin, 2019). We compared the cortical thickness from the atlas to our functional estimates based on white matter location and determined a scale factor of 17%. Accordingly, a 17% reduction was applied to the mapping of the recording sites onto the atlas schematics.

Quantification and Statistical Analysis. Analyses were performed using custom MATLAB scripts or SPSS and displayed using Corel Draw. For all statistical analyses, we used alpha=0.05 as significant threshold, unless otherwise stated. Data are presented as mean +/- standard error of the mean, unless otherwise stated. Analyses focused on large amplitude target and distractor stimuli.

Multiunit Activity (MUA) Analyses. Behavioral and combined behavioral-recording sessions were truncated to include a single engaged period (a continuous bout of at least 10 minutes of task performance with no gaps in responding (licking) greater than 60 seconds). MUA was identified as negative-going threshold crossings over 3×standard deviation of the band-pass filtered voltage fluctuations throughout that session.

For MC recordings we used linear multielectrode arrays with 100 µm spacing. Channels 1 to 7 (spanning the superficial 600 µm) were considered as superficial layers.

The remaining channels (8 to 16) were considered as deep layers. For DLS data analyses, we first determined the location of the white matter, as the site within the middle 5-12 sites with the minimum average spiking. The recording sites below that were considered as putative DLS sites.

Spike counts were binned in 5 ms bins throughout each recording session and combined as needed for larger window analyses. We calculated sensory detection and choice probability values using signal detection theory (Zareian et al., 2021). Briefly, the sensory detection was calculated by considering the area under receiver operating characteristic (ROC) curve constructed from plotting cumulative distributions of spiking of a post-stimulus window against pre-stimulus baseline activity. For baseline activity, three consecutive epochs with the same size as the post-stimulus window were considered. Post-stimulus window sizes were either 5 ms bins for continuous d-prime traces (Figure 4.4 A-D) or a single 100 ms window immediately post-stimulus (Figure 4.4 E and F). For latency to reaction time analyses, a window of 1 s before the reaction time was considered as baseline.

Similarly, choice probability was calculated as the area under the ROC curve constructed from plotting the cumulative distributions of spiking activity on hit trials against miss trials. The choice probability traces were calculated from 50 ms sliding windows with 90% overlap. For statistical comparisons, the session choice probability values were compared to chance level (50%). For choice probability analysis, sufficient hit and miss trials were assessed based on previously described criteria (Zareian et al.,

2021). Choice probability latency was determined as the time from stimulus onset to rise above 60% choice probability.

Muscimol Inactivation Analyses. For the muscimol inactivation experiments, we obtained task engagement time, hit rate, false alarm rate, d-prime, and criterion using a 1-hour time window of selective detection task performance (Figures 4.7, 4.8). Data were averaged across all sessions and all mice for each set of analyses (from n=7 total mice, see Table 2 for the number of sessions used). Task engagement times (Figure 4.7D) were calculated as the sum of all times mice were active during the task, as defined by no lapse in licking greater than 1 minute.

Statistical Analyses. For statistical comparisons of recording experiments, t-test or ANOVA were used. ANOVA statistics was calculated using either SPSS or MATLAB. We considered region and hemisphere effects by running 2-way ANOVA tests; performance measures were grouped regionally (main effect of MC vs. DLS regions regardless of the hemisphere) and grouped by hemisphere (main effect of target-aligned vs. distractor-aligned regions regardless of brain regions). 'Target-aligned' or 'distractor-aligned' refers to the hemisphere contralateral to the whisker field that receives target or distractor paddle deflections, respectively. Interaction effects were also considered (regional × hemisphere). For pairwise comparisons, Tukey-Kramer post-hoc multiple comparison test using *multcompare* function in MATLAB were conducted between pair of conditions (tMC, tDLS, dMC, dDLS). For muscimol inactivation studies, we

additionally compared overall performance rates using Chi-square tests and compared inactivation sessions to non-injected control sessions using unpaired t-tests.

Results

Behavioral Task, Model Predictions, and Regions of Interest. We trained mice in a head-fixed, whisker-based selective detection task (Aruljothi et al., 2020; Marrero et al., 2021; Zareian et al., 2021). In this task, mice learned to respond (lick) to small, transient whisker deflections within one whisker field (target) and to ignore identical whisker deflections in the opposite whisker field (distractor) (Figure 4.1A). Due to the lateralization of the somatosensory system, this task configuration establishes "target-aligned" and "distractor-aligned" cortical and striatal fields that are symmetric across midline and contralateral to the deflected whiskers. In the task structure, we impose a 200 ms lockout between stimulus onset and response window, and mice learn to withhold responding across this delay (Figure 4.1B). Mice are considered expert in this task once they achieve a separation (d-prime) between hit rate (response to target) and false alarm rate (response to distractor), greater than 1, for three consecutive days (for training details, see Methods and (Aruljothi et al., 2020).

Electrophysiological recording and muscimol inactivation studies were conducted in expert mice, while they were performing the selective detection task. These physiological studies focused on two major outputs of primary somatosensory cortex (S1): the S1-projection sub-regions of both the motor cortex (MC) and the dorsolateral

striatum (DLS) (Mao et al., 2011). Figure 4.2 depicts examples of MC and DLS targeting, relative to S1-projections.

We recognize four possible functional organizations of these S1-output pathways. If sensory selection is primarily mediated through motor cortex (Figure 4.1C), we would expect greater sensory and motor activities in MC than DLS, and for inactivations of MC to cause larger impairments of task performance. If selection is primarily mediated through the basal ganglia (Figure 4.1D), we would expect DLS to show greater sensory and motor activities and larger performance impairments from inactivations. From the cortical bottleneck model (Figure 4.1E), we would expect robust sensory and motor activities in both MC and DLS, yet inactivating MC to have the larger effects on task performance. From the basal ganglia bottleneck model (Figure 4.1F), we would expect robust sensory and motor activities in both regions, yet inactivating DLS to have the larger effects on task performance. Subsequent experiments and analyses were designed to distinguish between these models.

Robust Sensory-Related and Motor-Related Spiking Activities in MC and DLS. We performed laminar electrophysiological recordings and compared the multiunit activity (MUA) signals from MC and DLS. For each recording session, we identified the site with the largest sensory encoding (neurometric d-prime, see Methods for details) and used the activity at that site for all subsequent analyses. For MC, the laminar electrode spanned all layers, and sensory encoding was invariable largest in deep layers (1023 +/- 37 μm, n=30 sessions, n=11 sessions in target-aligned MC and n=19 sessions in distractor-aligned

MC). For DLS, sensory encoding was largest 2136 +/- 55 μm from the cortical surface and 452 +/- 53 μm below the putative white matter (n=21 sessions, n=10 sessions in target-aligned DLS and n=11 sessions in distractor-aligned DLS). The approximate locations of these recording sites are shown in Figures 4.2C and 4.2F.

In Figure 4.3, we display post-stimulus and pre-response activities for target stimuli in target-aligned MC (tMC) and in target-aligned DLS (tDLS). In both regions, MUA appeared at short latency after stimulus onset (Figure 4.3A, B left columns). We consider this activity to be 'sensory' because it occurs regardless of trial outcome (Figure 4.3C, F) and is time-locked to stimulus onset (within the first 100 ms) regardless of the reaction time (Figure 4.3D, G). We do note differences in activity levels on hit vs miss trials (both pre-stimulus and post-stimulus) (Figure 4.3C, F), which we analyze further below. To view pre-response activity, we aligned the spiking on each trial to the reaction time (Figure 4.3A, B right columns). Both tMC and tDLS displayed elevated activity before the response. However, pre-response ramping activity was more evident in tDLS than tMC. This was also appreciated by clustering trials according to reaction time (Figure 4.3E, H), demonstrating more pronounced transient activations in tDLS within 100 ms before the response (Figure 4.3H), potentially reflecting motor response triggering. These qualitative observations are followed up with more quantitative analyses below. However, they suggest that both MC and DLS contain robust sensory-related and motor-related activity (consistent with models in Figure 4.1E, F), with DLS more robustly signaling response triggering.

Lateralized Sensory Encoding in MC and DLS. In the subsequent analyses, we present data from four brain regions: target-aligned MC (tMC), target-aligned DLS (tDLS), distractor-aligned MC (dMC), and distractor-aligned DLS (dDLS). As such, our main quantification approach follows a 2x2 ANOVA design, assessing for main effects of region (MC vs DLS) or hemisphere (target-aligned vs distractor-aligned).

To quantify sensory encoding in MC and DLS, we computed the neurometric d-prime for each recording session (Figure 4.4). We limited this analysis only to 'response' trials (hits for target trials, false alarms for distractor trials), which presumably contain sensory-motor transformations. On hit trials, we observed that target-aligned regions (both tMC and tDLS) showed large, rapid-onset peaks in their d-prime profiles (Figure 4.4A, B), compared to more slowly rising sensory encoding in distractor-aligned regions (Figure 4.4C, D). Averaging across all recording sessions, sensory encoding for hit trials within the first 100 ms post-stimulus (which is 100 ms before the earliest reaction times) peaked at (d-prime): tMC, 1.54 +/- 0.15; tDLS, 1.30 +/- 0.22; dMC, 0.49 +/- 0.09; dDLS, 0.42 +/- 0.13 (Figure 4.4E). From ANOVA testing, we observed a significant main effect of hemisphere (target-aligned vs. distractor-aligned, $F(1,47)=44.41$, $p<0.01$), no significant main effect of region (MC vs. DLS, $F(1,47)=1.08$, $p=0.30$), and no significant interaction ($F(1,47)=0.35$, $p=0.55$). Such findings indicate sensory encoding on hit trials that is lateralized and similar in tMC and tDLS.

We conducted similar sensory encoding analyses on false alarm trials (Figure 4.4F). Again, the only statistically significant effect was of hemisphere (target-aligned vs. distractor-aligned, $F(1,39)=7.51$, $p<0.01$), yet with larger encoding in distractor-aligned

regions. Together, these analyses establish robust and lateralized sensory encoding in MC and DLS, and argue against purely cortical or purely basal ganglia selection models.

Pre-Response Peak Firing and Significant Choice Probability in MC Precedes DLS. Next, we sought to assess the order of activation leading to response triggering. To accomplish this, we analyzed the time course of spiking activity in each region preceding reaction times on hit trials (Figure 4.5). In all regions, we observed ramping activity preceding reaction times (Figure 4.5 A-D). However, the time course of these ramping activations differed between regions. We quantified the delay between the 80% percentile of normalized peak neuronal activation and the reaction time (for tMC and tDLS example sessions see Figure 4.5E). The activation-RT delay for each region was (sec): tMC, 0.18 +/- 0.01; tDLS, 0.11 +/ -0.02; dMC, 0.13 +/- 0.02; dDLS, 0.09 +/- 0.02. Unlike analyses of sensory encoding, activation-RT delay ANOVA testing revealed a significant main effect of region (MC vs. DLS, $F(1,47)=9.84$, $p<0.01$) (Figure 4.5F), with longer delays for MC compared to DLS. We did not observe significant effects of hemisphere or interaction. These analyses suggest that, with regards to response triggering, MC is upstream of DLS.

Next, we used choice probability analyses to gain insights into the temporal latencies of the sensory-motor transformations within each region (Figure 4.6). Choice probability is the quantification of a relationship between neuronal activity and behavioral outcome, independent of stimulus amplitude (Britten et al., 1996). Above chance (0.5) choice probability indicates epochs in which neural activity is not solely

accounted for by sensory processing and may instead reflect decision making and/or motor response processing. In Figure 4.6A-D, we plot the choice probability time course for target stimuli, as the separation of spiking activity on hit versus miss trials. Target-aligned MC shows prominent early choice probability peaks within 100 ms post-stimulus (Figure 4.6A). This finding in MC is consistent with our previous report of early choice probability in layer 5 of MC (Zareian et al., 2021). Distractor-aligned MC shows moderate latency choice probability (Figure 4.6C), whereas target-aligned and distractor-aligned DLS show more gradual rises in choice probability, peaking during the response window >200 ms post-stimulus onset (Figure 4.6B, D). A comparison of latencies to reach choice probability of 0.6 revealed significantly earlier increases in MC than DLS (sec): tMC, 0.06 +/- 0.02; tDLS, 0.15 +/- 0.04; dMC, 0.11 +/- 0.01; dDLS, 0.20 +/- 0.04; significant main effect of region (MC vs. DLS), $F(1,25)=6.97$, $p=0.01$; no significant effect of hemisphere, $F(1,25)=2.52$, $p=0.12$, or interaction, $F(1,25)=0$, $p=1.00$. These analyses suggest that sensory-motor transformation signaling occurs earlier in MC compared to DLS.

We recently reported lower than chance (negative) choice probability before stimulus onset throughout dorsal neocortex, indicating that lower pre-stimulus activity is more likely to result in response (versus no response) outcomes (Marrero et al., 2021). Interestingly, here we observed below chance pre-stimulus choice probability in both MC and DLS (Figure 4.6A-E). These pre-stimulus baseline differences can also be appreciated in plots of the average spike rates preceding hit and miss trials (Figure 4.3C

and 4.3F). Thus, noise suppression preceding whisker stimulus detection may generalize to cortical and subcortical structures.

In summary, we find robust sensory, motor, and choice-related signals in both MC and DLS. Sensory signals are lateralized, whereas motor and choice signals are more regionally organized. Notably, we find a temporal ordering of motor and choice signals between regions, suggesting a functional organization with MC upstream to DLS, and DLS activations more directly linked to response triggering.

Task Performance Requires Target-Aligned DLS. Next, we performed muscimol ($GABA_A$ receptor agonist) inactivation studies to determine the essential functional contributions of MC and DLS to task performance. Muscimol provides stable inactivation of the exposed region during behavioral testing, enabling assessment of its essential functions that cannot be compensated for on the order of minutes to hours (with full recovery of neural activity within 6 hours, (Arikan et al., 2002)). In mice that had achieved expert performance, we alternated muscimol injected and control (non-injected) testing sessions, randomizing muscimol inactivation among the four sites (tMC, tDLS, dMC, dDLS).

For each behavioral testing session (Figure 4.7A), we first tested mice in a classical conditioning version of the task in which an auditory cue the mice had previously associated with reward (opening of a solenoid) was presented along with a fluid reward. This was performed to assess global deficiencies in motivation or response initiation/execution. In all inactivation conditions, mice performed this classical

conditioning task at a high rate (Figure 4.7B), with no significant differences between conditions (Pearson Chi-square value = 4.554, p-value = 0.208). These findings argue against global deficits in motivation or response execution. In contrast, we did observe substantial group variance during subsequent performance in the operant, selective detection task (Figure 4.7C) (Chi-square value = 10.521, p-value = 0.015). Deficits in performance were particularly notable for target-aligned DLS inactivations, in which 50% of the behavioral sessions failed to attain a minimum number of rewards (<10 rewards within 1 hour, compared to an average of 62 rewards for control mice, see also Methods for descriptions of performance thresholds). Additionally, we assessed task engagement time (Figure 4.7D), quantified as the total time of engagement in the selective detection task (see Methods for assessment details). A 2-way ANOVA test determined significant main effects of region ($F(1,44)=11.5$, $p=<0.01$) and hemisphere ($F(1,44)=5.21$, $p=0.03$), with target-aligned DLS inactivations displaying the greatest reductions in task engagement.

To better understand the contributions of each site to task performance, we assessed effects of inactivations on hit rate, false alarm rate, behavioral d-prime (separation between hit rate and false alarm rate), and criterion (tendency to respond on target and distractor trials) during the 1-hour selective detection task (Figure 4.8). For all performance measures, we observed significant main effects of region ($p=<0.01$), with additional main effects of hemisphere for hit rate and criterion ($p=0.03$ and $p=0.02$, respectively). Overall, DLS inactivations resulted in lower hit rates, lower false alarm rates, poorer target-distractor discrimination (d'), and reduced tendency to respond (c).

For each measure, the largest impairments were observed for target-aligned DLS inactivations. Moreover, for each measure, target-aligned DLS inactivation sessions were significantly different than non-injected control sessions (task engagement time: control, 5460 +/- 270 seconds; tDLS, 1510 +/- 470 seconds, 72% reduction, p=<0.01; hit rate: control, 0.71 +/- 0.03; tDLS, 0.25 +/- 0.11, 65% reduction, p=<0.01; false alarm rate: control, 0.16 +/- 0.01; tDLS: 0.06 +/- 0.02, 63% reduction, p=0.019; d-prime: control, 1.91 +/- 0.11; tDLS, 0.56 +/- 0.31, 71% reduction, p=<0.01; criterion: control, 0.13 +/- 0.08; tDLS, 1.43 +/- 0.30, 11 fold increase, p=<0.01). These data identify target-aligned DLS, rather than MC, as most critical for responding to task-related stimuli.

Interestingly, we found that muscimol inactivation did not invariably reduce response rates. Inactivations of MC resulted in increased false alarm rates compared to control sessions (Figure 4.8B), which was statistically significant for distractor-aligned MC inactivations (control, 0.16 +/- 0.03; dMC, 0.29 +/- 0.05, 81% increase p=<0.01). For multiple measures, effects of target-aligned DLS inactivation vs distractor-aligned MC inactivation were significantly different from each other and opposite in direction compared to control sessions. This includes hit rate (tDLS, 0.25 +/ - 0.11; dMC: 0.82 +/- 0.07, p=<0.01), false alarm rate (tDLS, 0.06 +/-0.02; dMC, 0.29+/ -0.05, p<0.01), and criterion (c) (tDLS, 1.43 +/- 0.30; dMC, -0.33 +/- 0.20, p=<0.01). These findings highlight the divergent functional contributions of these two regions on task performance, with target-aligned DLS dominantly contributing to sensory selection and distractor-aligned MC dominantly contributing to distractor response suppression.

Discussion

In this study, we compared motor cortex (MC) and dorsolateral striatum (DLS) contributions to performance in a learned selective detection task. First, we identified the S1-project sites within MC and DLS as our target regions (Figure 4.2). Next, we demonstrated that both regions display robust sensory encoding (Figure 4.3 and 4.4) as well as motor-related and choice-related signals (Figures 4.3, 4.5, 4.6) during expert task performance. Lastly, targeted pharmacological inactivation studies identified DLS as essential for responding to task-related stimuli (Figures 4.7, 4.8). Collectively, our data support DLS, and not MC, as a crucial bottleneck in linking task-related stimuli to prepotent responses in this learned task (Figure 4.9).

One important consideration when interpreting inactivation studies, particularly for Go/NoGo tasks, is that reductions in task performance may reflect global deficits in motivation, sensation, or response execution rather than specific deficits in task-related processing (Carandini & Churchland, 2013). We interpret the robust impairments during DLS inactivation as reflecting specific deficits in task-related processing for multiple reasons. Most importantly, during the same behavioral sessions, mice with DLS inactivations responded at high rates to auditory-cued reward delivery (Figure 4.7B), ruling out severe global deficits. Additionally, we observed robust post-stimulus (sensory) and pre-response (possibly motor command) signals within DLS, as would be required for participation in sensory-motor transformations. Whether the actual sensory-to-motor transformation is computed within DLS or is computed elsewhere and

propagated to DLS remains unknown. However, our data support DLS as an indispensable node in the sensory-motor transformation process in this task.

Our findings support current frameworks for the importance of DLS in learned tasks (Atallah et al., 2007; Dhawale et al., 2021). An unexpected finding, however, is that target-aligned DLS inactivations did not only reduce responding to target stimuli (Figure 4.8A), but also robustly reduced responding to distractor stimuli (Figure 4.8B). We speculate that through learning, response triggering for target and distractor stimuli become conditioned on the activation of target-aligned DLS. Understanding the neural mechanisms underlying this conditioned response triggering, and its possible dependence on dopamine neuromodulation (Gerfen et al., 1990; Gerfen & Surmeier, 2011; Kravitz et al., 2010; Surmeier et al., 1996) are important topics of future research.

It was recently proposed that baseline (prestimulus) activity within the striatum may regulate task engagement, with higher prestimulus activity priming motor execution by bringing the network closer to response threshold (Steinmetz et al., 2019). This framework would have predicted above chance prestimulus choice probability for target-aligned DLS. In contrast, we find that bilateral DLS, like the rest of dorsal neocortex (Marrero et al., 2021), displays below chance prestimulus choice probability in response to target stimuli (Figure 4.6E). This difference may be due to sensory modality or task design. Nonetheless, our data suggest that for both cortical and subcortical structures within the whisker system, noise reduction enhances stimulus detection.

An important open question is which basal ganglia outputs are most relevant for response triggering. The basal ganglia may project back to regions of motor/frontal

cortex not studied here, which may ultimately signal the motor command. And yet, there is growing appreciation of direct projections from the basal ganglia to subcortical motor structures, including the superior colliculus and other brainstem motor structures (Lee & Sabatini, 2021; Saitoh et al., 2003; Takakusaki et al., 2003; Takakusaki et al., 2011). We speculate that, at least in the rodent, striatal selection does not require motor cortex for response execution.

In comparison to DLS, our findings indicate that MC is less critical for responding to task-related stimuli, despite this region demonstrating robust sensory and early choice-related signals. We interpret this discrepancy between representation and function in MC as due to redundant sensory-motor processing through the DLS. Recent studies have shown that motor cortex is required for skill learning, yet is dispensable for performing well-learned tasks (Hwang et al., 2021; Kawai et al., 2015). Thus, it is possible that sensory-motor processing through MC is more important during learning than during expert performance as tested in this study.

Although our data support that MC is not critical for sensory detection in expert mice, we do find evidence for MC involvement in distractor response suppression, especially for distractor-aligned MC (Figure 4.8B). This finding is consistent with a growing literature, primarily in rodents, suggesting essential roles of motor cortices in suppressing prepotent responses (Ebbesen & Brecht, 2017; Murakami et al., 2017; Zagha et al., 2015). Further studies are required to determine the mechanisms underlying this function.

We do recognize important limitations of our study. Foremost, the multiunit activities analyzed here represent the summed spiking outputs of neuronal ensembles consisting of different cell-types. While we do observe systematic differences in the dynamics of pre-response and choice-related signals in MC and DLS, we recognize that there is likely a much larger heterogeneity of responses of single units. Second, our pharmacological inactivations do not distinguish between the multiple output pathways that may be responsible for the consequent behavioral effects. Follow-up studies with cell-type resolution and pathway-specificity will provide many important mechanistic insights into how DLS and MC contribute to sensory selection.

Figures and Legends

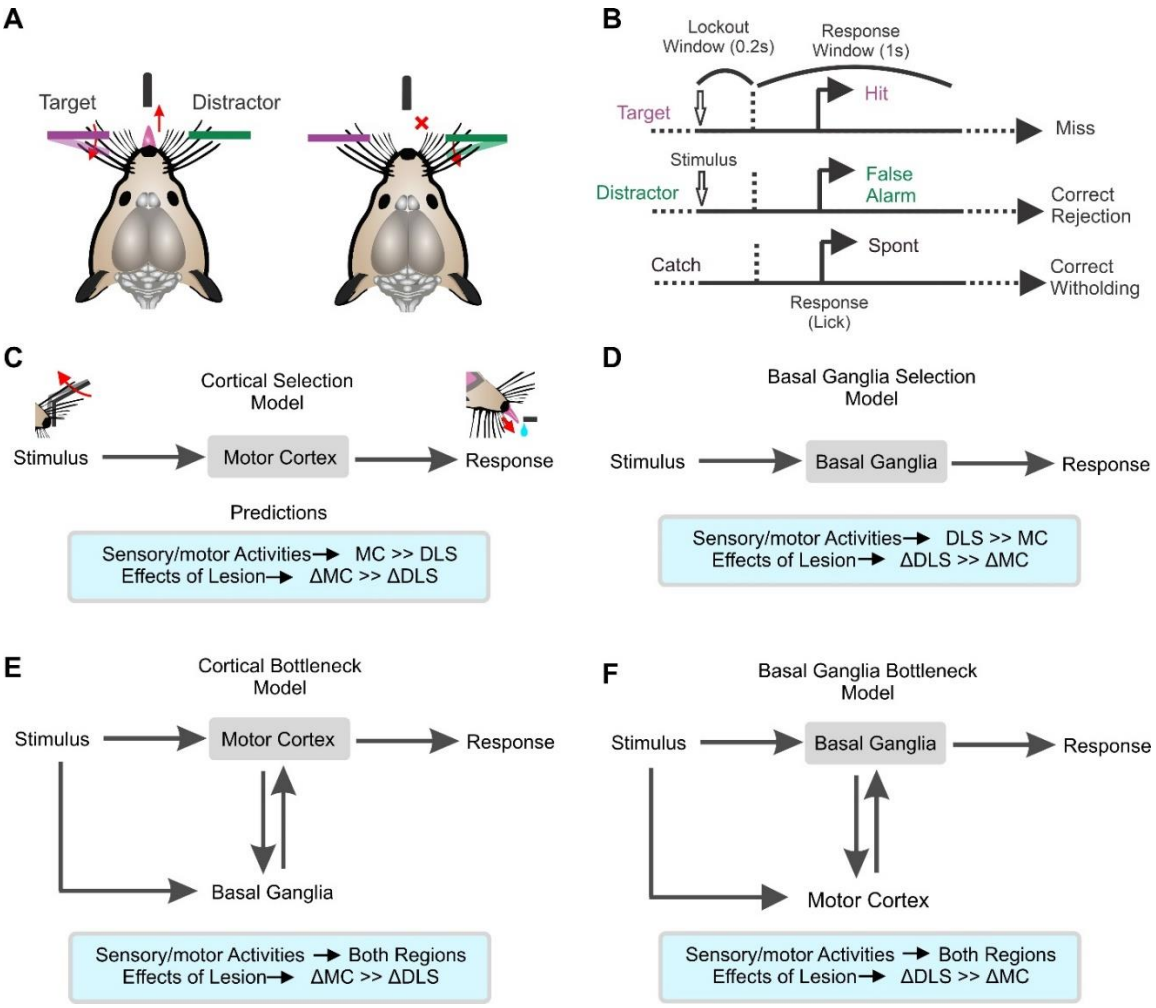

Figure 4.1. Behavioral task, trial structure and possible functional organizations underlying sensory selection.

(A) Illustration of the behavioral task. Mice learn to respond (lick) to small, transient whisker deflections in one of their whisker fields (purple - target) and to withhold licking to identical deflections in their opposite whisker field (green - distractor) (modified from (Aruljothi et al., 2020)). **(B)** Diagram of task structure for the operant, selective detection task (also see methods). Following a variable (5-9s) intertrial interval, mice receive either a target stimulus, distractor stimulus, or catch trial. After stimulus onset, a lockout window of 0.2s is implemented in which responding is punished by immediately restarting the intertrial. Responses during the response window of target trials are considered hits and responses during the response window of distractor trials are considered false alarms. **(C-F)** Different models (top) and their experimental predictions (bottom) for the pathways involved in converting whisker stimuli into motor responses. The models differ in the involvement and importance of sensory-to-motor transformations through the motor cortex versus the basal ganglia.

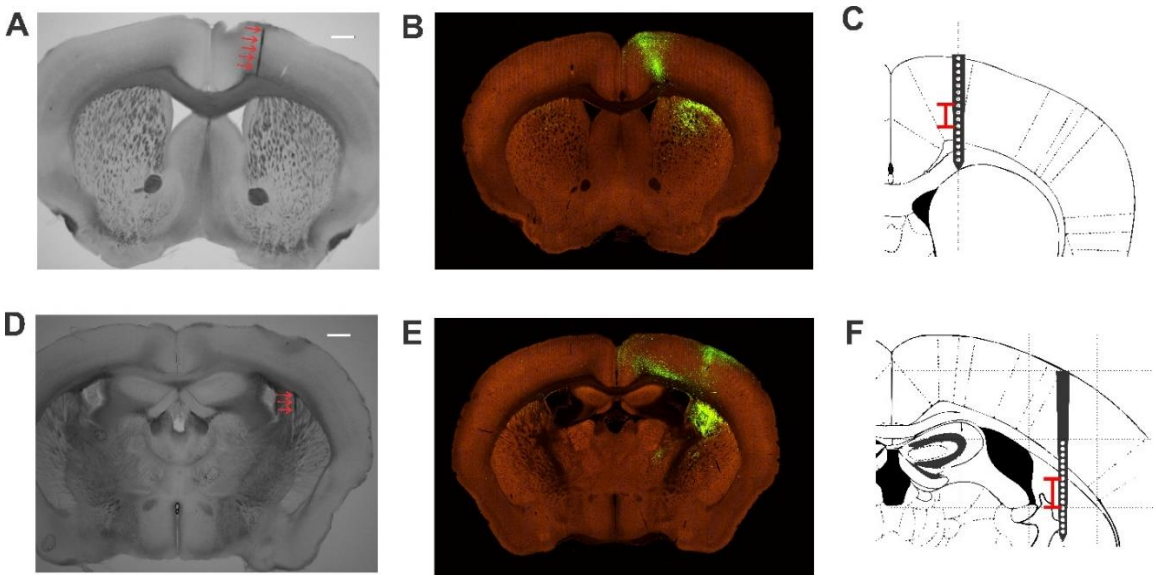

Figure 4.2. MC and DLS sub-region targeting.

(A, D) Coronal brain sections depicting the needle tracts (red arrows) from targeting MC **(A)** and DLS **(D)**. **(B, E)** Findings from whisker-related S1 anterograde labeling from the Allen Brain Atlas: Mouse Connectivity (experiment 126907302), showing the S1-projection sites (green) in MC (B, section 49) and DLS (E, section 62). **(C, F)** Schematics of the same coronal sections as in [A, B] and [D, E], respectively, illustrating the coverage of the laminar multi-site electrode recordings. Red bars indicate the mean +/- 1 standard deviation for the sites with maximum sensory encoding within each region. Scale bars in [A] and [D] are 1 mm.

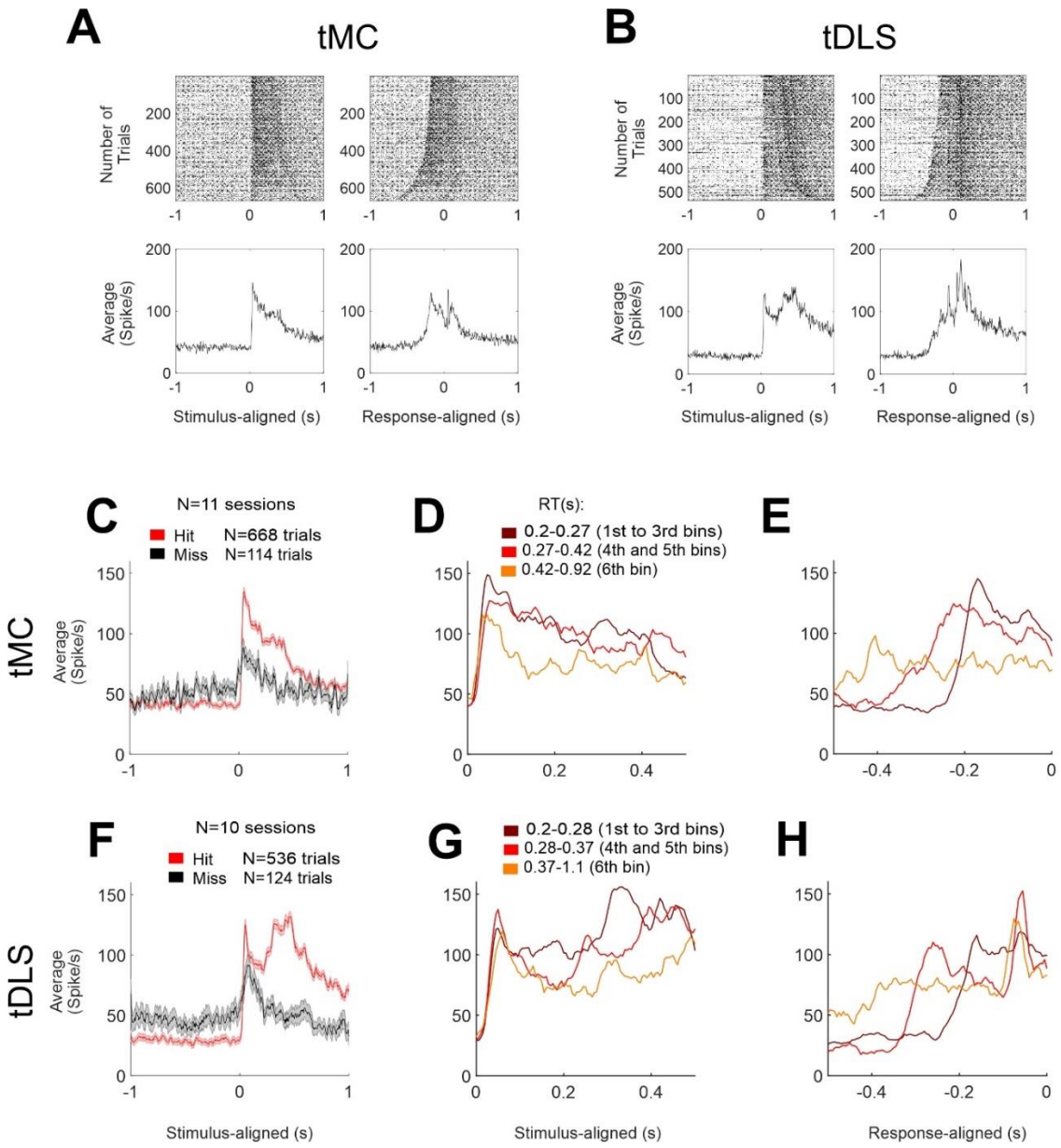
A
tMC
B
tDLS
Number of Trials
Average (Spike/s)
Stimulus-aligned (s)
Response-aligned (s)
C
N=11 sessions
Hit N=668 trials
Miss N=114 trials
D
RT(s):
0.2-0.27 (1st to 3rd bins)
0.27-0.42 (4th and 5th bins)
0.42-0.92 (6th bin)
E
tMC
F
N=10 sessions
Hit N=536 trials
Miss N=124 trials
G
0.2-0.28 (1st to 3rd bins)
0.28-0.37 (4th and 5th bins)
0.37-1.1 (6th bin)
H
tDLS

Figure 4.3. Robust post-stimulus and pre-response spiking activities in target-aligned MC and DLS.

(A) MUA recorded from deep layers of target-aligned MC for all hit trials, pooled across sessions. The left column depicts MUA aligned to the target stimulus onset and the right column depicts MUA aligned to the reaction time. Top panels show raster plots sorted based on reaction times from fast (top) to slow (bottom) hits trials. Bottom panels show average of all trials shown in the top panels. Note the rapid post-stimulus (left, putative sensory) and the robust pre-response (right, putative motor) spiking activities. **(B)** Same as [A] but recorded from target-aligned DLS. **(C)** Average of all hit (red) and miss trials (black), recorded from deep layers of target-aligned MC (n=11 sessions). **(D)** Hit trials, pooled across sessions, from target-aligned MC, grouped based on reaction time, aligned to the stimulus onset. Darker colors depict faster reaction time trials. Note the early 'sensory' peak, invariant to reaction time. **(E)** Hit trials, pooled across sessions, from target-aligned MC, grouped based on reaction time (as in [D]), aligned to the reaction time. (F,G and H) Same as [C, D and E] but recorded from target-aligned DLS, also displaying robust sensory and motor alignments.

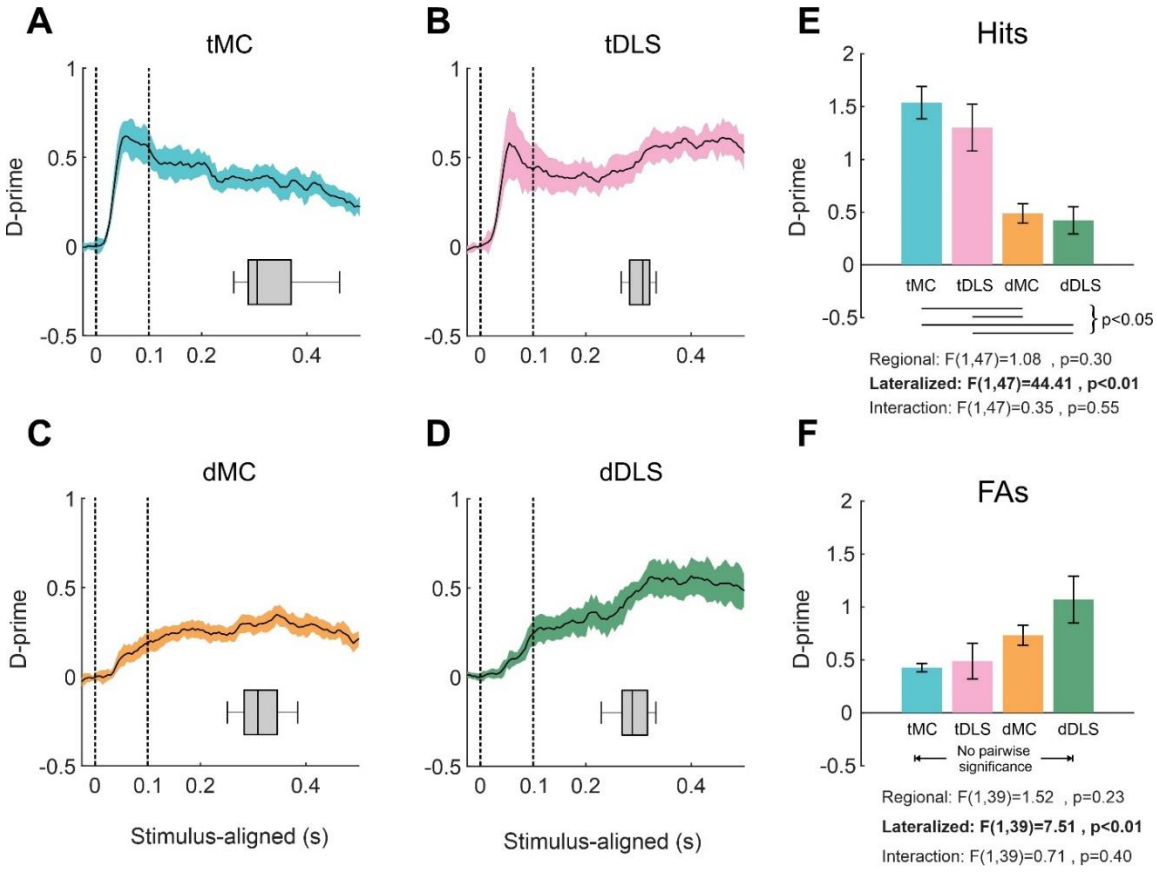

Figure 4.4. Lateralized sensory responses in MC and DLS.

(A) Average peak sensory encoding of target stimulus responses (hits) in deep layers of target-aligned MC. The x-axis denotes time from stimulus onset in seconds. The y-axis denotes neurometric d-prime (as the separation between distributions of pre-stimulus and post-stimulus MUA). Dashed lines indicate the 100 ms post-stimulus window used for quantification in [E]. **(B-D)** Same as [A], but for target-aligned DLS **(B)**, distractor-aligned MC **(C)**, and distractor-aligned DLS **(D)**. Note the rapid and large increase in d-prime after stimulus onset in target-aligned regions compared to distractor-aligned regions. **(E)** Sensory encoding of hit trials within each region calculated for the first 100 ms post-stimulus across recording sessions. Lines under the bar graph indicate significant pairwise differences. **(F)** Same as E, but for distractor stimulus responses (false alarms).

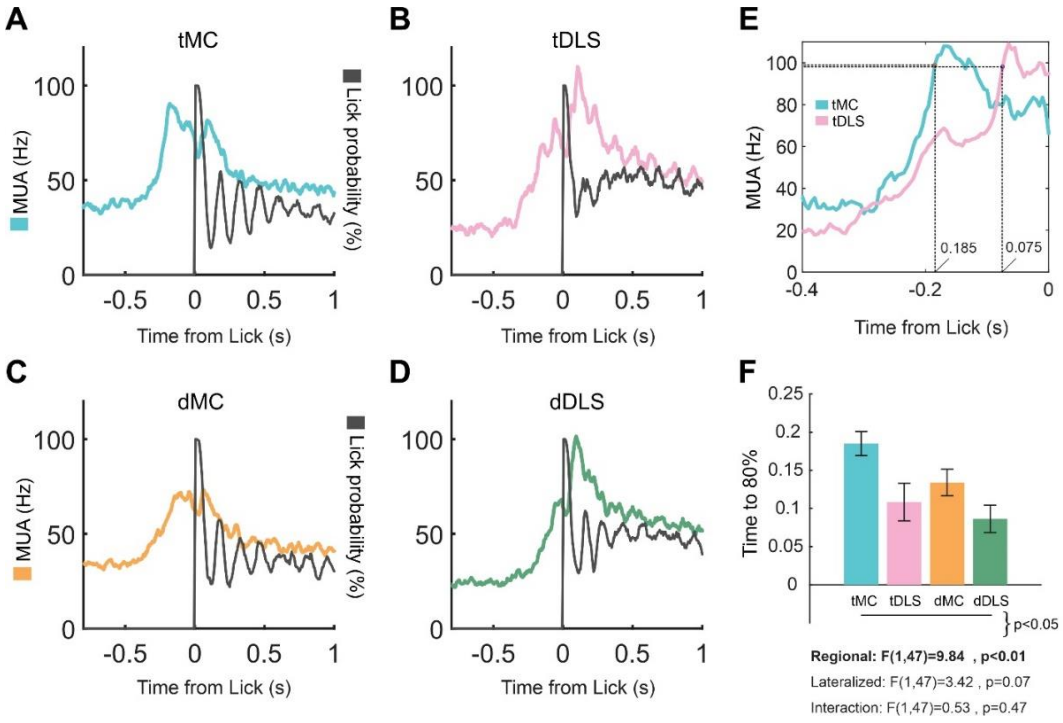

Figure 4.5. Pre-response peak firing in MC precedes pre-response peak firing in DLS.

(A) Average peak multiunit activity aligned to the lick responses on hit trials in deep layers of target-aligned MC. The blue trace shows spike rate (Hz) whereas the black trace shows the lick probability (%). Note the increase in spiking activity before the licking response. **(B-D)** Same as [A], but for target-aligned DLS **(B)**, distractor-aligned MC **(C)**, and distractor-aligned DLS **(D)**. **(E)** Average peak multiunit activity for lick responses for example sessions from tMC and tDLS. Dashed lines show the 80% percentile of peak neuronal activation. **(F)** Delay between the 80% percentile of peak neuronal activation and reaction time across sessions for each recording site. Lines under the bar graph indicate significant pairwise differences.

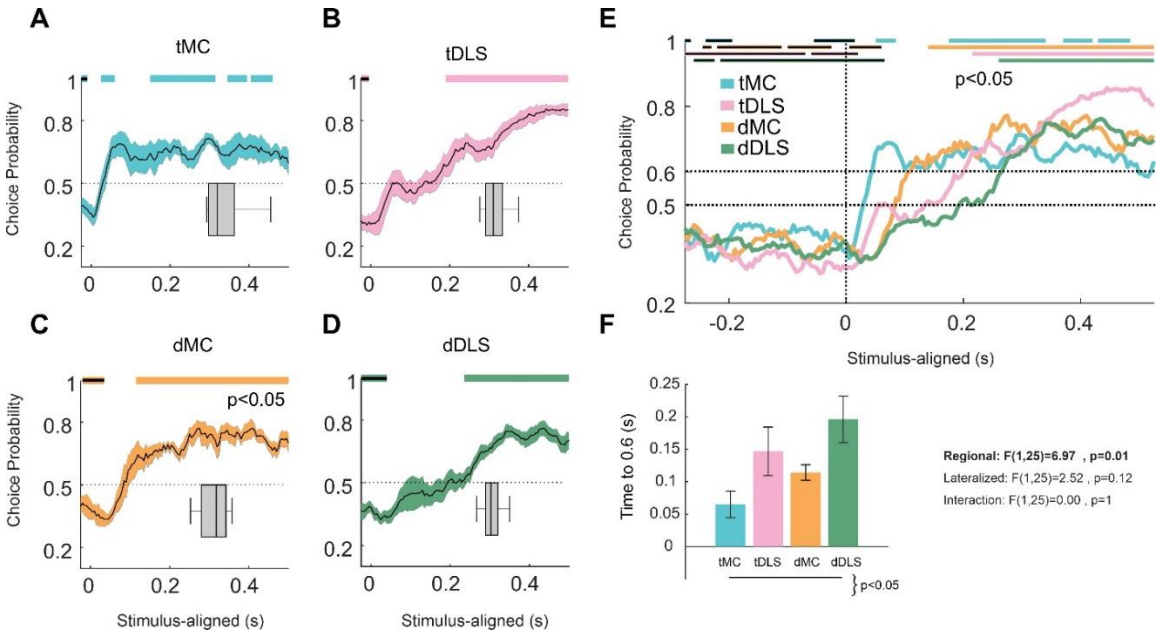

Figure 4.6. Choice probability in MC precedes DLS.

(A) Average choice probability on target trials in deep layers of target-aligned MC. The x-axis denotes time from stimulus onset in seconds. The y-axis denotes choice probability calculated as the separation of spiking activity on hit and miss trials in 50 ms sliding windows with 90% overlap. Significant positive and negative choice probability time points are depicted by plain and filled color bars, respectively, at the top of the panel. Chance level (equal spiking on hit and miss trials) is depicted by the dashed line at 0.5. The grey box-and-whisker plot indicates the reaction time distributions for the same recording sessions. Note the early above chance choice probability, well-preceding the reaction time. **(B-D)** Same as [A] but for target-aligned DLS **(B)**, distractor-aligned MC **(C)**, and distractor-aligned DLS **(D)**. **(E)** Choice probability traces, overlapped for all four regions, demonstrating differences in temporal profiles. In addition to chance (0.5), an arbitrary threshold at 0.6 is depicted by a dashed line. **(F)** Time to reach choice probability of 0.6 across sessions for each recording site. Lines under the bar graph indicate significant pairwise differences.

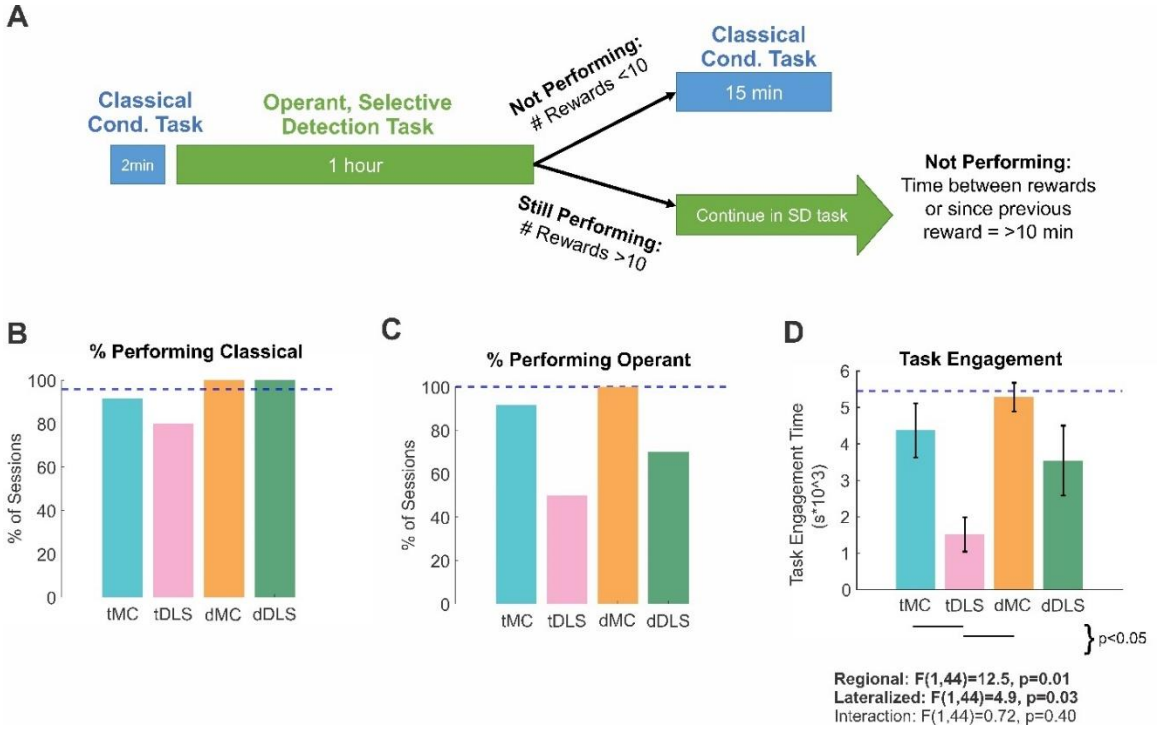

Figure 4.7. Muscimol inactivation impacts on task performance.

(A) Behavioral training workflow for muscimol inactivation experiments (see also Methods). For each behavioral training session, mice were first presented with a classical conditioning task for 2 minutes, followed by the operant, selective detection task for 1 hour. For mice that did not perform the selective detection task, they were again presented with the classical conditioning task for 15 minutes. Mice that did perform the selective detection task continued in this task until unmotivated. **(B)** Percentage of sessions meeting threshold performance for the classical conditioning task, according to region of inactivation. **(C)** Percentage of sessions meeting threshold performance for the operant, selective detection task. **(D)** Length of task engagement within the selective detection task, averaged across all sessions according to the region of inactivation. Lines under the bar graph indicate significant pairwise differences. For [B-D], the horizontal dashed line reflects performance measures from non-injected control sessions.

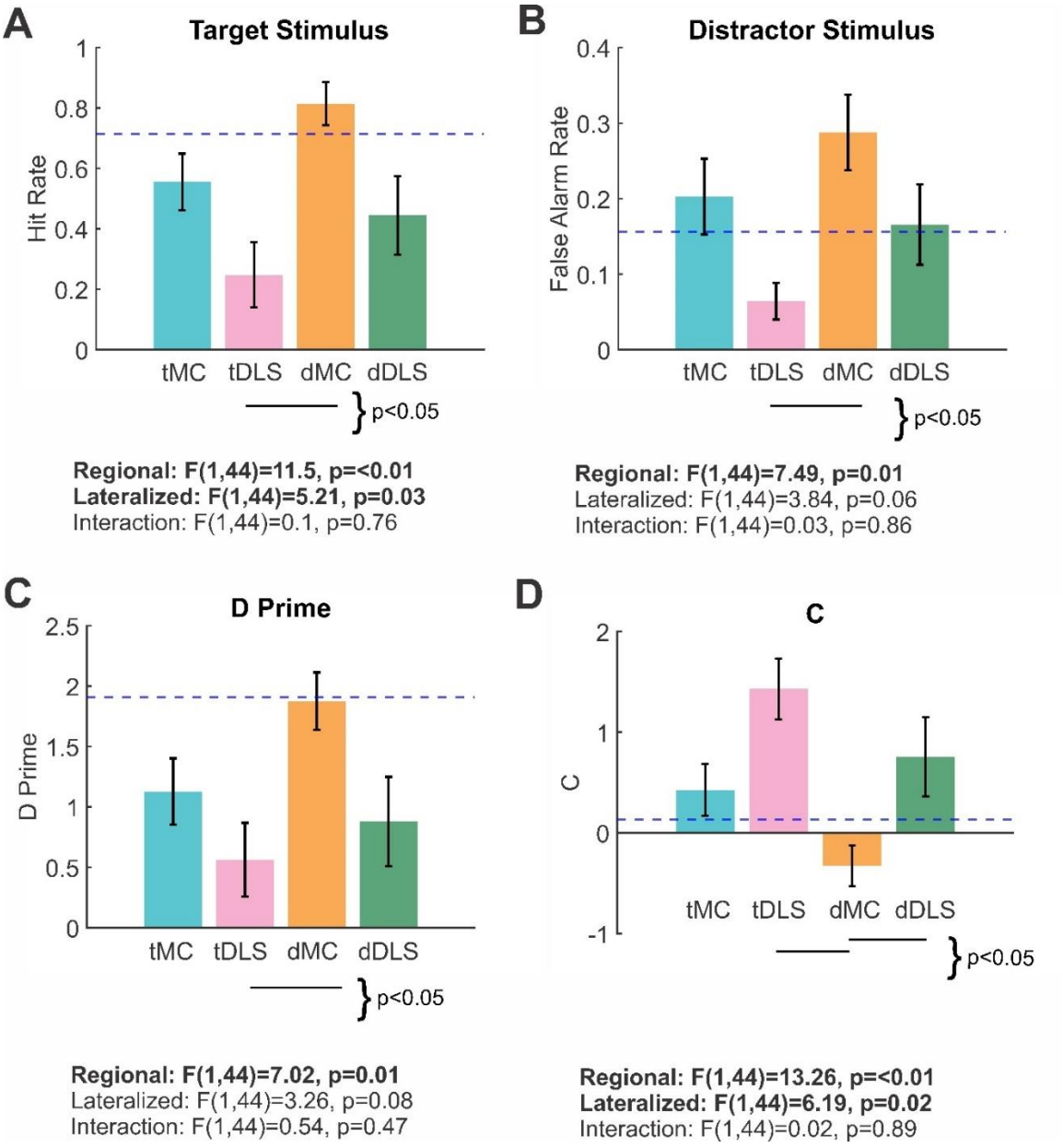

Figure 4.8. Target-aligned DLS inactivation reduces responding to task-related stimuli.

(A) Hit rates within the selective detection task, averaged across all sessions according to the region of inactivation. Lines under the bar graph indicate significant pairwise differences. The horizontal dashed line reflects performance measures from non-injected control sessions. **(B-D)** Same as [A], but for false alarm rates **(B)**, behavioral d-prime **(C)**, and criterion **(D)**. Note that target-aligned DLS inactivations (pink) caused large decreases in hit rates and false alarm rates, and corresponding increases in the criterion.

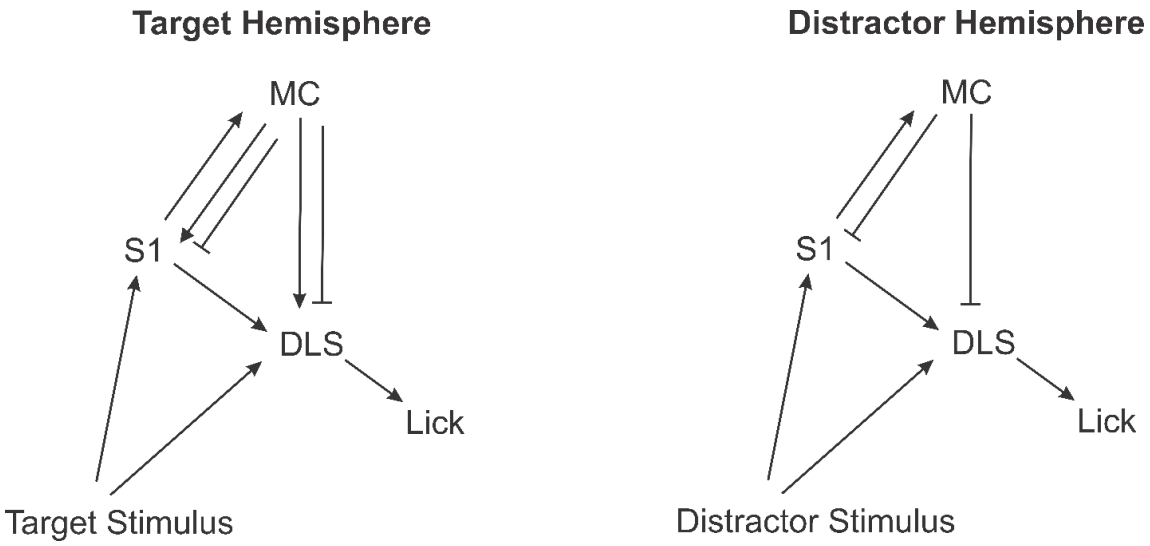

Figure 4.9. Functional circuit model for how MC and DLS interact to implement sensory selection.

Arrows depict net excitatory pathways whereas blunt arrows depict net inhibitory pathways. In this model, target-aligned DLS functions as a critical node in transforming sensory inputs into motor outputs, potentially integrating sensory evidence from S1, MC, and subcortical regions. In contrast, MC acts primarily to modulate the sensory-to-motor transformations that occur through the DLS pathway.

Session Ns					
Electrophysiological Experiments	Figure 4.3	Figure 4.4, Hits	Figure 4.4, FAs	Figure 4.5	Figure 4.6
tMC	11	11	7	11	7
tDLS	10	10	9	10	8
dMC	Not used	19	17	19	6
dDLS	Not used	11	10	11	8
Total Sessions	21	51	43	51	29

Table 4.1. Session number (N) used for electrophysiological recordings.

The number of sessions for each region used for analyses in different figures, related to recording experiments.

Session Ns	
Inactivation Experiment Type	Figures 4.7, 4.8
Control	72
tMC	12
tDLS	10
dMC	13
dDLS	10
Total Sessions	117

Table 4.2. Session number (N) used for muscimol inactivation.

The number of sessions for each region used for analyses in different figures, related to control and inactivation experiments.

References

Alexander, G. E., & Crutcher, M. D. (1990). Functional architecture of basal ganglia circuits: neural substrates of parallel processing. Trends in neurosciences, 13(7), 266-271.

Antzoulatos, E. G., & Miller, E. K. (2011). Differences between neural activity in prefrontal cortex and striatum during learning of novel abstract categories. Neuron, 71(2), 243-249.

Arikan, R., Blake, N. M. J., Erinjeri, J. P., Woolsey, T. A., Giraud, L., & Highstein, S. M. (2002). A method to measure the effective spread of focally injected muscimol into the central nervous system with electrophysiology and light microscopy. Journal of Neuroscience Methods, 118(1), 51-57.

Aruljothi, K., Marrero, K., Zhang, Z., Zareian, B., & Zagha, E. (2020). Functional localization of an attenuating filter within cortex for a selective detection task in mice. Journal of Neuroscience, 40(28), 5443-5454.

Atallah, H. E., Lopez-Paniagua, D., Rudy, J. W., & O'Reilly, R. C. (2007). Separate neural substrates for skill learning and performance in the ventral and dorsal striatum. Nature neuroscience, 10(1), 126-131.

Bergstrom, H. C., Lieberman, A. G., Graybeal, C., Lipkin, A. M., & Holmes, A. (2020). Dorsolateral striatum engagement during reversal learning. Learning & Memory, 27(10), 418-422.

Bergstrom, H. C., Lipkin, A. M., Lieberman, A. G., Pinard, C. R., Gunduz-Cinar, O., Brockway, E. T., Taylor, W. W., Nonaka, M., Bukalo, O., & Wills, T. A. (2018). Dorsolateral striatum engagement interferes with early discrimination learning. Cell reports, 23(8), 2264-2272.

Britten, K. H., Newsome, W. T., Shadlen, M. N., Celebrini, S., & Movshon, J. A. (1996). A relationship between behavioral choice and the visual responses of neurons in macaque MT. Visual neuroscience, 13(1), 87-100.

Brockett, A. T., Tennyson, S. S., deBettencourt, C. A., Kallmyer, M., & Roesch, M. R. (2022). Medial prefrontal cortex lesions disrupt prepotent action selection signals in dorsomedial striatum. Current Biology.

Carandini, M., & Churchland, A. K. (2013). Probing perceptual decisions in rodents. Nature neuroscience, 16(7), 824-831.

Clarke, H. F., Robbins, T. W., & Roberts, A. C. (2008). Lesions of the medial striatum in monkeys produce perseverative impairments during reversal learning similar to those produced by lesions of the orbitofrontal cortex. Journal of Neuroscience, 28(43), 10972-10982.

de Lafuente, V., & Romo, R. (2006). Neural correlate of subjective sensory experience gradually builds up across cortical areas. Proceedings of the National Academy of Sciences, 103(39), 14266-14271.

Dhawale, A. K., Wolff, S. B. E., Ko, R., & Olveczky, B. P. (2021). The basal ganglia control the detailed kinematics of learned motor skills. Nat Neurosci, 24(9), 1256-1269.

Ebbesen, C. L., & Brecht, M. (2017). Motor cortex—to act or not to act? Nature Reviews Neuroscience, 18(11), 694-705.

Esmaeili, V., Tamura, K., Muscinelli, S. P., Modirshanechi, A., Boscaglia, M., Lee, A. B., Oryshchuk, A., Foustoukos, G., Liu, Y., & Crochet, S. (2021). Rapid suppression and sustained activation of distinct cortical regions for a delayed sensory-triggered motor response. Neuron, 109(13), 2183-2201. e2189.

Finkelstein, A., Fontolan, L., Economo, M. N., Li, N., Romani, S., & Svoboda, K. (2021). Attractor dynamics gate cortical information flow during decision-making. Nature neuroscience, 24(6), 843-850.

Foster, N. N., Barry, J., Korobkova, L., Garcia, L., Gao, L., Becerra, M., Sherafat, Y., Peng, B., Li, X., & Choi, J.-H. (2021). The mouse cortico–basal ganglia–thalamic network. Nature, 598(7879), 188-194.

Frank, M. J., Loughry, B., & O'Reilly, R. C. (2001). Interactions between frontal cortex and basal ganglia in working memory: a computational model. Cognitive, Affective, & Behavioral Neuroscience, 1(2), 137-160.

Gordon, E. M., Laumann, T. O., Marek, S., Newbold, D. J., Hampton, J. M., Seider, N. A., Montez, D. F., Nielsen, A. M., Van, A. N., & Zheng, A. (2022). Individualized Functional Subnetworks Connect Human Striatum and Frontal Cortex. Cerebral Cortex, 32(13), 2868-2884.

Graybiel, A. M., Aosaki, T., Flaherty, A. W., & Kimura, M. (1994). The basal ganglia and adaptive motor control. Science, 265(5180), 1826-1831.

Grillner, S., Hellgren, J., Menard, A., Saitoh, K., & Wikström, M. A. (2005). Mechanisms for selection of basic motor programs–roles for the striatum and pallidum. Trends in neurosciences, 28(7), 364-370.

Guo, Z. V., Inagaki, H. K., Daie, K., Druckmann, S., Gerfen, C. R., & Svoboda, K. (2017). Maintenance of persistent activity in a frontal thalamocortical loop. Nature, 545(7653), 181-186.

Guo, Z. V., Li, N., Huber, D., Ophir, E., Gutnisky, D., Ting, J. T., Feng, G., & Svoboda, K. (2014). Flow of cortical activity underlying a tactile decision in mice. Neuron, 81(1), 179-194.

Hanes, D. P., & Schall, J. D. (1996). Neural control of voluntary movement initiation. Science, 274(5286), 427-430.

Hintiryan, H., Foster, N. N., Bowman, I., Bay, M., Song, M. Y., Gou, L., Yamashita, S., Bienkowski, M. S., Zingg, B., & Zhu, M. (2016). The mouse cortico-striatal projectome. Nature neuroscience, 19(8), 1100-1114.

Hong, Y. K., Lacefield, C. O., Rodgers, C. C., & Bruno, R. M. (2018). Sensation, movement and learning in the absence of barrel cortex. In Nature (Vol. 561, pp. 542-546): Nature Publishing Group.

Hoover, J. E., & Strick, P. L. (1999). The organization of cerebellar and basal ganglia outputs to primary motor cortex as revealed by retrograde transneuronal transport of herpes simplex virus type 1. Journal of Neuroscience, 19(4), 1446-1463.

Hunnicutt, B. J., Jongbloets, B. C., Birdsong, W. T., Gertz, K. J., Zhong, H., & Mao, T. (2016). A comprehensive excitatory input map of the striatum reveals novel functional organization. elife, 5, e19103.

Hwang, E. J., Dahlen, J. E., Mukundan, M., & Komiyama, T. (2021). Disengagement of motor cortex during long-term learning tracks the performance level of learned movements. Journal of Neuroscience, 41(33), 7029-7047.

Inagaki, H. K., Fontolan, L., Romani, S., & Svoboda, K. (2019). Discrete attractor dynamics underlies persistent activity in the frontal cortex. Nature, 566(7743), 212-217.

Jin, X., & Costa, R. M. (2010). Start/stop signals emerge in nigrostriatal circuits during sequence learning. Nature, 466(7305), 457-462.

Kawai, R., Markman, T., Poddar, R., Ko, R., Fantana, A. L., Dhawale, A. K., Kampff, A. R., & Ölveczky, B. P. (2015). Motor cortex is required for learning but not for executing a motor skill. Neuron, 86(3), 800-812.

Kupferschmidt, D. A., Juczewski, K., Cui, G., Johnson, K. A., & Lovinger, D. M. (2017). Parallel, but dissociable, processing in discrete corticostriatal inputs encodes skill learning. Neuron, 96(2), 476-489. e475.

Lee, C. R., Yonk, A. J., Wiskerke, J., Paradiso, K. G., Tepper, J. M., & Margolis, D. J. (2019). Opposing influence of sensory and motor cortical input on striatal circuitry and choice behavior. Current Biology, 29(8), 1313-1323. e1315.

Lee, J., & Sabatini, B. L. (2021). Striatal indirect pathway mediates exploration via collicular competition. Nature, 599(7886), 645-649.

Li, N., Chen, T.-W., Guo, Z. V., Gerfen, C. R., & Svoboda, K. (2015). A motor cortex circuit for motor planning and movement. Nature, 519(7541), 51-56.

Li, N., Daie, K., Svoboda, K., & Druckmann, S. (2016). Robust neuronal dynamics in premotor cortex during motor planning. Nature, 532(7600), 459-464.

Mao, T., Kusefoglu, D., Hooks, Bryan M., Huber, D., Petreanu, L., & Svoboda, K. (2011). Long-Range Neuronal Circuits Underlying the Interaction between Sensory and Motor Cortex. Neuron, 72(1), 111-123.

Marrero, K., Aruljothi, K., Zareian, B., Gao, C., Zhang, Z., & Zagha, E. (2021). Global, Low-Amplitude Cortical State Predicts Response Outcomes in a Selective Detection Task in Mice. Cerebral Cortex.

McGeorge, A., & Faull, R. (1987). The organization and collateralization of corticostriate neurones in the motor and sensory cortex of the rat brain. Brain research, 423(1-2), 318-324.

Middleton, F. A., & Strick, P. L. (2000). Basal ganglia output and cognition: evidence from anatomical, behavioral, and clinical studies. Brain and cognition, 42(2), 183-200.

Mink, J. W. (1996). The basal ganglia: focused selection and inhibition of competing motor programs. Progress in neurobiology, 50(4), 381-425.

Moran, J., & Desimone, R. (1985). Selective attention gates visual processing in the extrastriate cortex. Science, 229(4715), 782-784.

Muhammad, R., Wallis, J. D., & Miller, E. K. (2006). A comparison of abstract rules in the prefrontal cortex, premotor cortex, inferior temporal cortex, and striatum. Journal of cognitive neuroscience, 18(6), 974-989.

Murakami, M., Shteingart, H., Loewenstein, Y., & Mainen, Z. F. (2017). Distinct sources of deterministic and stochastic components of action timing decisions in rodent frontal cortex. Neuron, 94(4), 908-919. e907.

Pasupathy, A., & Miller, E. K. (2005). Different time courses of learning-related activity in the prefrontal cortex and striatum. Nature, 433(7028), 873-876.

Paxinos, G., & Franklin, K. B. (2019). Paxinos and Franklin's the mouse brain in stereotaxic coordinates. Academic press.

Peters, A. J., Fabre, J. M., Steinmetz, N. A., Harris, K. D., & Carandini, M. (2021). Striatal activity topographically reflects cortical activity. Nature, 591(7850), 420-425.

Pimentel-Farfan, A. K., Báez-Cordero, A. S., Peña-Rangel, T. M., & Rueda-Orozco, P. E. (2022). Cortico-striatal circuits for bilaterally coordinated movements. Science advances, 8(9), eabk2241.

Redgrave, P., Prescott, T. J., & Gurney, K. (1999). The basal ganglia: a vertebrate solution to the selection problem? Neuroscience, 89(4), 1009-1023.

Saitoh, K., Hattori, S., Song, W. J., Isa, T., & Takakusaki, K. (2003). Nigral GABAergic inhibition upon cholinergic neurons in the rat pedunculopontine tegmental nucleus. Eur J Neurosci, 18(4), 879-886.

Salinas, E., & Romo, R. (1998). Conversion of sensory signals into motor commands in primary motor cortex. Journal of Neuroscience, 18(1), 499-511.

Salkoff, D. B., Zagha, E., McCarthy, E., & McCormick, D. A. (2020). Movement and performance explain widespread cortical activity in a visual detection task. Cerebral Cortex, 30(1), 421-437.

Saunders, A., Oldenburg, I. A., Berezovskii, V. K., Johnson, C. A., Kingery, N. D., Elliott, H. L., Xie, T., Gerfen, C. R., & Sabatini, B. L. (2015). A direct GABAergic output from the basal ganglia to frontal cortex. Nature, 521(7550), 85-89.

Siegel, M., Buschman, T. J., & Miller, E. K. (2015). Cortical information flow during flexible sensorimotor decisions. Science, 348(6241), 1352-1355.

Sippy, T., Lapray, D., Crochet, S., & Petersen, C. C. (2015). Cell-type-specific sensorimotor processing in striatal projection neurons during goal-directed behavior. Neuron, 88(2), 298-305.

Stephenson-Jones, M., Samuelsson, E., Ericsson, J., Robertson, B., & Grillner, S. (2011). Evolutionary conservation of the basal ganglia as a common vertebrate mechanism for action selection. Current Biology, 21(13), 1081-1091.

Takakusaki, K., Habaguchi, T., Ohtinata-Sugimoto, J., Saitoh, K., & Sakamoto, T. (2003). Basal ganglia efferents to the brainstem centers controlling postural muscle tone and locomotion: a new concept for understanding motor disorders in basal ganglia dysfunction. Neuroscience, 119(1), 293-308.

Takakusaki, K., Obara, K., Nozu, T., & Okumura, T. (2011). Modulatory effects of the GABAergic basal ganglia neurons on the PPN and the muscle tone inhibitory system in cats. Arch Ital Biol, 149(4), 385-405.

Utter, A. A., & Basso, M. A. (2008). The basal ganglia: an overview of circuits and function. Neuroscience & Biobehavioral Reviews, 32(3), 333-342.

Yin, H. H., & Knowlton, B. J. (2006). The role of the basal ganglia in habit formation. Nature Reviews Neuroscience, 7(6), 464-476.

Yin, H. H., Knowlton, B. J., & Balleine, B. W. (2004). Lesions of dorsolateral striatum preserve outcome expectancy but disrupt habit formation in instrumental learning. European journal of neuroscience, 19(1), 181-189.

Zagha, E., Ge, X., & McCormick, D. A. (2015). Competing neural ensembles in motor cortex gate goal-directed motor output. Neuron, 88(3), 565-577.

Zareian, B., Zhang, Z., & Zagha, E. (2021). Cortical Localization of the Sensory-Motor Transformation in a Whisker Detection Task in Mice. Eneuro, 8(1).

Chapter 5 : Conclusions and Future Directions

Brief Overview for the Findings of all the Chapters. This dissertation investigates the brain mechanisms of sensory-motor transformation. I trained mice to perform sensory-motor behavior. The mice learned the task in about 11 days. Using whisker imaging, I showed that the expert mice were able to maintain their whiskers fixed before the arrival of a stimulus, to detect a small deflection in their whisker field (Chapter 2). They extended their tongue long enough to reach a waterspout and receive water in a short window after stimulus onset. Using wide-field calcium imaging, my colleagues found regions that were active during task performance in the dorsal cortex (Chapter 2). I confirmed their findings with a greater temporal resolution by recording LFPs in active regions.

For my primary investigations (Chapters 3 and 4), I mostly used the method of electrophysiological recording of brain regions, especially regions other than S1. During the past 50 years, a good understanding of sensory brain regions, such as primary sensory cortices and their relationship with behavior is well established (however see Chapter 1 for a discussion related to rodents). However, the function of brain regions that were anatomically connected to the primary sensory cortices remained puzzling. Electrophysiological recordings became extremely insightful in capturing the function of these regions in mice for various reasons. 1) For instance, wMC has layers with heterogeneous activities during behavior, which we have only captured using electrophysiological recording (unpublished). However, the recording experiments themselves are harder to implement in S1 than wMC for mice considering that motor

cortices in mice lie on the flat surface in front of the brain, compared to S1 which resides below an arc on the side of the brain. 2) Also, involved regions of interest reside deep inside the brain, inaccessible even with the most current imaging methods.

Here, I extensively characterized the electrophysiological properties of wMC, which is a follow-up of the research of my supervisor (Zagha et al., 2013; Zagha et al., 2015). Using methods for quantification of behavior such as alignment to task events and signal detection theory, we were able to redefine/revitalize concepts such as sensory, motor, and choice signals in brain regions in rodents (Chapter 3). From Chapter 3, we now know how regional activities are related to behavior, especially at the population level. We especially know ALM is a purely motor region in our task and does not promote response suppression, at least not in a proactive sense.

Toward the end of my research, I focused more on DLS, which is less understood in terms of functionality in selective detection behavior. I showed that this region has sensory representation similar to wMC, but a motor representation in DLS appears closer to the time of response, later than wMC. Along with other experiments, we were able to show that DLS is a bottleneck of sensory-motor transformation (Chapter 4). Collectively, from chapters 3 and 4, we now know sensory-motor transformation is distributed across multiple regions, at least within the cortex and the basal ganglia.

Future Directions

Functional Connectivity Between S1, wMC, and the Striatum. Striatal neurons receive many axonal inputs from different cortical regions (Shepherd, 2003). Also, the density of

synaptic contacts from each axon is small. This and other connectivity properties of corticostriatal inputs entail that there is no exclusive control from a part of the cortex; rather there exists a combinatorial logic. For instance, cortical region A and cortical region B converge into the striatum and if both regions become active, neuron C that gets input from both regions becomes active. This type of mapping is independent of the spatial proximity of projecting regions. More interestingly, sensory and motor regions related to the same body part may project to the same striatal regions. The anatomical connectivity of inputs to the striatum from the cortex and other brain regions has been investigated in mice using tracing, recently (Foster et al., 2021; Hunnicutt et al., 2016).

It remains to be investigated how S1 and wMC modulate DLS activity in our task. In Chapter 3 we inactivated and recorded wMC and DLS; however, these experiments were not simultaneous. One future direction is to see if the striatum activity is influenced by the absence of wMC (or S1) and whether any of these cortical regions are necessary for the involvement of the striatum. A more targeted experiment is to optogenetically inhibit or stimulate S1 and wMC, and to assess the ongoing and task-evoked activity in the striatum, as well as influences on the sensory-motor behavior. Similar experiments have been performed in the past and revealed mixed roles of S1 and wMC on choice behavior. 1) Lee et al. showed that stimulating S1 corticostriatal neurons in mice inhibits responding and stimulating wMC corticostriatal neurons promote responding (Lee et al., 2019). 2) Sun et al. showed that activation of S1 corticostriatal neurons improved performance (Sun et al., 2021). 3) Pimentel-Farfan et al. showed that stimulating motor cortex corticostriatal neurons increases the duration of task-related movements (Pimentel-

Farfan et al., 2022). Based on these findings, I predict that stimulating S1 and wMC corticostriatal neurons, at least in the target-aligned hemisphere promotes responding to the target stimulus (increase in hit rate) during our sensory-motor behavior. In chapter 4, we observed that inhibition of wMC does not reduce task-relevant responses. However, I speculate that this is due to fast compensation by other cortical regions. In this framework, inhibiting both cortical regions diminish the activity in the striatum and impair task performance.

Exploring Upstream of the Striatum for Next Stages of Sensory-Motor Transformation. The dominant view in the field is focused on corticostriatal pathways and their importance in sensory-motor tasks. But thalamostriatal pathways may be important in sensory-motor behavior. There are inputs from the posterior medial thalamus to the striatum that could deliver sensory information, bypassing the cortex (Smith et al., 2012). The importance of this pathway in our task remains to be investigated. It is likely that the input from whiskers gets directly routed to DLS via thalamic pathways since we were able to see a fast sensory response in DLS (Chapter 4, Figure 4.4). The way to investigate these pathways is by injecting retrograde optogenetically-sensitive viruses into DLS and stimulating or inhibiting the destination (soma) of striatal projecting neurons in the thalamus during the task performance. Alternatively, these regions could be found using retrograde labeling and lesioned in separate sets of mice to inform about their functions.

The Possibility of Assessing Communication Across Regions Using Synchronization. LFPs, current source densities (CSDs), and spiking activities give different information about neuronal events, but all are recorded using the same method from the brain (recording voltage fluctuations using a probe). I used spiking activities in the projects of this dissertation extensively. Although we investigated the LFPs in Chapter 2 in three cortical regions, it remains to be known what LFPs informs about the function of the striatum and whether LFPs in the striatum (and their relation to underlying spiking activity) are different with the cortex. Furthermore, LFPs may provide information about communication among cortical regions and between the cortex and the striatum, possibly mediated via synchronization. CSD can be informative in terms of input and output to the layers of the cortex. For instance, using spiking activity, I found that the sensory information reaches the superficial layers of wMC in both target-aligned and distractor-aligned hemispheres, but they did not propagate further to deep layers in the distractor-aligned wMC, confirming the results of widefield calcium imaging in Chapter 2 (unpublished). This was in contrast with sustained and strong activation of deep layers in target-aligned wMC. I used CSD to validate the appearance of input in superficial layers of wMC and found that there was indeed CSD activity in superficial layers of wMC in both hemispheres (unpublished).

Aside from the purely representational aspects of extracellular recording, combining it with manipulation tools such as optogenetics and microstimulation may provide additional insights about the intrinsic excitability of a region, or about functional coupling among multiple regions. I measured intrinsic excitability by optogenetically

stimulating a brain region at different power levels and recording the changes in spiking activities and LFPs. Similarly, I measured functional coupling by optogenetically stimulating a region at different power levels and recording the spiking activities and LFPs in a destination region (which is anatomically targeted by the source region). Using this methodology, I found that the intrinsic excitability of wMC and the communication between S1 and wMC are not different in the two hemispheres (unpublished). This methodology is quite novel and rarely used in the field and may provide insights for localizing seizures in the brain (Klorig et al., 2019). It may be helpful to investigate and compare the intrinsic excitability of the cortex and the striatum, and the functional coupling between these regions in the sensory-motor task for healthy and diseased models.

Learning Transfer in Mice. We trained our mice for a period of 10 days to 2 weeks in this task to become an expert (high stimulus detection rate) (Chapter 2). It remains to be investigated whether training induces long-term changes in the brain or whether the knowledge obtained in whisker-based tasks transfers to visual tasks. Confirming my findings, researchers found that the activity of wMC remains stable even after other regions disengage from the task after an extended period of learning (Kupferschmidt et al., 2017). Recently, there is an interest in studying the same brain regions and neurons in multiple tasks that reveal important insights about the function of brain regions as well as plasticity (Arlt et al., 2022; Lee et al., 2022). I predict that wMC remains the site of

sensory-motor transformation in a visual task that transforms a visual stimulus into a licking behavior.

Insights for Translational and Comparative Studies. In my recent investigations, I discovered that there is a good deal of overlap between our research on the whisker system and research on the haptic system in humans. It has been suggested that the haptic system in humans has "where" and "what" pathways similar to vision modality (Lederman & Klatzky, 2009). Similarly, it has been proposed that the mouse whisker system has "where" and "what" pathways (Ni & Chen, 2017). The pathway between S1 and wMC has been associated with the "where" pathway, related to the localization of objects. Thus our findings about wMC may be informative about the haptic sensory-motor transformation regions in the cortex and their impairment in humans.

Open-Access Electrophysiology. The insights obtained from targeted electrophysiological recordings (Chapters 3 and 4) may not be obtained by using macro-scale brain imaging techniques, because the method I used is more intricate, on a faster timescale, and more specific. Thus, the data is extremely valuable. As a result, there have been considerable challenges in the reproducibility of this type of research across labs.

There have been recent efforts to unify electrophysiological data across tasks, experiments, and labs. For instance, there has been research studies on introducing a type of file that is readable and sharable among different electrophysiological approaches (Garcia et al., 2014). Similarly, the datasets and relevant codes that I obtained can be

uploaded to a repository accessible to everyone to promote open-access research. This saves time and energy from the other labs that aim at reproducing the behavioral and neuronal results I found in my research. This in turn reduces the number of mice used for neuroscience research.

Final Conclusions

The brain is made up of distinct parts and each has its own unique cellular architecture and characteristics. During a behavior, different networks may become activated. I studied one of these networks by focusing on a few specific nodes. My research builds a bridge between large-scale brain activities and the local circuit activities in those nodes. Ultimately, I would like for my research to contribute to a more efficient therapy for patients with different health problems such as ADHD and Parkinson's disease.

In my research, I avoided extensive data collection and computational methods, which often need additional interpretation. However, the type of research I performed required analytical thinking. There were many points where simple but logically correct inference worked better than more sophisticated computational methods. Nevertheless, the type of research I performed, required close partnership with other types of experiments. These include, but are not limited to, the following: 1) Inactivation experiments in which a region or set of regions in the brain becomes inactivated (Chapter 4) 2) Widefield calcium imaging or a global method of assessing the whole brain activity to find out the active brain regions. 3) Computational neuroscience to find out the best models that explain the data.

This research is also closely related to both seizure localization and the study of consciousness; and more broadly, it relates to all the cases in which there is the involvement and/or impairment of the motor cortex and the dorsolateral striatum and interaction of these regions among themselves or with respect to primary sensory cortices. My hope is that both the scientific and methodological aspects and contents of my research will be of use in the future.

References

Arlt, C., Barroso-Luque, R., Kira, S., Bruno, C. A., Xia, N., Chettih, S. N., Soares, S., Pettit, N. L., & Harvey, C. D. (2022). Cognitive experience alters cortical involvement in goal-directed navigation. *Elife*, *11*, e76051.

Garcia, S., Guarino, D., Jaillet, F., Jennings, T., Pröpper, R., Rautenberg, P. L., Rodgers, C. C., Sobolev, A., Wachtler, T., & Yger, P. (2014). Neo: an object model for handling electrophysiology data in multiple formats. *Frontiers in neuroinformatics*, *8*, 10.

Klorig, D., Alberto, G., Smith, T., & Godwin, D. (2019). Optogenetically-induced population discharge threshold as a sensitive measure of network excitability. *Eneuro*, *6*(6).

Kupferschmidt, D. A., Juczewski, K., Cui, G., Johnson, K. A., & Lovinger, D. M. (2017). Parallel, but dissociable, processing in discrete corticostriatal inputs encodes skill learning. *Neuron*, *96*(2), 476-489. e475.

Lederman, S. J., & Klatzky, R. L. (2009). Haptic perception: A tutorial. *Attention, Perception, & Psychophysics*, *71*(7), 1439-1459.

Lee, C. R., Yonk, A. J., Wiskerke, J., Paradiso, K. G., Tepper, J. M., & Margolis, D. J. (2019). Opposing influence of sensory and motor cortical input on striatal circuitry and choice behavior. *Current Biology*, *29*(8), 1313-1323. e1315.

Lee, J. J., Krumin, M., Harris, K. D., & Carandini, M. (2022). Task specificity in mouse parietal cortex. *Neuron*.

Ni, J., & Chen, J. L. (2017). Long-range cortical dynamics: a perspective from the mouse sensorimotor whisker system. *European Journal of Neuroscience*, *46*(8), 2315-2324.

Pimentel-Farfan, A. K., Báez-Cordero, A. S., Peña-Rangel, T. M., & Rueda-Orozco, P. E. (2022). Cortico-striatal circuits for bilaterally coordinated movements. *Science advances*, *8*(9), eabk2241.

Shepherd, G. M. (2003). *The Synaptic Organization of the Brain* (G. M. Shepherd, Ed. 5th ed.). Oxford University Press.

Smith, J. B., Mowery, T. M., & Alloway, K. D. (2012). Thalamic POm projections to the dorsolateral striatum of rats: potential pathway for mediating stimulus–response associations for sensorimotor habits. *Journal of neurophysiology*, *108*(1), 160-174.

Sun, Z., Schneider, A., Alyahyay, M., Karvat, G., & Diester, I. (2021). Effects of optogenetic stimulation of primary somatosensory cortex and its projections to striatum on vibrotactile perception in freely moving rats. *Eneuro*, *8*(2).

Zagha, E., Casale, A. E., Sachdev, R. N., McGinley, M. J., & McCormick, D. A. (2013). Motor cortex feedback influences sensory processing by modulating network state. *Neuron*, *79*(3), 567-578.

Zagha, E., Ge, X., & McCormick, D. A. (2015). Competing neural ensembles in motor cortex gate goal-directed motor output. *Neuron*, *88*(3), 565-577.